University of Wroclaw
Faculty of Physics and Astronomy
Institute of Theoretical Physics

Stability and properties of striped phases in systems of interacting fermions or hard-core bosons

Volodymyr Derzhko

Thesis submitted for the degree of Doctor of Physical Sciences at the University of Wroclaw

Supervisor:
dr hab. Janusz Jędrzejewski

Wroclaw, 2006

Uniwersytet Wrocławski
Wydział Fizyki i Astronomii
Instytut Fizyki Teoretycznej

Stabilność i własności faz pasemkowych w układach oddziałujących fermionów lub bozonów z twardym rdzeniem

Volodymyr Derzhko

Praca doktorska

praca wykonana pod kierunkiem:
dr. hab. Janusza Jędrzejewskiego

Wrocław, 2006

Abstract

In this thesis we deal with the specific collective phenomena in condensed matter — striped-structures formation. Such structures are observed in different branches of condensed matter physics, like surface physics or physics of high-temperature superconductors. These quasi-one-dimensional objects appear in theoretical analyses as well as in computer simulations of different theoretical models. Here, the main topic of interest is the stability of striped structures in certain quantum models, where a tendency towards crystallization competes with a tendency towards phase separation, and some basic properties of these structures.

We consider two strongly correlated two-component quantum systems, consisting of quantum mobile particles and immobile ones. By immobile particles we mean those particles whose occupation numbers are invariant with respect to the hamiltonian evolution. But this does not mean that these occupation numbers serve as a kind of a fixed disorder field. They are varied to reach the minimum of the energy of the total system (an analog of annealing). The both systems are described by Falicov-Kimball-like Hamiltonians on a square lattice, extended by direct short-range interactions between the immobile particles, that favor phase separation. In the first system the mobile particles are spinless fermions while in the second one they are hardcore bosons. We construct rigorously ground-state phase diagrams of the both systems in the strong-coupling regime and at half filling. Two main conclusions are drawn. Firstly, short-range interactions in quantum gases are sufficient for the appearance of charge stripe-ordered phases. When they occur, a first order phase transition between a checkerboard-crystal phase and phase-separated state (a segregated phase) is impossible: by varying the intensity of a direct nearest-neighbor interaction between the immobile particles, the both systems can be driven from a segregated phase via striped phases (for instance, via a diagonal-striped phase in the case of fermions, and via vertical- (horizontal-) striped phases in the case of hardcore bosons) to the checkerboard phase. Secondly, the phase diagrams of the two systems (mobile fermions or mobile hardcore bosons) are definitely different. However, if the strongest effective interaction in the fermionic case gets frustrated gently, then the phase diagram becomes similar to that of the bosonic case.

We show that any anisotropy of nearest-neighbor hopping eliminates the $\pi/2$-rotation degeneracy of the so called dimeric and axial-stripe phases and orients them in the direction of a weaker hopping. Moreover, due to the same anisotropy the obtained phase diagrams of fermions show a tendency to become similar to those of hardcore bosons.

Finally, introducing a next-nearest-neighbor hopping, small enough not to destroy the striped structure, we examine rigorously how the presence of the next-nearest-neighbor hopping anisotropy reduces the $\pi/2$-rotation degeneracy of the diagonal-striped phase. The effect appears to be similar to that in the case of anisotropy of the nearest-neighbor hopping: the stripes are oriented in the direction of the weaker next-nearest-neighbor hopping.

Contents

1 Introduction

In the passing decade, some specific phases, having quasi-one-dimensional structure, the so called striped phases, have been a highly debated subject in condensed-matter physics. Apparently, a broad interest in such phases was initiated by reports presenting experimental evidence for the existence of charge stripes in doped layered perovskites, some of which constitute materials exhibiting high-temperature superconductivity [1, 2].

However, striped phases had been observed much earlier, for instance in physisorbed monolayers on metallic surfaces (see [3] and references therein), or in ultrathin magnetic films [4]. Many other instances of experimental observations of stripe-ordered phases are listed in [5], where Monte-Carlo studies of formation of striped phases in a continuous gas with hardcore and short-range repulsive interactions are reported. Theoretical descriptions, including computer simulations, of these phenomena involve various kinds of classical lattice-gas models (also termed classical spin models) with competing interactions: for physisorbed monolayers see Ref.[6], for ultrathin magnetic films see Ref.[7]. Striped phases have been also studied in the framework of quantum-spin models, like XY model for instance [8]. Interesting theoretical considerations of stripe phases in a two-dimensional electron gas, physically realizable in MOSFET's, based on classical spin models with competing interactions, can be found in Ref.[9].

Quite interestingly, theoretical studies of striped phases in systems of strongly correlated electrons [10, 11, 12, 13] have preceded experimental observations of such phases. But only after those observations, the discussion became much more vigorous, and the nature of stripe-ordered phases started to attract attention of numerous researchers. In the context of the Hubbard model, a comprehensive review of the problem can be found in [14]. The existence of the same kind of striped phases was investigated also in the t–J model [15, 16, 17]. A bird's eye view on the problem of stripe-ordered phases in high-temperature superconductors, but emphasizing its general relevance for contemporary condensed-matter physics can be found in [18]. The general relevance of striped phases is underlined also in [19], where they are viewed as an emergent phenomenon resulting from collective motions of microscopic particles, somewhat analogous to quasi-particles like phonons.

The Hubbard or t–J-like models belong to the most realistic models, in the framework of which the problem of striped-ordered phases in doped layered perovskites can be investigated (see a review paper by Oleś [14]). In the both models, the spin and the charge degrees of freedom are taken into account, and it is believed that it is the competition between these degrees of freedom that is decisive for the formation of striped phases. The major difference between Hubbard, t–J, and similar quantum-particle models for stripe formation, on one side, and the classical or quantum spin models (mentioned above) on the second side, is the role of the kinetic energy. It is absent in the second group of models while it plays a crucial role in the first group. The model studied by us in this thesis belong to the first group.

The question of formation of striped phases is closely related to the question of relative stability of these phases against mixtures of an electron-reach phase and a hole-reach phase (segregated phases). Due to the tiny energy differences between both phases, the results obtained by means of approximate methods, which introduce hardly-controllable errors, are disparate. Therefore, as pointed out in [19, 20] further careful studies are

necessary to settle the problem of formation of stripe-ordered phases. One of possible ways of attacking this problem is to formulate analog problems in less realistic but simpler models, where some control over the results obtained by means of various methods of statistical physics and many-body physics can be gained. This leads hopefully to a deeper insight into the, mentioned above, stability problem.

Such an approach has been adopted by many researchers, using models of the both groups mentioned above. Here are two examples concerning classical spin models. To investigate the phenomenon of frustrated phase separation in high-temperature superconductors, Löw et al [21] consider a spin 1 two-dimensional Ising model with short-range ferromagnetic coupling competing with long-range antiferromagnetic Coulomb interactions, where spin variables are coarsegrained representations of the local density of mobile holes. By means of combined analytical and numerical techniques they show that the transition between ferromagnetic and antiferromagnetic states proceeds via numerous phases, among which there are striped phases. In a recent paper, Valdez-Balderas and Stroud [22] investigate, by means of Monte Carlo techniques, a competition between superconductivity and other types of order in two dimensions. Each site of the underlying lattice, occupied by a classical XY spin (plane rotator), is interpreted by them as a mobile, positively charged superconducting domain, and the orientation of the spin as a phase of the superconducting order parameter of this domain. Vacant sites represent negatively charged nonsuperconducting domains. The nearest neighbor spins are coupled ferromagnetically (a representation of Josephson tunneling) and the occupied sites repel each other with a kind of a screened Coulomb interaction. By varying the relative strength of the two competing interactions, the system is driven from a phase separated state to a checkerboard-like state via a series of complex patterns of self-organization, including some kinds of striped phases.

And here are examples concerning quantum-particle models. Buhler et al [23] have found, by means of Monte Carlo simulations, that upon hole doping antiferromagnetic spin domains and charge stripes, whose properties are in very good agreement with experiments, appear in a spin-fermion model for cuprates. Using the so called restricted phase diagrams, the stability problem of charge-stripe phases has been studied in the spinless Falicov–Kimball model by Lemański et al [20, 24]. In their study the formation of charge stripe-ordered phases can be looked upon as a way the system interpolates between a periodic charge-density wave phase (the chessboard phase) and the segregated phase (a mixture of completely filled and completely empty phases), as the degree of doping varies. A considerable reduction of the Hilbert space dimension in a spinless fermion model with infinite nearest-neighbor repulsion (as compared to a Hubbard model) has been exploited by Zhang and Henley [19, 25] to study carefully, by means of an exact diagonalization technique, the formation of charge stripe-ordered phases upon doping. They addressed also an interesting question of the role of quantum statistics in the problem of striped phases, by replacing fermion particles with hardcore-boson ones.

Our work has been inspired mainly by the recent studies of Lemański et al [20, 24] and by Zhang and Henley [19, 25]. To investigate the key question, whether charge stripe-ordered phases are stable compared to a phase-separated state, we study rigorously the strong-coupling limit of an extended spinless Falicov–Kimball model on a square lattice, with mobile particles being spinless fermions or hardcore bosons. The usual spinless Falicov–Kimball Hamiltonian (such as that studied in [26]) has been augmented by a

direct, Ising-like interaction between the immobile particles.

In the framework of striped-structures formations, one of the interesting questions, the influence of hopping anisotropy on striped phases, was investigated by means of the Hartree–Fock method in [14, 27]. They showed that under an anisotropy in hopping intensities, stripes become oriented in the direction of weaker hopping. This problem is investigated here rigorously, using the introduced model.

The thesis is organized as follows. In the next section we give some insight into the Falicov–Kimball model, providing its main properties, and we introduce technics which are used for deriving our results. Then, in Section 3 we present the considered models and construct phase diagrams due to truncated effective interactions. After that, in Sections 4 and 5, we analyze the influence of hopping anisotropy on striped phases. Finally, we draw conclusions and provide a summary. Various technical details a placed in Appendices (from A to E). Our original results are contained in Sections 3,4, and 5, and have been published in [28, 29, 30], respectively.

2 The Falicov–Kimball models

In this section we give the definition of the spinless Falicov–Kimball model and it basic properties. First of all, we discuss possible interpretations of the model in respect to history of its development. We also shortly mention about today's topics of interest. In the second paragraph we present some useful properties of the model. The following paragraphs deal with technics we use to investigate the model: we make a sketch of a perturbation scheme and discuss the m-potential method in more details.

2.1 Definition

The spinless Falicov–Kimball model, on arbitrary lattice Λ is described by the Hamiltonian:

$$H_{FK} = -\sum_{(x,y)\subset\Lambda} \left(t_{xy} c_x^+ c_y + h.c.\right) + U \sum_{x\in\Lambda} \left(c_x^+ c_x - \frac{1}{2}\right) \cdot s_x, \tag{1}$$

where sites on lattice Λ are denoted as $x, y, \ldots$, whose number is $|\Lambda|$, and the first summation is over the pairs of different sites x and y, with each pair counted once. The system described by Hamiltonian (1) consists of two sorts of spinless particles: quantum which can hop (usually between nearest-neighbors sites) on the lattice with hopping amplitude $t_{xy} = t_{yx}^*$ (we call them *electrons*) and classical which are immobile (*ions*). The electrons, as quantum particles, are described by creation and annihilation operators on site x: c_x^+ and c_x, respectively, which satisfy the appropriate commutation relations: canonical anticommutation relations for spinless fermions or commutation relations of spin 1/2 operators S_x^+, S_x^-, S_x^z for hard-core bosons. The total electron-number operator is $N_e = \sum_x n_x^e = \sum_x c_x^+ c_x$ and corresponding electron density is $\rho_e = N_e/|\Lambda|$. Classical ions, are described by pseudo-spin (or simply, *spin*) s_x on cite x: if $s_x = 1$, site x is occupied by an ion and, if $s_x = -1$ the site x is empty. Ions are described in terms of spins for convenience: instead of spin variable s_x we can use occupation-number variable $n_x^i = (s_x+1)/2$. The collection of spins values $\{s_x\}_{x\in\Lambda}$ is called the *ion configuration*. The total number of ions is $N_i = \sum_x n_x^i = \sum_x (s_x+1)/2$ and the ion density is $\rho_i = N_i/|\Lambda|$. There is no direct interaction either between the electrons or between the ions, although there is the simple on-site interaction between the two kinds of particles with coupling constant U. It is clear that the particle-number operators N_e, N_i, and spins s_x are conserved. Therefore, the description of the classical subsystem in terms of the ion configurations $S = \{s_x\}_{x\in\Lambda}$ remains valid. Whenever periodic configurations of pseudo-spins are considered, it is assumed that Λ is sufficiently large, so that it accommodates an integer number of elementary cells.

The Falicov–Kimball model was first considered by Hubbard [31] and Gutzwiller [32] as a simplification of the one-band Hubbard model,

$$H_{Hubbard} = -\sum_{\sigma=\uparrow,\downarrow} \sum_{(x,y)\subset\Lambda} t_{xy}^{(\sigma)} c_{x\sigma}^+ c_{y\sigma} + 2U \sum_{x\in\Lambda} n_{x\uparrow} n_{x\downarrow}, \tag{2}$$

where $t_{xy}^{(\uparrow)} = 0$, and $t_{xy}^{(\downarrow)} = t_{xy}$ for arbitrary sign of coupling constant U. This is an approximation of the Hubbard model in the case of infinitely heavy spin-up electrons.

In 1969 this model was introduced by Falicov and Kimball in order to explain metal–insulator transitions in mixed valence compounds of rare-earth materials [33]. Experiments suggested that these transitions occur only due to the interactions between electrons: localized immobile f-electrons (ions) and d-electrons in Bloch-like states. The model described by (1) is the simplification of the original model, suggested in [33].

In 1986, Kennedy and Lieb reinvestigated Falicov–Kimball model as a "static Hubbard model". It was used in [34] and [35] to study crystallization. Some rigorous results concerning the model were presented in these works for the first time. Mainly, they proved the existence of the phase transition in the model for any value of U and for sufficiently low temperature.

In the last years the Falicov–Kimball model is intensively studied in the frame of the dynamical mean field theory, where properties of the system could be calculated exactly in the limit of infinite dimension (see review [36]).

We would like to mention about the numerical studies of the Falicov–Kimball-like models, which are provided on finite clusters and are performed by Farkašovský and co-workers (see for e.g. [37], [38], [39]).

Due to the relative simplicity of the model, a variety of modifications have been applied to it. First of all it can be considered on different types of lattices. In [40], the model was considered on a triangular lattice. Due to increasing interest of such systems on lattices such as Kagomé or pyrochlore, studies of the Falicov–Kimball model on them are going to be instructive.

An interesting problem arises on changing the statistic of quantum particles. In [40] the electron subsystem, whose particles obey Fermi statistic where replaced by a system of hard-core bosons. Since two bosons cannot occupy the same site, because of hard-core interaction, the subsystem consists of interacting particles. A comparison of this two statistics might be useful for computer simulations, where fermions are often replaced by hard-core bosons, in order to make computations easier.

One of the alterations, which was studied recently, is the so-called *correlated hopping*, i.e. the hopping intensity t_{xy} depends on occupation numbers of ions on sites x and y. Influence of the correlated hopping on the phase diagram of the simple Falicov–Kimball model was investigated in [41] in the case of 1D model, and in [42] and [43] in 2D.

Another simple modification, which perhaps makes the model more realistic, is introduction of a spin degree of freedom. It was studied by Brandt et al. in [44] and [45]. Recently, using perturbation technique, the Falicov–Kimball model in case of infinite Coulomb repulsion between classical ions with different spin orientation at the same site was investigated in [46]. The model with an additional spin-depended Ising-type interaction (Ising–Falicov–Kimball model) was studied recently in [47].

Historical review and list of new trends, as well as extended comments, concerning the field of the Falicov–Kimball model are given in a short guide [48].

2.2 Symmetries and other basic properties

We are interested in ground-state properties of the Falicov–Kimball model. We describe its ground state from the point of ion subsystem, so the main question is the ground-state configuration of ions. Here the model on a square lattice is considered, though many properties of the model can be extended to a wider class of latices. The most convenient

ensemble for our purposes is the grand-canonical ensemble. Let,

$$H(\mu_e, \mu_i) = H_{FK} - \mu_e N_e - \mu_i N_i, \tag{3}$$

where μ_e, μ_i are chemical potentials of electrons and ions, respectively.

First, we notice, that for a fixed configuration $\{s_x\}_{x\in\Lambda}$ Hamiltonian (1), in the case when electrons obey Fermi statistic, describes a system of free Fermi particles in an external field $U \cdot s_x$. The Hamiltonian (1) is the second-quantized version of the single particle Hamiltonian

$$h = -T + US, \tag{4}$$

where h is $|\Lambda| \times |\Lambda|$-matrix with the elements $h_{xy} = t_{xy} + U s_x \delta_{xy}$. However, the configuration of ions $\{s_x\}_{x\in\Lambda}$ is not fixed in the system: the configuration of ions should minimize the whole Hamiltonian $H(\mu_e, \mu_i)$, and the main question of describing the ion subsystem is to find such a configuration for specific values of (μ_e, μ_i). This follows from the form of a partition function,

$$Z_\Lambda = \sum_S \text{Tr } \exp\left[-\beta H(\mu_e, \mu_i)\right], \tag{5}$$

where the sum runs over all the configurations and the trace is taken over the fermion Fock space (β is the inverse temperature). In other words, if $E_S(\mu_e, \mu_i)$ is the ground-state energy of $H(\mu_e, \mu_i)$ for a given configuration S of the ions, then we are looking for the ground-state energy of $H(\mu_e, \mu_i)$, which is given by,

$$E_G(\mu_e, \mu_i) = \min_S E_S(\mu_e, \mu_i). \tag{6}$$

The minimum is attained at the set G of the ground-state configurations of ions. The task is to determine the set G in the (μ_e, μ_i)-plane.

For this purpose, it is useful to examine the spectrum of the Hamiltonian (4) (in the case of fermions). When $\max |t_{xy}| = t$ and $|U| > zt$, where z is the coordination number of the underlaying lattice ($z = 4$, for square lattice), there is a gap in the spectrum $(-|U| + zt, |U| - zt)$ (the so-called *universal gap*). This gap is of great importance, because if we suppose the chemical potential of electrons μ_e to be in the universal gap,

$$\mu_e \in (-|U| + zt, |U| - zt), \qquad (|U| > zt), \tag{7}$$

then the ground-state energy expansion, we use below, is absolutely convergent, and uniformly in Λ. Quite interestingly, a similar condition holds in the case when quantum particles are hard-core bosons,

$$\mu_e \in (-|U| + 4zt, |U| - 4zt), \qquad (|U| > 4zt). \tag{8}$$

This condition was obtained by Messager and Miracle-Solé in [49], using a cluster expansion. Under conditions (7) and (8), for U positive (negative) and in the zero-temperature limit, the *half-filling condition*, $N_e + N_i = |\Lambda|$ (*neutrality condition*, $N_e = N_i$), is implied, either for fermions or hard-core bosons.

In studies of grand-canonical phase diagrams an important role is played by unitary transformations (*hole–particle transformations*) that exchange particles and holes: $c_x^+ c_x \to 1 - c_x^+ c_x$, for electrons, and $s_x \to -s_x$, for ions.

The peculiarity of the model is that the case of attraction ($U < 0$) and the case of repulsion ($U > 0$) are related by a unitary transformation (the hole–particle transformation for ions): if $S = \{s_x\}_{x\in\Lambda}$ is a ground-state configuration at (μ_e, μ_i) for $U > 0$, then $-S = \{-s_x\}_{x\in\Lambda}$ is the ground-state configuration at $(\mu_e, -\mu_i)$ for $U < 0$. This property holds for both statistics, and does not depend on the form of hopping term. Consequently, without any loss of generality one can fix the sign of the coupling constant U. In the following paragraphs we choose $U > 0$ and express all the other parameters of the Hamiltonian (3) in the units of U, i.e. formally we set $U = 1$, preserving previous notations.

In the case, when only nearest-neighbor (n.n.) hopping terms are present, i.e. $t_{xy} = 0$ for all $\langle x, y\rangle_i$, $i \geqslant 2$, this transformation for some (μ_e^0, μ_i^0) leave the Hamiltonian $H(\mu_e, \mu_i)$ invariant. An example of such transformation for the electrons is given by $c_x^+ \to \epsilon_x c_x$, where $\epsilon_x = 1$ for bosons; for fermions $\epsilon_x = 1$ at the even sublattice of Λ and $\epsilon_x = -1$ at the odd one. Since H_{FK} is invariant under the joint hole–particle transformation of mobile and localized particles (when only n.n. hopping is non-zero), $H(\mu_e, \mu_i)$ is hole–particle invariant at the point $(0, 0)$. At the hole–particle symmetry point, the system under consideration has very special properties, which simplify studies of its phase diagram [34]. Moreover, by means of the defined above hole–particle transformations one can determine a number of symmetries of the grand-canonical phase diagram [50]. With the sign of U fixed, applying joint hole–particle transformation for electrons and ions, one concludes that there is an *inversion symmetry* of the grand-canonical phase diagram. If S is a ground-state configuration at (μ_e, μ_i), then $-S$ is the ground-state configuration at $(-\mu_e, -\mu_i)$. Therefore, it is enough to determine the phase diagram in a half-plane specified by fixing the sign of one of the chemical potentials.

Let us note, that in the case when the next-nearest-neighbor (n.n.n.) hopping amplitude is nonzero, $t_{xy} \neq 0$ for $\langle x, y\rangle_2$, Hamiltonian (3) is not invariant with respect to the joint hole–particle transformation for any values of μ_e and μ_i.

Let us consider symmetry properties of the model with the following restrictions: n.n. hopping is supposed to be independent of direction, i.e. $t_{xy} = t$, for $\langle x, y\rangle_1$, and n.n.n. hopping amplitude differs $t_{xy} = \{t_+, t_-\}$ in two different directions. Moreover, we consider the system of fermions only. Then applying the hole–particle transformation for electrons, i.e. $c_x \to \varepsilon_x c_x^+$, and the hole–particle transformation for ions, one finds that if S is the ground-state configuration at $(t, t_+, t_-, \mu_e, \mu_i)$, then $-S$ is the ground-state configuration at $(t, -t_+, -t_-, -\mu_e, -\mu_i)$. Thus, it is enough to consider only one sign of n.n.n. hopping. We shall consider the case of positive n.n.n. hopping intensities: $t_+, t_- > 0$. Using another hole–particle transformation for electrons, $c_x \to c_x^+$, and the hole-particle transformation for ions, we obtain that if S is the ground-state configuration at $(t, t_+, t_-, \mu_e, \mu_i)$, then $-S$ is the ground-state configuration at $(-t, -t_+, -t_-, -\mu_e, -\mu_i)$. Applying consecutively the two joint (with respect to electrons and ions) hole–particle transformations, we obtain that if S is the ground-state configuration at $(t, t_+, t_-, \mu_e, \mu_i)$, it is also the ground-state configuration at $(-t, t_+, t_-, \mu_e, \mu_i)$. So the relative sign of n.n. and n.n.n. hopping amplitudes does not play any role in the model.

Above, we have briefly discussed those properties of our model, which shall be useful

in the sequel. For more extended picture of the Falicov–Kimball model, its modifications, results and applications, readers are referred to a series of reviews [48], [51], [52] and [53].

2.3 Strong-coupling expansion of the ground-state energy at half-filling — the method

There are different ways of obtaining ground-state energy expansion. In the case of fermions, when $zt < 1$ and $|\mu_e| < 1 - zt$, the ground-state energy of the model can be written in the form [50, 51]:

$$E_S\left(\mu_e, \mu_i\right) = -\frac{1}{2}\mathrm{Tr}|h| - (\mu_i - \mu_e)N_i - \mu_e|\Lambda|, \tag{9}$$

where the one-particle Hamiltonian $h = -T + US$ is given by (4), and $|h| = \sqrt{h^2}$. The trace of $|h|$, can be rewritten in the form

$$\mathrm{Tr}|h| = \mathrm{Tr}\sqrt{I + \Delta}, \tag{10}$$

where, I is the unity operator, $\Delta = T^2 - (TS + ST)$ stands for small perturbation, $S^2 = I$. Expanding the square root into a power series of Δ, one obtains the ground-state energy expansion. Such a "square root expansion" was applied in [50].

An alternative way for fermions, the "resolvent expansion", was used in [40]. Ground-state energy (9) can be rewritten in the form

$$E_S\left(\mu_e, \mu_i\right) = -\frac{1}{2}\sum_{x\in\Lambda} s_x + \int_{\mathcal{C}} \frac{dz}{2\pi i}\mathrm{Tr}\left[\frac{z}{z-h}\right] - (\mu_i - \mu_e)N_i - \mu_e|\Lambda|, \tag{11}$$

where $\mathcal{C}$ is a contour in the complex plain enclosing all the negative eigenvalues of h. In order to calculate the above integral trace of resolvent is expanded into a power series of t_{xy}.

Unfortunately, the above methods are not applicable in the case when quantum hopping particles are hard-core bosons. To obtain the ground-state energy expansion in this case, a closed-loop expansion is used, which was first applied in [49] for fermions, and then used for hard-core bosons in [40].

We use another, more powerful method, the method of unitary-equivalent interactions, which is suitable not only for both systems, fermions and hard-core bosons, but can also be applied to a wide class of Hamiltonians. It was proposed in a series of papers [54], [55], [56] and summarized in [57]. The main advantage of this method is that the unitary transformations are applied locally, and that is why the method is well-defined: the expansion is convergent, uniformly in $|\Lambda|$.

The idea of the method is the following. Considering the Hamiltonians which are sums of local terms, $H = \sum_X H_X$ (X is a finite set of sites in Λ), they are supposed to consist of two parts: classical, which is diagonal in some basis, and small quantum perturbation, which is off-diagonal. With λ being the small parameter considered in the model, we are looking for some unitary operator $U_\Lambda^{(n)}(\lambda)$, which makes the original Hamiltonian $H_\Lambda(\lambda)$ block-diagonal to order λ^n in some basis, i.e.

$$H_\Lambda^{(n)}(\lambda) = U_\Lambda^{(n)}(\lambda)H_\Lambda(\lambda)\, U_\Lambda^{(n)\,*}(\lambda) = H_{0\Lambda}^{(n)}(\lambda) + V_\Lambda^{(n)}(\lambda),$$

where the leading block-diagonal part $H_{0\Lambda}^{(n)}(\lambda)$ contains terms up to the n-th order in λ, and off-diagonal part $V_{\Lambda}^{(n)}(\lambda)$ consists of $(n+1)$-th and higher order terms. Following this procedure, the convergence of the expansion can be rigorously proven. Moreover, by applying quantum Pirogov–Sinai theory, it was established that some parts of the grand-canonical zero-temperature phase diagram of the leading part is modified "slightly" when the whole expansion is taken into account at zero or low-temperature regimes [57].

Here we present a scheme of obtaining the ground-state energy expansion for the Falicov–Kimball model up to the fourth order. We consider the case where nearest-neighbor and next-nearest-neighbor hopping intensities are anisotropic.

2.3.1 Local projections

First we consider the system, where quantum hopping particles obey Fermi statistic. Following [57], we rewrite FK Hamiltonian (3) in the form convenient for perturbation (up to some constant), i.e. "classical part" plus "small quantum perturbation":

$$H_{FK} = H_0 + V_1, \tag{12}$$

where the classical part,

$$H_0 = \sum_{x\in\Lambda} \Phi_{0x}, \tag{13}$$

with the classical on-site potential,

$$\Phi_{0x} = 2n_x^e n_x^i - \mu_e n_x^e - \mu_i n_x^i; \tag{14}$$

and the quantum perturbation,

$$\begin{aligned} V_1 &= \sum_{\langle x,y\rangle_{1,h}\subset\Lambda} Q_{\langle x,y\rangle_{1,h}} + \sum_{\langle x,y\rangle_{1,v}\subset\Lambda} Q_{\langle x,y\rangle_{1,v}} + \sum_{\langle x,y\rangle_{2,+}\subset\Lambda} Q_{\langle x,y\rangle_{2,+}} + \sum_{\langle x,y\rangle_{2,-}\subset\Lambda} Q_{\langle x,y\rangle_{2,-}} \\ &= \sum_i \sum_{\langle x,y\rangle_i\subset\Lambda} Q_{\langle x,y\rangle_i}. \end{aligned} \tag{15}$$

Operators $Q_{\langle x,y\rangle_i}$ are defined in the following way:

$$\begin{aligned} Q_{\langle x,y\rangle_{1,h}} &= t_h \left(c_x^+ c_y + c_y^+ c_x\right), \\ Q_{\langle x,y\rangle_{1,v}} &= t_v \left(c_x^+ c_y + c_y^+ c_x\right), \\ Q_{\langle x,y\rangle_{2,+}} &= t_+ \left(c_x^+ c_y + c_y^+ c_x\right), \\ Q_{\langle x,y\rangle_{2,-}} &= t_- \left(c_x^+ c_y + c_y^+ c_x\right), \end{aligned} \tag{16}$$

and the role of the small parameter λ is played by $t = \max\{t_h, t_v, t_+, t_-\}$, (the so-called *strong-coupling regime*). The method is applied in the situation where for certain value of energy of the classical part there are infinitely many states. Then, it is possible that the quantum perturbation reduces this degeneracy by splitting the energy levels. Let us look at the classical part, or the "zeroth order". The phase diagram of the classical interaction (Fig. 1) is partitioned into four parts. On each boundary line between any two phases the degeneracy is infinite. We are interested in the case of half-filling which corresponds

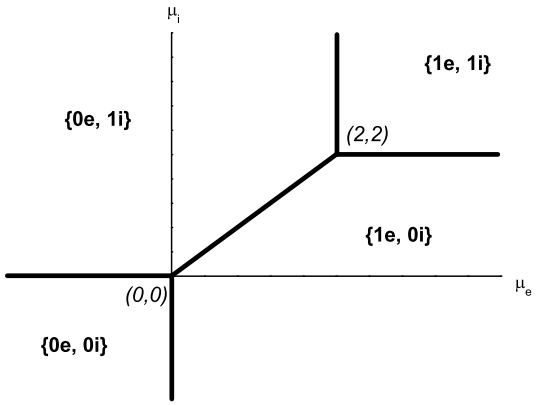

Figure 1: Ground-state phase diagram for $H_0 = \sum_{x\in\Lambda} (2n_x^e n_x^i - \mu_e n_x^e - \mu_i n_x^i)$. Numbers of electrons and ions at each site of lattice Λ, which determine the state of the system, are given in curly brackets.

to the boundary line $\mu_e = \mu_i$, $(0 < \mu_e < 2)$, the configurations on this line with the lowest energy are characterized by the condition: each site of lattice Λ is occupied by one particle only, either ion or electron.

On the line $\mu_e = \mu_i$ we introduce the projection onto the ground state at site x:

$$P_x^0 = n_x^e \left(1 - n_x^i\right) + n_x^i \left(1 - n_x^e\right) = \left(n_x^e - n_x^i\right)^2 . \tag{17}$$

The projection onto excited states $P_x^1 = 1 - P_x^0$. It is easy to extend these projections to the ground-state projection on $Y \subset \Lambda$:

$$P_Y^0 = \prod_{x\in Y} P_x^0. \tag{18}$$

In this case unity is given by $\mathbb{1}_Y = P_Y^0 + P_Y^1$, and hence the definition of the projection onto exited states at the set Y:

$$P_Y^1 = \mathbb{1}_Y - P_Y^0 \qquad\qquad \text{(note, that } P_Y^1 \neq \prod_{x\in Y} P_x^1\text{)}. \tag{19}$$

For calculation we need the following simple relations:

$$\begin{aligned} c_x^+ P_x^0 &= P_x^1 c_x^+, \\ c_x^+ P_x^1 &= P_x^0 c_x^+, \end{aligned} \tag{20}$$

If $y \neq x$, then c_x^+ or c_x commute with any projection at site y. These relations give immediately very useful properties for any operator $Q_{\langle x,y\rangle_i}$, with pair $x \neq y$ on lattice Λ:

$$\begin{aligned} P_{\langle x,y\rangle_i}^0 Q_{\langle x,y\rangle_i} &= Q_{\langle x,y\rangle_i} P_x^1 P_y^1, \\ P_{\langle x,y\rangle_i}^1 Q_{\langle x,y\rangle_i} &= Q_{\langle x,y\rangle_i} \left(1 - P_x^1 P_y^1\right). \end{aligned} \tag{21}$$

Another pairs of relations which correspond to (20) and (21) are obtained by Hermitian conjugation.

Using these properties and the partition of unity, for $Y = \langle x, y\rangle_i$, we can rewrite $Q_{\langle x,y\rangle_i}$:

$$Q_{\langle x,y\rangle_i} = Q^{00}_{\langle x,y\rangle_i} + Q^{01}_{\langle x,y\rangle_i} + Q^{11}_{\langle x,y\rangle_i}, \tag{22}$$

for $i = \{1h, 1v, 2+, 2-\}$; where

$$\begin{aligned} Q^{00}_{\langle x,y\rangle_i} &= P^0_{\langle x,y\rangle_i} Q_{\langle x,y\rangle_i} P^0_{\langle x,y\rangle_i} = 0 \\ Q^{01}_{\langle x,y\rangle_i} &= P^0_{\langle x,y\rangle_i} Q_{\langle x,y\rangle_i} P^1_{\langle x,y\rangle_i} + P^1_{\langle x,y\rangle_i} Q_{\langle x,y\rangle_i} P^0_{\langle x,y\rangle_i} \\ &= P^0_x P^0_y Q_{\langle x,y\rangle_i} P^1_x P^1_y + P^1_x P^1_y Q_{\langle x,y\rangle_i} P^0_x P^0_y, \\ Q^{11}_{\langle x,y\rangle_i} &= P^1_{\langle x,y\rangle_i} Q_{\langle x,y\rangle_i} P^1_{\langle x,y\rangle_i}. \end{aligned} \tag{23}$$

So the whole Hamiltonian (12) is rewritten in the form:

$$H_{FK} = H_0 + V^{01} + V^{11}, \tag{24}$$

where,

$$\begin{aligned} V^{01} &= \sum_{\langle x,y\rangle_{1,h}} Q^{01}_{\langle x,y\rangle_{1,h}} + \sum_{\langle x,y\rangle_{1,v}} Q^{01}_{\langle x,y\rangle_{1,v}} + \sum_{\langle x,y\rangle_{2,+}} Q^{01}_{\langle x,y\rangle_{2,+}} + \sum_{\langle x,y\rangle_{2,-}} Q^{01}_{\langle x,y\rangle_{2,-}} = \\ &= \sum_i \sum_{\langle x,y\rangle_i} Q^{01}_{\langle x,y\rangle_i}, \\ V^{11} &= \sum_{\langle x,y\rangle_{1,h}} Q^{11}_{\langle x,y\rangle_{1,h}} + \sum_{\langle x,y\rangle_{1,v}} Q^{11}_{\langle x,y\rangle_{1,v}} + \sum_{\langle x,y\rangle_{2,+}} Q^{11}_{\langle x,y\rangle_{2,+}} + \sum_{\langle x,y\rangle_{2,-}} Q^{11}_{\langle x,y\rangle_{2,-}} = \\ &= \sum_i \sum_{\langle x,y\rangle_i} Q^{11}_{\langle x,y\rangle_i}. \end{aligned} \tag{25}$$

2.3.2 First-order unitary transformation for fermions

We are looking for a unitary transformation, that eliminates the first-order off-diagonal term V^{01}. The transformation can be written in the form:

$$U^{(1)} = \exp\left(S^{(1)}\right), \tag{26}$$

where the operator $S^{(1)} = S^{(1)}(t_h, t_v, t_+, t_-)$ is of order one, i.e. it depends on $t_h^a t_v^b t_+^c t_-^d$ with $a + b + c + d = 1$. Applying the first unitary transformation (26) and using the Lie–Schwinger series, the transformed Hamiltonian can be written as

$$\begin{aligned} H^{(1)} &= e^{S^{(1)}} H_{FK} e^{-S^{(1)}} = \\ &= H_{FK} + \left[S^{(1)}, H_{FK}\right] + \frac{1}{2!}\left[S^{(1)}, \left[S^{(1)}, H_{FK}\right]\right] + \ldots = \\ &= \sum_{n=0}^{\infty} \frac{1}{n!} \mathrm{ad}^n S^{(1)}(H_{FK}), \end{aligned} \tag{27}$$

where, the operation $\mathrm{ad}A(B)$ is defined as follows

$$\begin{aligned}\mathrm{ad}^0 A(B) &= B,\\ \mathrm{ad}^1 A(B) &= [A,B],\\ \mathrm{ad}^n A(B) &= \left[A, \mathrm{ad}^{n-1}A(B)\right].\end{aligned}$$

Rewriting (27),

$$\begin{aligned}H^{(1)} &= H_0 + V^{01} + V^{11} + \mathrm{ad}^1 S^{(1)}\left(H_0\right) + \mathrm{ad}^1 S^{(1)}\left(V^{01}+V^{11}\right) + \\ &+ \sum_{n=2}^{\infty} \frac{1}{n!}\,\mathrm{ad}^n S^{(1)}\left(H_0 + V^{01} + V^{11}\right),\end{aligned} \tag{28}$$

and choosing the operator $S^{(1)}$ in the way to eliminate V^{01},

$$\mathrm{ad}^1 H_0\left(S^{(1)}\right) = V^{01},$$

we obtain:

$$H^{(1)} = H_0 + V^{11} + V_2 + \sum_{n=2}^{\infty} \frac{1}{n!}\,\mathrm{ad}^n S^{(1)}\left(\frac{n}{n+1}V^{01} + V^{11}\right).$$

In the above formula,

$$V_2 = \mathrm{ad}S^{(1)}\left(\frac{1}{2}V^{01} + V^{11}\right).$$

Now our problem is to find the operator $S^{(1)}$. If we suppose it to be a sum of local operators,

$$S^{(1)} = \sum_i \sum_{\langle x,y\rangle_i} S^{(1)}_{\langle x,y\rangle_i}, \tag{29}$$

in order to satisfy the condition $[H_0, S^{(1)}] = V^{01}$, $S^{(1)}_{\langle x,y\rangle_i}$ can be chosen in the form:

$$S^{(1)}_{\langle x,y\rangle_i} = \sum_i \mathrm{ad}^{-1}\overline{H}_{0,\langle x,y\rangle_i}\left(Q^{01}_{\langle x,y\rangle_i}\right), \tag{30}$$

where $\overline{H}_{0,\langle x,y\rangle_i} = \Phi_{0x} + \Phi_{0y}$. Introducing the spectral decomposition of $\overline{H}_{0,\langle x,y\rangle_i}$,

$$\overline{H}_{0,\langle x,y\rangle_i} = \sum_j E^{(j)}_{\langle x,y\rangle_i} P^{(j)}_{\langle x,y\rangle_i},$$

$S^{(1)}$ can be rewritten as

$$S^{(1)}_{\langle x,y\rangle_i} = \sum_i \sum_{\substack{j,k\\(j\neq k)}} \frac{P^{(j)}_{\langle x,y\rangle_i} Q^{01}_{\langle x,y\rangle_i} P^{(k)}_{\langle x,y\rangle_i}}{E^{(j)}_{\langle x,y\rangle_i} - E^{(k)}_{\langle x,y\rangle_i}}. \tag{31}$$

In the spectral decomposition of Φ_{0x} there are three eigensubspaces with eigenvalues $E_x^{(l)}$ and with the corresponding projections $P_x^{(l)}$, $l = 0, 1, 2$:

$$\begin{aligned} E_x^{(0)} &= -\bar{\mu}, & P_x^{(0)} &= n_x^e + n_x^i - 2n_x^e n_x^i, \\ E_x^{(1)} &= 0, & P_x^{(1)} &= 1 - n_x^e - n_x^i + n_x^e n_x^i, \\ E_x^{(2)} &= 2(1-\bar{\mu}), & P_x^{(2)} &= n_x^e n_x^i, \end{aligned}$$

where $\bar{\mu} = \mu_i = \mu_e$. Note, that $P_x^{(0)} = P_x^0$, and $P_x^{(1)} + P_x^{(2)} = P_x^1$. Then, the spectral decomposition of $\overline{H}_{0,\langle x,y\rangle_i}$ consists of six eigenvalues $E^{(l)}_{\langle x,y\rangle_i}$ and eigenprojections $P^{(l)}_{\langle x,y\rangle_i}$, $l = 0, \ldots, 5$:

$$\begin{aligned} E^{(0)}_{\langle x,y\rangle_i} &= -2\bar{\mu}, & P^{(0)}_{\langle x,y\rangle_i} &= P_x^{(0)} P_y^{(0)}, \\ E^{(1)}_{\langle x,y\rangle_i} &= -\bar{\mu}, & P^{(1)}_{\langle x,y\rangle_i} &= P_x^{(0)} P_y^{(1)} + P_x^{(1)} P_y^{(0)}, \\ E^{(2)}_{\langle x,y\rangle_i} &= 2 - 3\bar{\mu}, & P^{(2)}_{\langle x,y\rangle_i} &= P_x^{(0)} P_y^{(2)} + P_x^{(2)} P_y^{(0)}, \\ E^{(3)}_{\langle x,y\rangle_i} &= 0, & P^{(3)}_{\langle x,y\rangle_i} &= P_x^{(1)} P_y^{(1)}, \\ E^{(4)}_{\langle x,y\rangle_i} &= 2(1-\bar{\mu}), & P^{(4)}_{\langle x,y\rangle_i} &= P_x^{(1)} P_y^{(2)} + P_x^{(2)} P_y^{(1)}, \\ E^{(5)}_{\langle x,y\rangle_i} &= 4(1-\bar{\mu}), & P^{(5)}_{\langle x,y\rangle_i} &= P_x^{(2)} P_y^{(2)}. \end{aligned}$$

Considering the products $P^{(j)}_{\langle x,y\rangle_i} Q^{01}_{\langle x,y\rangle_i} P^{(k)}_{\langle x,y\rangle_i}$, one finds that only two of them are nonzero: $P^{(0)}_{\langle x,y\rangle_i} Q^{01}_{\langle x,y\rangle_i} P^{(4)}_{\langle x,y\rangle_i}$ and $P^{(4)}_{\langle x,y\rangle_i} Q^{01}_{\langle x,y\rangle_i} P^{(0)}_{\langle x,y\rangle_i}$, for any i. Using the projections defined above, we can write the expression for operator $S^{(1)}$:

$$S^{(1)} = -\frac{1}{2} \sum_i \sum_{\langle x,y\rangle_i} \left(P_x^0 P_y^0 Q^{01}_{\langle x,y\rangle_i} P_x^1 P_y^1 - P_x^1 P_y^1 Q^{01}_{\langle x,y\rangle_i} P_x^0 P_y^0 \right). \tag{32}$$

To proceed, we have to consider commutators $\mathrm{ad}^1 A(B) = AB - BA$, where $A = \sum_i \sum_{\langle x,y\rangle_i} A_{\langle x,y\rangle_i}$ and $B = \sum_j \sum_{\langle m,n\rangle_j} B_{\langle m,n\rangle_j}$. First, let us note that the commutator for $\left[A_{\langle x,y\rangle_i}, B_{\langle m,n\rangle_j}\right]$ vanishes unless $\langle x,y\rangle_i \cap \langle m,n\rangle_j \neq \emptyset$. In this case, the product,

$$AB = \sum_{\substack{i,j \\ (i \leqslant j)}} \left(\delta_{ij} \sum_{x:\langle x,y\rangle_i} A_{\langle x,y\rangle_i} B_{\langle x,y\rangle_i} + \sum_{x:\langle x,y\rangle_i} \sum_{z:\langle y,z\rangle_j} \left(A_{\langle x,y\rangle_i} B_{\langle y,z\rangle_j} + A_{\langle y,z\rangle_j} B_{\langle x,y\rangle_i} \right) \right). \tag{33}$$

The first term in the brackets runs over all the possible pairs of sites, i.e. $i = \{1h, 1v, 2+, 2-\}$. In the second term we introduce the extended indices of summation, $x : \langle x,y\rangle_i$ and $z : \langle y,z\rangle_j$, in order to stress that first sum runs over all $x \in \Lambda$ and pair (x,y) is the n.n. pair of the i-type, and the second sum runs over z (shown on Figs. 2,3,4), such that pair (y,z) is the n.n. pair of j-th type. Whenever we skip the index of direction (like 'h' or '$-$') this means that the summation is over all the possible directions. So, the notation $\sum_{\langle x,y\rangle_2}$ stands for sum over all n.n.n. pairs, each counted once.

The second-order term is V_2, which after somewhat lengthy calculations can be written in the form:

$$V_2^{00} = -\frac{1}{2} \sum_i \sum_{x:\langle x,y\rangle_i} P_x^0 P_y^0 Q^2_{\langle x,y\rangle_i} P_x^0 P_y^0,$$

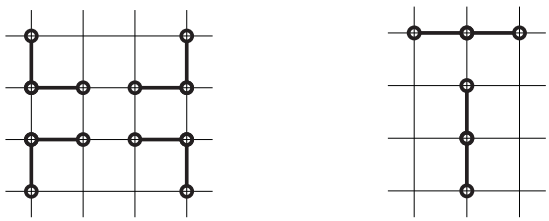

Figure 2: The set of paths over which the sum $\sum_{x:\langle x,y\rangle_1}\sum_{z:\langle y,z\rangle_1}$ runs in (33). Sums run over the set of paths shown here, and their translations. Sites x and z are at the ends of each path (x can be chosen arbitrary), and site y is always between them.

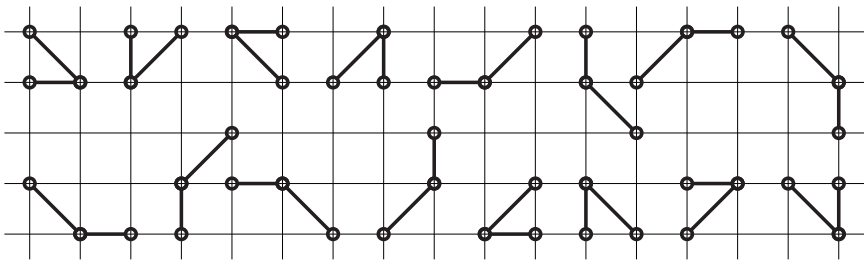

Figure 3: The set of paths over which the sum $\sum_{x:\langle x,y\rangle_1}\sum_{z:\langle y,z\rangle_2}$ runs in (33). Sums run over the set of paths shown here, and their translations. Sites x and z are at the ends of each path (x can be chosen arbitrary), and site y is always between them.

$$
\begin{aligned}
V_2^{01} = &-\frac{1}{2}\sum_{i\leqslant j}\sum_{x:\langle x,y\rangle_i}\sum_{z:\langle y,z\rangle_j}\Big(P_x^0P_y^0P_z^0\left[Q_{\langle x,y\rangle_i}Q_{\langle y,z\rangle_j}+Q_{\langle y,z\rangle_j}Q_{\langle x,y\rangle_i}\right]P_x^1P_y^0P_z^1\\
&+P_x^1P_y^0P_z^1\left[Q_{\langle x,y\rangle_i}Q_{\langle y,z\rangle_j}+Q_{\langle y,z\rangle_j}Q_{\langle x,y\rangle_i}\right]P_x^0P_y^0P_z^0\Big),\\
V_2^{11} = &\sum_{i\leqslant j}\Bigg(\frac{\delta_{ij}}{2}\sum_{x:\langle x,y\rangle_i}P_x^1P_y^1Q_{\langle x,y\rangle_i}^2P_x^1P_y^1-\\
&-\frac{1}{2}\sum_{x:\langle x,y\rangle_i}\sum_{z:\langle y,z\rangle_j}\Big[P_x^0P_y^0P_z^1Q_{\langle x,y\rangle_i}Q_{\langle y,z\rangle_j}P_x^1P_y^0P_z^0-P_x^1P_y^1P_z^0Q_{\langle x,y\rangle_i}Q_{\langle y,z\rangle_j}P_x^0P_y^1P_z^1-\\
&-P_x^0P_y^1P_z^1Q_{\langle y,z\rangle_j}Q_{\langle x,y\rangle_i}P_x^1P_y^1P_z^0+P_x^1P_y^0P_z^0Q_{\langle y,z\rangle_j}Q_{\langle x,y\rangle_i}P_x^0P_y^0P_z^1+\\
&-P_x^1P_y^1P_z^1\left[Q_{\langle x,y\rangle_i}Q_{\langle y,z\rangle_j}+Q_{\langle y,z\rangle_j}Q_{\langle x,y\rangle_i}\right]P_x^0P_y^1P_z^0-\\
&-P_x^0P_y^1P_z^0\left[Q_{\langle x,y\rangle_i}Q_{\langle y,z\rangle_j}+Q_{\langle y,z\rangle_j}Q_{\langle x,y\rangle_i}\right]P_x^1P_y^1P_z^1\Big]\Bigg).
\end{aligned}
$$

We have got all the elements which are necessary for obtaining the effective Hamiltonian up to the third order (the second-order ground-state energy expansion):

$$E_S^{(2)} = P_\Lambda^0 H^{(1)} P_\Lambda^0 = P_\Lambda^0\left(H_0+V_2^{00}\right)P_\Lambda^0.$$

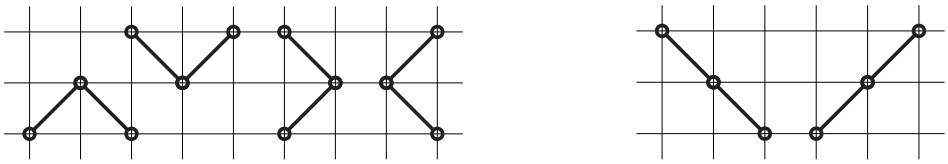

Figure 4: The set of paths over which the sum $\sum_{x:\langle x,y\rangle_2}\sum_{z:\langle y,z\rangle_2}$ runs in (33). Sums run over the set of paths shown here, and their translations. Sites x and z are at the ends of each path (x can be chosen arbitrary), and site y is always between them.

Hence,

$$E_S^{(2)} = \sum_x \Phi_{0x} - \frac{1}{2}\sum_i \sum_{x:\langle x,y\rangle_i} P_x^0 P_y^0 Q^2_{\langle x,y\rangle_i} P_x^0 P_y^0.$$

In the ground state $n_x^e + n_x^i = 1$, so

$$Q^2_{\langle x,y\rangle_i} = t_i^2\left[n_x^e\left(1-n_y^e\right) + n_y^e\left(1-n_x^e\right)\right] = -\frac{t_i^2}{2}\left(s_x s_y - 1\right),$$

$$V_2^{00} = \sum_i \frac{t_i^2}{4}\sum_{\langle x,y\rangle_i}\left(s_x s_y - 1\right) \tag{34}$$

and finally the second-order ground-state energy expansion is of the form:

$$E_S^{(2)} = -\frac{1}{2}\sum_x\left(\mu s_x + \nu\right) + \sum_i \frac{t_i^2}{4}\sum_{\langle x,y\rangle_i}\left(s_x s_y - 1\right), \tag{35}$$

where $\mu = \mu_i - \mu_e$ and $\nu = \mu_i + \mu_e$.

2.3.3 Second-order unitary transformation for fermions

Applying the second unitary transformation, we obtain:

$$\begin{aligned}
H^{(2)} &= e^{S^{(2)}} H^{(1)} e^{-S^{(2)}} \\
&= H^{(1)} + \mathrm{ad}^1 S^{(2)}\left(H^{(1)}\right) + \frac{1}{2!}\mathrm{ad}^2 S^{(2)}\left(H^{(1)}\right) + \ldots \\
&= H_0 + V^{11} + V_2^{00} + V_2^{01} + V_2^{11} + \mathrm{ad}^1 S^{(2)}\left(H_0\right) + \frac{1}{2!}\mathrm{ad}^2 S^{(1)}\left(\frac{2}{3}V^{01}V^{11}\right) + \\
&\quad + \mathrm{ad}^1 S^{(2)}\left(V^{11}\right) + \frac{1}{3!}\mathrm{ad}^3 S^{(1)}\left(\frac{3}{4}V^{01} + V^{11}\right) + \mathrm{ad}^1 S^{(2)}\left(V_2^{00} + V_2^{01} + V_2^{11}\right) + \\
&\quad + \frac{1}{2!}\mathrm{ad}^2 S^{(2)}\left(H_0\right) + \tilde{V}^{(5)},
\end{aligned} \tag{36}$$

where $\tilde{V}^{(5)}$ is the remainder of the fifth order:

$$\begin{aligned}\tilde{V}^{(5)} &= \sum_{n\geqslant 4}\frac{1}{n!}\,\mathrm{ad}^n S^{(1)}\left(\frac{n}{n+1}V^{01}+V^{11}\right)+\\ &+ \mathrm{ad}^1 S^{(2)}\left(\sum_{n\geqslant 2}\frac{1}{n!}\,\mathrm{ad}^n S^{(1)}\left(\frac{n}{n+1}V^{01}+V^{11}\right)\right)+\\ &+ \frac{1}{2!}\,\mathrm{ad}^2 S^{(2)}\left(V^{11}+V_2^{00}+V_2^{01}+V_2^{11}+\sum_{n\geqslant 2}\frac{1}{n!}\,\mathrm{ad}^n S^{(1)}\left(\frac{n}{n+1}V^{01}+V^{11}\right)\right)+\\ &+ \sum_{m\geqslant 3}\frac{1}{m!}\,\mathrm{ad}^m S^{(2)}\left(H_0+V^{11}+V_2^{00}+V_2^{01}+V_2^{11}+\sum_{n\geqslant 2}\frac{1}{n!}\,\mathrm{ad}^n S^{(1)}\left(\frac{n}{n+1}V^{01}+V^{11}\right)\right).\end{aligned}$$

In order to eliminate the second-order off-diagonal term V_2^{01}, we put:

$$\mathrm{ad}^1 H_0\left(S^{(2)}\right)=V_2^{01},$$

then

$$H^{(2)}=H_0+V^{11}+V_2^{00}+V_2^{11}+V_3+V_4+\tilde{V}^{(5)},$$

and

$$V_3 = \mathrm{ad}^2 S^{(1)}\left(\frac{2}{3!}V^{01}+\frac{1}{2!}V^{11}\right)+\mathrm{ad}^1 S^{(2)}\left(V^{11}\right), \tag{37}$$

$$V_4 = \mathrm{ad}^3 S^{(1)}\left(\frac{3}{4!}V^{01}+\frac{1}{3!}V^{11}\right)+\mathrm{ad}^1 S^{(2)}\left(V_2^{00}+\frac{1}{2}V_2^{01}+V_2^{11}\right). \tag{38}$$

The operator $S^{(2)}$ can be chosen in the form:

$$S^{(2)}=\sum_{i\leqslant j}\sum_{x:\langle x,y\rangle_i}\sum_{z:\langle y,z\rangle_j}S^{(2)}_{\langle x,y\rangle_i\cup\langle y,z\rangle_j},$$

where, analogously as for $S^{(1)}$,

$$S^{(2)}_{\langle x,y\rangle_i\cup\langle y,z\rangle_j}=\sum_{\alpha,\beta}P^{(\alpha)}_{\langle x,y\rangle_i\cup\langle y,z\rangle_j}\frac{V^{01}_{2,\langle x,y\rangle_i\cup\langle y,z\rangle_j}}{E^{(\alpha)}_{\langle x,y\rangle_i\cup\langle y,z\rangle_j}-E^{(\beta)}_{\langle x,y\rangle_i\cup\langle y,z\rangle_j}}P^{(\beta)}_{\langle x,y\rangle_i\cup\langle y,z\rangle_j}.$$

The spectral decomposition used in the above formula, is given by

$$\Phi_{0x}+\Phi_{0y}+\Phi_{0z}=\sum_{\alpha}E^{(\alpha)}_{\langle x,y\rangle_i\cup\langle y,z\rangle_j}P^{(\alpha)}_{\langle x,y\rangle_i\cup\langle y,z\rangle_j}.$$

Operator $S^{(2)}$ is constructed in the similar way as $S^{(1)}$ was. It reads:

$$\begin{aligned}S^{(2)} = \frac{1}{4}\sum_{i\leqslant j}\sum_{x:\langle x,y\rangle_i}\sum_{z:\langle y,z\rangle_j}\Big(&P^0_{\langle x,y\rangle_i\cup\langle y,z\rangle_j}\left[Q_{\langle x,y\rangle_i}Q_{\langle y,z\rangle_j}+Q_{\langle y,z\rangle_j}Q_{\langle x,y\rangle_i}\right]P^1_{\langle x,y\rangle_i\cup\langle y,z\rangle_j}-\\ &-P^1_{\langle x,y\rangle_i\cup\langle y,z\rangle_j}\left[Q_{\langle x,y\rangle_i}Q_{\langle y,z\rangle_j}+Q_{\langle y,z\rangle_j}Q_{\langle x,y\rangle_i}\right]P^0_{\langle x,y\rangle_i\cup\langle y,z\rangle_j}\Big).\end{aligned} \tag{39}$$

The next step, consists in calculating double commutators, $[A,[B,C]]$ that appear in in (37) and (38). Each commutant X, of these commutators, has the form $X = \sum_{x:\langle x,y\rangle_i} X_{\langle x,y\rangle_i}$. Applying the same argument as before (commutators vanish unless commutants are defined on subsets intersection of which is not empty), we restrict ourselves to the products where the sets of sites, on which each multiplier is defined, forms a connected path, i.e. each site on a path has nearest neighbor, or next-nearest neighbor, or both. Another thing, worth mentioning, is that, even considering the fourth order only, we do not need to calculate all the expressions in (37) and (38). The result, we are interested in, is projected onto ground state, hence, some of the terms vanish. The following property of operators $Q_{\langle x,y\rangle_i}$ is useful. Because of relations (20) it is clear, that if we consider the path, $path = \{i_1, i_2, \ldots, i_q\}$, the expression

$$P^0_{path} Q_{\langle i_1,i_2\rangle_a} Q_{\langle i_3,i_4\rangle_b} \cdots Q_{\langle i_{q-1},i_q\rangle_z} P^0_{path} \neq 0, \tag{40}$$

only if each of indices i_j in the subscript of Q repeated even number of times. With this condition satisfied, let us note that any operator $A^{01} = P^0AP^1 + P^1AP^0$ or $A^{11} = P^1AP^1$ is equal to zero after projecting onto ground states. We will use these properties during calculations third- and fourth order terms.

Third order. The calculation of the third order terms is the calculation of V_3. First note, that in our case there is only one type of path that consists of three pairs of n.n. or n.n.n sites and product of three operators Q on it satisfies the condition (40) (see Fig. 5). In addition, after ground-state projection only V_3^{00} is nonzero. Using the multiplication

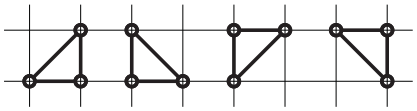

Figure 5: The set of paths of P_1-type which appear in the third-order calculations.

rule in a way described above, we obtain:

$$\begin{aligned} V_3^{00} &= \frac{1}{4}\sum_{P_1} P^0_x P^0_y P^0_z \left(Q_{1xy}Q_{1yz}Q_{2xz} + Q_{1yz}Q_{1xy}Q_{2xz} + Q_{1xy}Q_{2xz}Q_{1yz} + \right. \\ &\left. + Q_{1yz}Q_{2xz}Q_{1xy} + Q_{2xz}Q_{1xy}Q_{1yz} + Q_{2xz}Q_{1yz}Q_{1xy}\right) P^0_x P^0_y P^0_z, \end{aligned}$$

or in terms of spin variables:

$$V_3^{00} = \frac{3}{4}\left[-t_h t_v \left(t_+ + t_-\right)\sum_x s_x + \frac{t_h t_v t_+}{2}\sum_{P_{1,+}} s_{P_{1,+}} + \frac{t_h t_v t_-}{2}\sum_{P_{1,-}} s_{P_{1,-}}\right], \tag{41}$$

where the set of paths P_1 splits into two parts, $P_{1,+}$ and $P_{1,-}$, where n.n.n. part of the path has the slope $+1$ and -1, respectively. The $s_{P_{1,i}}$ stands for the product of spins which belong to $P_{1,i}$. This is the third-order correction to the effective Hamiltonian.

Fourth order. To consider fourth-order products, we start with describing connected paths that satisfy condition (40) for a product of four operators Q. There are three types of such paths: X-type path, i.e the path consisting of the pair (n.n. or n.n.n.) of two sites X; XY-type path, i.e. the path consisting of three sites that formed by two pairs X and Y; $XYZW$-type path, i.e. the path consisting of four sites which are in the form of closed loop and are formed by four different pairs of sites, — X, Y, Z and W. The corresponding product of Q's to the X-type path is Q_X^4. The product proportional to $Q_X^2 Q_Y^2$ corresponds to XY-type path. The product of the type $Q_X Q_Y Q_Z Q_W$ corresponds to the $XYZW$-type path. Only these types of products contribute to the ground-state projection of V_4. Another thing connected with calculations, is that some terms, like $\mathrm{ad}^1 S^{(2)}(V_2^{11})$, vanish on projecting onto the ground-state. Performing all necessary calculations, we finally obtain:

$$
\begin{aligned}
8 \cdot V_4^{00} = & \sum_{\alpha} \sum_{x:\langle x,y\rangle_\alpha} Q^4_{\langle x,y\rangle_\alpha} + \\
& + \sum_{\substack{\alpha,\beta \\ (\alpha \leqslant \beta)}} \sum_{x:\langle x,y\rangle_\alpha} \sum_{z:\langle y,z\rangle_\beta} \left(2Q^2_{\langle x,y\rangle_\alpha} Q^2_{\langle y,z\rangle_\beta} - Q_{\langle x,y\rangle_\alpha} Q^2_{\langle y,z\rangle_\beta} Q_{\langle x,y\rangle_\alpha} - Q_{\langle y,z\rangle_\beta} Q^2_{\langle x,y\rangle_\alpha} Q_{\langle y,z\rangle_\beta} \right) - \\
& - \sum_{i=2}^{6} \sum_{x:x\in P_i} \Bigg(\frac{1}{2} \cdot \left[Q_{\langle x,y\rangle_\alpha} Q_{\langle z,j\rangle_\gamma} + Q_{\langle z,j\rangle_\gamma} Q_{\langle x,y\rangle_\alpha} \right] \cdot \left[Q_{\langle y,z\rangle_\beta} Q_{\langle x,j\rangle_\omega} + Q_{\langle x,j\rangle_\omega} Q_{\langle y,z\rangle_\beta} \right] + \\
& \qquad + \frac{1}{2} \cdot \left[Q_{\langle y,z\rangle_\beta} Q_{\langle x,j\rangle_\omega} + Q_{\langle x,j\rangle_\omega} Q_{\langle y,z\rangle_\beta} \right] \cdot \left[Q_{\langle x,y\rangle_\alpha} Q_{\langle z,j\rangle_\gamma} + Q_{\langle z,j\rangle_\gamma} Q_{\langle x,y\rangle_\alpha} \right] + \\
& \qquad + \left[Q_{\langle x,y\rangle_\alpha} Q_{\langle y,z\rangle_\beta} + Q_{\langle y,z\rangle_\beta} Q_{\langle x,y\rangle_\alpha} \right] \cdot \left[Q_{\langle z,j\rangle_\gamma} Q_{\langle x,j\rangle_\omega} + Q_{\langle x,j\rangle_\omega} Q_{\langle z,j\rangle_\gamma} \right] + \\
& \qquad + \left[Q_{\langle y,z\rangle_\beta} Q_{\langle z,j\rangle_\gamma} + Q_{\langle z,j\rangle_\gamma} Q_{\langle y,z\rangle_\beta} \right] \cdot \left[Q_{\langle x,j\rangle_\omega} Q_{\langle x,y\rangle_\alpha} + Q_{\langle x,y\rangle_\alpha} Q_{\langle x,j\rangle_\omega} \right] + \\
& \qquad + \left[Q_{\langle z,j\rangle_\gamma} Q_{\langle x,j\rangle_\omega} + Q_{\langle x,j\rangle_\omega} Q_{\langle z,j\rangle_\gamma} \right] \cdot \left[Q_{\langle x,y\rangle_\alpha} Q_{\langle y,z\rangle_\beta} + Q_{\langle y,z\rangle_\beta} Q_{\langle x,y\rangle_\alpha} \right] + \\
& \qquad + \left[Q_{\langle x,j\rangle_\omega} Q_{\langle x,y\rangle_\alpha} + Q_{\langle x,y\rangle_\alpha} Q_{\langle x,j\rangle_\omega} \right] \cdot \left[Q_{\langle y,z\rangle_\beta} Q_{\langle z,j\rangle_\gamma} + Q_{\langle z,j\rangle_\gamma} Q_{\langle y,z\rangle_\beta} \right] \Bigg).
\end{aligned}
$$

The paths P_i are shown in Fig. 6. We group the terms and rewrite it using spins variables. Note, that during this procedure the summation over P_6 is replaced. Summing up, the fourth-order correction to the ground-state energy expansion, reads

$$
\begin{aligned}
V_4^{00} = & \left(t_h^4 + t_v^4 + t_+^4 + t_-^4 \right) \frac{|\Lambda|}{32} - \\
& - \left(\frac{3}{16} t_h^4 + \frac{3}{8} t_h^2 t_v^2 + \frac{3}{16} \left(2t_h^2 - t_v^2 \right) \left(t_+^2 + t_-^2 \right) + \frac{1}{8} \left(3t_h^2 + 2t_v^2 \right) t_+ t_- \right) \sum_{\langle x,y\rangle_{1,h}} s_x s_y + \\
& - \left(\frac{3}{16} t_v^4 + \frac{3}{8} t_h^2 t_v^2 + \frac{3}{16} \left(2t_v^2 - t_h^2 \right) \left(t_+^2 + t_-^2 \right) + \frac{1}{8} \left(3t_v^2 + 2t_h^2 \right) t_+ t_- \right) \sum_{\langle x,y\rangle_{1,v}} s_x s_y +
\end{aligned}
$$

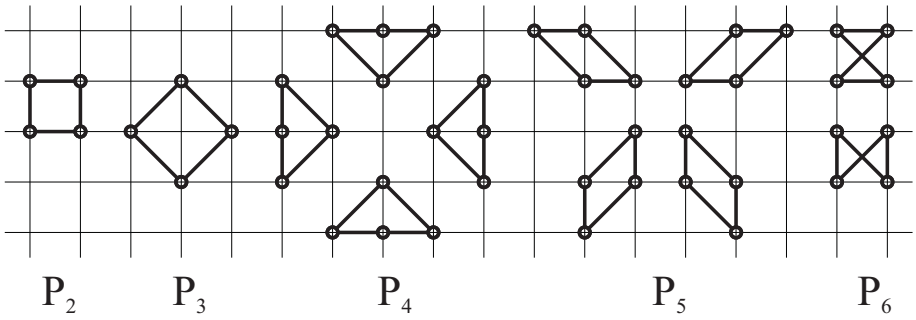

Figure 6: The sets of paths P_2, ... , P_6 which appear in the fourth order calculations.

$$
\begin{aligned}
&+\left(\frac{3}{16}t_h^2t_v^2-\frac{3}{16}\left(t_h^2+t_v^2\right)\left(2t_+^2+t_+t_-\right)-\frac{3}{16}t_+^4-\frac{3}{8}t_+^2t_-^2\right)\sum_{\langle x,y\rangle_{2,+}}s_xs_y+\\
&+\left(\frac{3}{16}t_h^2t_v^2-\frac{3}{16}\left(t_h^2+t_v^2\right)\left(2t_-^2+t_+t_-\right)-\frac{3}{16}t_-^4-\frac{3}{8}t_+^2t_-^2\right)\sum_{\langle x,y\rangle_{2,-}}s_xs_y+\\
&+\left(\frac{1}{8}t_h^4-\frac{1}{8}t_h^2t_+t_-+\frac{3}{16}t_+^2t_-^2\right)\sum_{\langle x,y\rangle_{3,h}}s_xs_y+\left(\frac{1}{8}t_v^4-\frac{1}{8}t_v^2t_+t_-+\frac{3}{16}t_+^2t_-^2\right)\sum_{\langle x,y\rangle_{3,v}}s_xs_y+\\
&+\frac{3}{16}t_h^2t_+^2\sum_{\langle x,y\rangle_{4,h+}}s_xs_y+\frac{3}{16}t_h^2t_-^2\sum_{\langle x,y\rangle_{4,h-}}s_xs_y+\frac{3}{16}t_v^2t_+^2\sum_{\langle x,y\rangle_{4,v+}}s_xs_y+\frac{3}{16}t_v^2t_-^2\sum_{\langle x,y\rangle_{4,v-}}s_xs_y+\\
&+\frac{1}{8}t_+^4\sum_{\langle x,y\rangle_{5,+}}s_xs_y+\frac{1}{8}t_-^4\sum_{\langle x,y\rangle_{5,-}}s_xs_y+\frac{1}{16}\left[t_h^2t_v^2+\left(t_h^2+t_v^2\right)t_+t_-\right]\sum_{P_2}\left(5s_{P_2}+1\right)+\\
&+\frac{1}{16}t_+^2t_-^2\sum_{P_3}\left(5s_{P_3}+1\right)+\frac{1}{16}t_h^2t_+t_-\sum_{P_{4,h}}\left(5s_{P_{4,h}}+1\right)+\frac{1}{16}t_v^2t_+t_-\sum_{P_{4,v}}\left(5s_{P_{4,v}}+1\right)+\\
&+\frac{1}{16}t_h^2t_+^2\sum_{P_{5,h+}}\left(5s_{P_{5,h+}}+1\right)+\frac{1}{16}t_h^2t_-^2\sum_{P_{5,h-}}\left(5s_{P_{5,h-}}+1\right)+\\
&+\frac{1}{16}t_v^2t_+^2\sum_{P_{5,v+}}\left(5s_{P_{5,v+}}+1\right)+\frac{1}{16}t_v^2t_-^2\sum_{P_{5,v-}}\left(5s_{P_{5,v-}}+1\right). \qquad (42)
\end{aligned}
$$

The whole ground-state energy expansion up to the fourth order,

$$E_S^{(4)}=H_0+V_2^{00}+V_3^{00}+V_4^{00}+R^{(4)}, \qquad (43)$$

where V_2^{00}, V_3^{00} and V_4^{00} are given by (34), (41) and (42), respectively. The remainder $R^{(4)}$ is independent of the chemical potentials, and collects all the terms proportional to $t_h^at_v^bt_+^ct_-^d$, with $a+b+c+d=5,6,\ldots$.

2.3.4 The case of hard-core bosons

On replacing the hopping fermions with hard-core bosons, the commutation rules change: operators of creation and annihilation at different sites commute. Using the same technic as in the case of fermions we obtain the ground-state energy expansion in the case of hard-core bosons. For the system of hard-core boson we consider only the case $t_+=t_-=0$.

The second order correction to the "classical" part H_0 remains the same as for fermions. The third order disappears (due to the absence of n.n.n. hopping, on the square lattice the path that satisfy condition (40) for a product of three Q operators does not exist), and the fourth-order correction, reads:

$$\begin{aligned}\left(V_4^{00}\right)_{hcb} =& \frac{t^4}{16}|\Lambda| - \left(\frac{3t_h^4}{16} + \frac{t_h^2 t_v^2}{8}\right) \sum_{\langle x,y\rangle_{1,h}} s_x s_y - \left(\frac{3t_v^4}{16} + \frac{t_h^2 t_v^2}{8}\right) \sum_{\langle x,y\rangle_{1,v}} s_x s_y + \frac{5t_h^2 t_v^2}{16} \sum_{\langle x,y\rangle_2} s_x s_y + \\ &+ \frac{t_h^4}{8} \sum_{\langle x,y\rangle_{3,h}} s_x s_y + \frac{t_v^4}{8} \sum_{\langle x,y\rangle_{3,v}} s_x s_y - \frac{t_h^2 t_v^2}{16} \sum_{P_2} (s_{P_2} + 5)\,. \end{aligned} \tag{44}$$

2.3.5 Building the ground-state phase diagram

We make some remarks on the expression of the ground-state energy expansion (43) in both cases: hopping fermions and hard-core bosons (in the case of hard-core bosons $V_3^{00} = 0$ and V_4^{00} in (43) is replaced with $(V_4^{00})_{hcb}$, given by (44)). In the above expressions we keep even the terms, that are independent of spin variables, hence have no influence on the phase diagram and so can be omitted. The effective Hamiltonian (43) depends only on $\mu = \mu_i - \mu_e$, which we call *the unique chemical potential parameter*.

The procedure of building the phase diagram is recursive. The phase diagram of the effective interaction truncated at the order k' is constructed on the basis of the phase diagram obtained at the preceding order k: the conditions imposed on the ground-state configurations by the k-th order effective Hamiltonian have to be obeyed by the ground-state configurations of the k'-th order effective Hamiltonian. In other words, the k'-th order terms of the expansion cannot change the hierarchy of configuration's energies established by the k-th order effective Hamiltonian; they can only split the energies of configurations in cases of degeneracy.

2.4 m-potential method

To proceed, we need to introduce some definitions. First, as was already mentioned, we denote the configuration of spins on the lattice Λ as $S = \{s_x\}_{x\in\Lambda}$, and s_x takes two values, either $+1$ or -1, at any site x. We call S_A the restriction of the configuration S to the subset of sites $A \subset \Lambda$ with $|A|$ sites, i.e. $S_A = \{s_x\}_{x\in A}$. Instead of talking about functions of spin variables s, it is convenient to use the function of configuration S (spin s_x depends on the configuration at site x, S_x). For $A \subset \Lambda$, let f_A be a function of configurations such that,

$$f_A(S) = f_A(S_A), \qquad \text{for any } S.$$

2.4.1 Definition of m-potentials

The concept of the m-potential was introduced in [58], and its idea is the following. Suppose that for some $A \subset \Lambda$, it is possible to write a Hamiltonian, which is a function of configurations, in the form,

$$H_\Lambda(S) = \sum_A H_A(S), \tag{45}$$

where by the sum $\sum_A H_A$ we understand the summation over all translations of A in Λ. Assume, that there exists a certain set of periodic configurations $\{\bar{S}\}$ (global configurations) which minimize the potential $H_A(S)$ for $\{\bar{S}_A\}$ (local configurations). If it holds for all translations of A in Λ, then we say that H_A is an m-potential and the set $\{\bar{S}\}$ is the set of the ground-state configurations.

Let us present two examples. Consider the antiferromagnetic Ising model on a square lattice ($J > 0$),

$$H_{Ising} = J \sum_{\langle x,y\rangle_1} s_x s_y. \tag{46}$$

The potential $H_{\langle x,y\rangle_1}(S) = J s_x s_y$ is an m-potential. Indeed, the local minimum for this potential is for configurations of nearest-neighbor pairs of spins where one is up and the second is down: $\{-1, 1\}$ or $\{1, -1\}$. There exist two global configurations, called the chessboard configurations, which minimize the potentials $H_{\langle x,y\rangle_1}$ for all $\langle x, y\rangle_1 \subset \Lambda$: if we choose any nearest-neighbor pair of sites, then the local configuration of the pair will be one of those which minimize the $H_{\langle x,y\rangle_1}$. In other words, if we can extend the local configuration (which is the ground-state configuration locally) to the global one, in a way that other local configurations with higher energy do not appear, we call the local potential H_A the m-potential, and the global configuration is the ground-state configuration because every potential under the sum has minimum on it.

Now, we consider the same Ising model (46) on a triangular lattice. As in the case of square lattice, local nearest-neighbor configurations remain the same. But the problem appears while trying to extend the local configurations to the whole lattice Λ: there is no such global configuration, which is ground-state configuration locally. This means that $H_{\langle x,y\rangle_1}$ is not an m-potential in this case (rewriting (46) as a sum over elementary triangles, it appears that the corresponding potential is m-potential, however the number of ground states is infinite).

Practically, potentials depend on some parameters and often they are m-potentials only for some range of these parameters. In order to find the complete phase diagram, i.e. all ground-state configurations for the whole range of the parameters, we are forced to build new m-potential. There is no recipe for constructing m-potentials. The only way to deal with the problem, as far as we know, is to introduce the so-called zero-potentials.

2.4.2 Definition of zero-potentials

The idea is simple: if some local potential does not satisfy the m-potential condition, then let's change it by adding zero, which means that we change it locally, but in a way that the total Hamiltonian remains the same. So the most general definition of zero-potential reads: a potential K_A, is a zero potential if it satisfies the zero-potential condition:

$$\sum_A K_A(S) = 0, \qquad \text{for any } S. \tag{47}$$

Now, it is clear that adding such a potential to the H_Λ,

$$H_\Lambda(S) = \sum_A H_A(S) = \sum_A \left(H_A(S) + K_A(S)\right) = \sum_A \widetilde{H}_A(S), \qquad \text{for any } S, \tag{48}$$

modifies only the local potential H_A. Under the zero-potential condition (47), K_A has no definite structure. In the sequel we shall consider two ways of constructing K_A.

2.4.3 First kind zero-potentials

In physics literature one can find two different ways of constructing zero-potentials. The first method was proposed in [50], where a part of the ground-state phase diagram of the Falicov–Kimball model was obtained for the first time in the fourth order. To illustrate the idea of this method we provide an example. Let us consider Hamiltonian H_Λ with a local potential H_A which is not an m-potential. Now we take some function (or several functions) of configurations on a set of sites A. For example, one of the simplest choices is $\alpha \sum\limits_{x\in A} s_x$, where α is a number. We add and subtract this function, so the Hamiltonian does not change,

$$H_\Lambda = \sum_A \left(H_A + \alpha \sum_{x\in A} s_x - \alpha \sum_{x\in A} s_x \right). \tag{49}$$

Next we chose a new set of sites A' (or several sets), and rewrite the Hamiltonian in the form:

$$\begin{aligned} H_\Lambda &= \sum_A \left(H_A + \alpha \sum_{x\in A} s_x \right) - \alpha \cdot |A| \sum_{x\in\Lambda} s_x = \sum_A \left(H_A + \alpha \sum_{x\in A} s_x \right) + \\ &+ \sum_{A'} \left(-\alpha \frac{|A|}{|A'|} \right) \sum_{x\in A'} s_x = \sum_A \widetilde{H}_A(\alpha) + \sum_{A'} \widehat{H}_{A'}(\alpha). \end{aligned} \tag{50}$$

The problem is to find such a value of the coefficient α that converts potentials $\widetilde{H}_A$ and $\widehat{H}_{A'}$ into m-potentials. Here it means that the m-potential condition must be satisfied for the both types of sets A and A': the restriction of a global ground-state configuration to any A and A' should minimize the corresponding potentials $\widetilde{H}_A$ and $\widehat{H}_{A'}$.

2.4.4 Second kind zero-potentials

Another method, was proposed in [59] and in [40]. In contrast to the first method, where zero-potentials are of the form $f_A(S) - f_A(S) = 0$ (i.e. the zero-potential condition is satisfied locally), no such restrictions are applied to its form. However, it is convenient to choose a zero-potential in a way that leaves the Hamiltonian's symmetry unchanged. We show here how to obtain zero potentials for the case when A is a 3×3-plaquette, later on called the T-plaquette (Fig. 7). We assume that H_T does not change under rotations

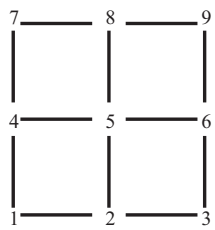

Figure 7: The sites of T-plaquette are labeled from the left to the right, starting at the bottom left corner and ending in the upper right one.

by $\pi/2$ and reflections.

Any function $f(S)$ can be rewritten in a form,

$$f(S) = \sum_{S'} \lambda(S')\chi(S', S), \tag{51}$$

where S' runs over all possible configurations, $\lambda(S')$ is a value of function $f(S)$ for specific configuration S' and $\chi(S', S)$ is an indicator function of configuration S', i.e. it is equal to 1 when $S = S'$ and is zero otherwise.

The construction of an indicator function $\chi(S', S)$ for specific configuration S' is simple. At a site x the indicator function for spin up is $\chi_x(+1, S_x) = (1 + s_x)/2$, for spin down is $\chi_x(-1, S_x) = (1 - s_x)/2$. The indicator function at A, is defined as

$$\chi_A(S'_A, S_A) = \prod_{x \in A} \chi_x(S'_x, S_x). \tag{52}$$

Performing the summation in (51) and taking into account the form of the indicator functions (52), any function $f_A(S_A)$, can be written as,

$$\begin{aligned} f_A(S_A) &= \lambda_0 + \sum_{x \in A} \lambda_x s_x + \sum_{\{x,y\} \subset A} \lambda_{xy} s_x s_y + \sum_{\{x,y,z\} \subset A} \lambda_{xyz} s_x s_y s_z + \ldots + \lambda_A \prod_{x \in A} s_x = \\ &= \sum_{X \subseteq A} \lambda_X s_X(S), \end{aligned} \tag{53}$$

where λ_X are the values which determine the function f_A. Notation $s_X(S)$ stands for the product of all spins which belong to X, $s_X = \prod_{x \in X} s_x$. For $X = \emptyset$, the coefficient $\lambda_X = \lambda_0$ and $s_X = 1$.

Another way to show the identity (53) and give a formula for finding the coefficients in (53) is to consider the functions $s_X(S)$ instead of indicator functions $\chi(S', S)$. If N_- is the number of spins in S_X oriented down, then $s_X(S) = (-1)^{N_-}$. Let us define the scalar product in the set of functions of configurations:

$$\langle f_A, g_B \rangle = \left(\frac{1}{2}\right)^{|\Lambda|} \sum_{S'} f_A(S') g_B(S'), \tag{54}$$

where S' runs over all possible configurations on Λ. Now we show, that

$$\langle s_X, s_Y \rangle = \begin{cases} 1, & \text{if } X = Y, \\ 0, & \text{if } X \neq Y. \end{cases} \tag{55}$$

Let us consider the product,

$$s_X(S) s_Y(S) = s_{X \cdot Y}(S),$$

which follows simply from the form of $s_X(S)$; here $X \cdot Y = (X \cup Y) \setminus (X \cap Y)$. Using the fact, that for any set X,

$$\sum_S s_X(S) = \begin{cases} 2^{|\Lambda|}, & \text{if } X = \emptyset \\ 0, & \text{if } X \neq \emptyset \end{cases} \tag{56}$$

we obtain expression (55). Since the functions s_X are orthonormal and there are as many s_X as χ_Λ, they constitute an orthonormal basis, and any function f_A, can be expanded as follows,

$$f_A(S) = \sum_{X \subseteq A} \lambda_X s_X(S)$$

which is equivalent to (53), where

$$\lambda_X = \langle s_X, f_A \rangle. \tag{57}$$

We are looking for a zero-potential $K_T(S)$ in a form (53). We can always set $\lambda_0 = 0$ although it can change the Hamiltonian only by a constant. So for a T-plaquette, which we will use later, we choose the zero-potential in a form:

$$\begin{aligned} K_T(S) &= \sum_{\emptyset \neq A \subseteq T} \lambda_A s_A(S) = \\ &= \sum_{x \in T} \lambda_x s_x + \sum_{\{x,y\} \subset T} \lambda_{xy} s_x s_y + \sum_{\{x,y,z\} \subset T} \lambda_{xyz} s_x s_y s_z + \ldots + \lambda_T s_T. \end{aligned} \tag{58}$$

Now applying to these objects the symmetry operations of the Hamiltonian and the zero-potential condition (47) we can eliminate some of the arbitrary coefficients λ_A. For instance, we consider the first term:

$$\sum_{x \in T} \lambda_x s_x = \lambda_1 s_1 + \lambda_2 s_2 + \lambda_3 s_3 + \lambda_4 s_4 + \lambda_5 s_5 + \lambda_6 s_6 + \lambda_7 s_7 + \lambda_8 s_8 + \lambda_9 s_9. \tag{59}$$

Demanding $\sum_{x \in T} \lambda_x s_x$ to be invariant with respect to symmetry operations (rotations or reflections), we obtain

$$\lambda_1 = \lambda_3 = \lambda_7 = \lambda_9, \qquad \lambda_2 = \lambda_4 = \lambda_6 = \lambda_8. \tag{60}$$

The zero-potential condition (47) now reads:

$$\sum_T \sum_{x \in T} \lambda_x s_x = \sum_i \lambda_i \sum_{x \in \Lambda} s_x = 0,$$

and holds for any configuration S. That directly implies the condition

$$\sum_i \lambda_i = 0. \tag{61}$$

Expressing λ_5 in terms of λ_1 and λ_2,

$$\lambda_5 = -4\left(\lambda_1 + \lambda_2\right), \tag{62}$$

only two coefficients remain independent, and the expression is of the form:

$$\sum_{x \in T} \lambda_x s_x = \lambda_1 \left(s_1 + s_3 + s_7 + s_9 - 4s_5\right) + \lambda_2 \left(s_2 + s_4 + s_6 + s_8 - 4s_5\right). \tag{63}$$

Similarly, we can obtain other zero-potentials applying the procedure sketched above to products of nearest-neighbors spins, next-nearest-neighbors, etc. Finally, we can rewrite $K_T(S)$ in the form

$$K_T(S) = \sum_i \alpha_i k_T^{(i)}(S), \tag{64}$$

where

$$\begin{aligned} k_T^{(1)}(S) &= s_1 + s_3 + s_7 + s_9 - 4s_5, \\ k_T^{(2)}(S) &= s_2 + s_4 + s_6 + s_8 - 4s_5, \end{aligned} \tag{65}$$

are the only two symmetric zero-potentials of the form (59). For a T-plaquette, there are 16 independent symmetrical zero potentials. The complete list of them is presented in Appendix A.

Now, having zero potentials, we are trying to find such a vector $\vec{\alpha} = (\alpha_1, \alpha_2, \ldots)$ that makes the total potential (the original potential H_A plus the zero potential K_A) an m-potential. Components α_i are called the zero-potential coefficients. Both, in the first and the second methods, there are no restrictions for $\vec{\alpha}$ but we suppose, that they are functions of the Hamiltonian's parameters p_i. For convenience, we write the set of parameters p_i as a vector $\vec{p} = (p_1, p_2, \ldots)$.

The both methods have their own advantages and disadvantages. For our purposes the second one is more suitable for two reasons. First of all, adding a zero-potential conserves the symmetry of the system. As a result, the number of block configurations whose energies we have to compare is reduced significantly. The second reason is that extending some local configurations to the whole lattice is much simpler in the case when we have one type of blocks, say T-plaquettes only. If other blocks are present, like A' in the first method, then we have to check if potential $\widehat{H}_{A'}$ in (50), is an m-potential for a configuration we have built using ground-state configurations of the potential $\widetilde{H}_A$, or vice versa.

2.4.5 Some remarks on constructing zero-potentials

Let the Hamiltonian, a function of configurations, be the linear function of parameters p_i (by linear function we understand function which is convex and concave simultaneously), and it is possible to rewrite it in the following form

$$H_\Lambda(\vec{p}; S) = \sum_A H_A(\vec{p}; S), \tag{66}$$

where H_A is linear in $\vec{p}$ and is not an m-potential. Adding the zero-potential K_A in the form (64), we suppose that a zero-potential vector $\vec{\alpha}$ is the linear function of a vector of parameters $\vec{p}$,

$$H_\Lambda(\vec{p}; S) = \sum_A \left(H_A(\vec{p}; S) + K_A(\vec{\alpha}(\vec{p}); S)\right) = \sum_A \widetilde{H}_A(\vec{p}; \vec{\alpha}(\vec{p}); S), \tag{67}$$

and we are looking for a vector $\vec{\alpha}$ for which the above potential is an m-potential for any vector of parameters $\vec{p}$. Unfortunately, we hardly ever succeed in finding a zero-potential

vector which converts $\widetilde{H}_A$ into an m-potential for the whole range of the parameters; usually coefficients $\vec{\alpha}(\vec{p})$ can be found in a certain range of the parameters only. So sometimes we need several sets of zero-potential coefficients to cover the whole range of the considered parameters. Such an approach is used in Section 3.

In studies of the minimum of the potentials, the following observation is useful. Consider two points in the parameters space, $\vec{x}$ and $\vec{y}$, and such $\vec{\alpha}'$, $\vec{\alpha}''$ in each point, respectively, that the potentials $\widetilde{H}_A(\vec{x};\vec{\alpha}';S)$ and $\widetilde{H}_A(\vec{y};\vec{\alpha}'';S)$ are minimized at some sets of local configurations $G_A(\vec{x},\vec{\alpha}')$ and $G_A(\vec{y},\vec{\alpha}'')$, respectively, and $G_A(\vec{x},\vec{\alpha}')\cap G_A(\vec{y},\vec{\alpha}'')\neq\emptyset$. There exist only one linear function $\vec{\alpha}(\vec{p})$ on the line segment between points $\vec{x}$ and $\vec{y}$ whose values are equal to $\vec{\alpha}'$ at $\vec{x}$ and $\vec{\alpha}''$ at $\vec{y}$:

$$\vec{\alpha}\Big(t\vec{x}+(1-t)\vec{y}\Big)=t\cdot\vec{\alpha}'+(1-t)\cdot\vec{\alpha}'',\qquad\text{for any } t\in[0,1]. \tag{68}$$

This definition ensures that potential $\widetilde{H}_A$ is linear in $\vec{p}$:

$$\begin{aligned}\widetilde{H}_A\Big(t\vec{x}+(1-t)\vec{y},\vec{\alpha}\,(t\vec{x}+(1-t)\vec{y})\,;S\Big)=\\ =t\cdot\widetilde{H}_A(\vec{x},\vec{\alpha}(\vec{x});S)+(1-t)\cdot\widetilde{H}_A(\vec{y},\vec{\alpha}(\vec{y});S),\qquad\text{for any } t\in[0,1].\end{aligned} \tag{69}$$

We claim that a set of block configurations that realizes the minimum of energy $\widetilde{H}_A(\vec{p};\vec{\alpha}(\vec{p});S)$ on the line segment between $\vec{x}$ and $\vec{y}$, is

$$G_A\big(t\vec{x}+(1-t)\vec{y},\vec{\alpha}\,(t\vec{x}+(1-t)\vec{y})\big)=G_A(\vec{x},\vec{\alpha}(\vec{x}))\cap G_A(\vec{y},\vec{\alpha}(\vec{y})),$$

for $0<t<1$.

Indeed, let $\widetilde{S}\in G_A(\vec{x},\vec{\alpha}(\vec{x}))\cap G_A(\vec{y},\vec{\alpha}(\vec{y}))$, i.e.:

$$\widetilde{H}_A(\vec{x},\vec{\alpha}(\vec{x});\widetilde{S})=\min_S\widetilde{H}_A(\vec{x},\vec{\alpha}(\vec{x});S)\quad\text{and}\quad\widetilde{H}_A(\vec{y},\vec{\alpha}(\vec{y});\widetilde{S})=\min_S\widetilde{H}_A(\vec{y},\vec{\alpha}(\vec{y});S). \tag{70}$$

Then by (69) and (70),

$$\begin{aligned}\widetilde{H}_A\Big(t\vec{x}+(1-t)\vec{y},\vec{\alpha}\,(t\vec{x}+(1-t)\vec{y})\,;\widetilde{S}\Big)=\\ =t\cdot\widetilde{H}_A(\vec{x},\vec{\alpha}(\vec{x});\widetilde{S})+(1-t)\cdot\widetilde{H}_A(\vec{y},\vec{\alpha}(\vec{y});\widetilde{S})\\ =t\cdot\min_S\widetilde{H}_A(\vec{x},\vec{\alpha}(\vec{x});S)+(1-t)\cdot\min_S\widetilde{H}_A(\vec{y},\vec{\alpha}(\vec{y});S)\\ \leqslant t\cdot\widetilde{H}_A(\vec{x},\vec{\alpha}(\vec{x});S)+(1-t)\cdot\widetilde{H}_A(\vec{y},\vec{\alpha}(\vec{y});S)\\ =\widetilde{H}_A\Big(t\vec{x}+(1-t)\vec{y},\vec{\alpha}\,(t\vec{x}+(1-t)\vec{y})\,;S\Big),\end{aligned}$$

for any configuration S and any $t\in[0,1]$, that is,

$$G_A(\vec{x},\vec{\alpha}(\vec{x}))\cap G_A(\vec{y},\vec{\alpha}(\vec{y}))\subseteq G_A\big(t\vec{x}+(1-t)\vec{y},\vec{\alpha}\,(t\vec{x}+(1-t)\vec{y})\big),$$

for any $t\in[0,1]$.

Now we shall demonstrate that for $t\in(0,1)$ the opposite inclusion holds. Let

$$\widehat{S}\in G_A\big(t\vec{x}+(1-t)\vec{y},\vec{\alpha}\,(t\vec{x}+(1-t)\vec{y})\big)$$

that is,

$$\widetilde{H}_A\Big(t\vec{x}+(1-t)\vec{y},\vec{\alpha}\,(t\vec{x}+(1-t)\vec{y})\,;\widehat{S}\Big)\leqslant \\ \leqslant \tilde{H}_A\Big(t\vec{x}+(1-t)\vec{y},\vec{\alpha}\,(t\vec{x}+(1-t)\vec{y})\,;S\Big),$$

for any S. In particular, the above inequality holds for $\widetilde{S}\in G_A(\vec{x},\vec{\alpha}(\vec{x}))\cap G_A(\vec{y},\vec{\alpha}(\vec{y}))$, and can be rewritten as

$$t\left[\widetilde{H}_A(\vec{x},\vec{\alpha}(\vec{x});\widehat{S})-\widetilde{H}_A(\vec{x},\vec{\alpha}(\vec{x});\widetilde{S})\right]+ \\ +(1-t)\left[\widetilde{H}_A(\vec{y},\vec{\alpha}(\vec{y});\widehat{S})-\widetilde{H}_A(\vec{y},\vec{\alpha}(\vec{y});\widetilde{S})\right]\leqslant 0, \quad (71)$$

for any $t\in(0,1)$. Simultaneously, since each of the energy differences (in square brackets) in (71) is nonnegative,

$$t\left[\widetilde{H}_A(\vec{x},\vec{\alpha}(\vec{x});\widehat{S})-\widetilde{H}_A(\vec{x},\vec{\alpha}(\vec{x});\widetilde{S})\right]+ \\ +(1-t)\left[\widetilde{H}_A(\vec{y},\vec{\alpha}(\vec{y});\widehat{S})-\widetilde{H}_A(\vec{y},\vec{\alpha}(\vec{y});\widetilde{S})\right]\geqslant 0. \quad (72)$$

By (71) and (72),

$$t\left[\widetilde{H}_A(\vec{x},\vec{\alpha}(\vec{x});\widehat{S})-\widetilde{H}_A(\vec{x},\vec{\alpha}(\vec{x});\widetilde{S})\right]+ \\ +(1-t)\left[\widetilde{H}_A(\vec{y},\vec{\alpha}(\vec{y});\widehat{S})-\widetilde{H}_A(\vec{y},\vec{\alpha}(\vec{y});\widetilde{S})\right]=0,$$

with $t>0$ and $1-t>0$, hence

$$\widetilde{H}_A(\vec{x},\vec{\alpha}(\vec{x});\widehat{S})-\widetilde{H}_A(\vec{x},\vec{\alpha}(\vec{x});\widetilde{S})=0 \qquad \text{and} \qquad \widetilde{H}_A(\vec{y},\vec{\alpha}(\vec{y});\widehat{S})-\widetilde{H}_A(\vec{y},\vec{\alpha}(\vec{y});\widetilde{S})=0,$$

which implies in turn that $\widehat{S}\in G_A(\vec{x},\vec{\alpha}(\vec{x}))\cap G_A(\vec{y},\vec{\alpha}(\vec{y}))$. Therefore,

$$G_A\big(t\vec{x}+(1-t)\vec{y},\vec{\alpha}\,(t\vec{x}+(1-t)\vec{y})\big)\subset G_A(\vec{x},\vec{\alpha}(\vec{x}))\cap G_A(\vec{y},\vec{\alpha}(\vec{y})).$$

This proof has a simple geometrical interpretation (Fig. 8). All energies are linear functions of t, so if there exist a point at $t\in(0,1)$ where some block configuration $\widehat{S}\neq\widetilde{S}$ has a lower energy than that of $\widetilde{S}$, then at least at one of the points, $\vec{x}$ or $\vec{y}$, the energy of $\widehat{S}$ is lower than the energy of local ground state configuration.

So, there is no need to find zero-potential coefficients everywhere: in order to find them for some interval $(\vec{x},\vec{y})$, it is enough to find them at $\vec{x}$ and at $\vec{y}$, where the sets of local ground state configurations are $G_{\vec{x}}$ and $G_{\vec{y}}$, respectively. The construction described above guarantees that with $\vec{\alpha}\,(t\vec{x}+(1-t)\vec{y})$ for $t\in(0,1)$, the set of local ground state configurations $G_{[\vec{x},\vec{y}]}$ on the line segment $(\vec{x},\vec{y})$ is given by $G_{[\vec{x},\vec{y}]}=G_{\vec{x}}\cap G_{\vec{y}}$. Such an approach is used in Section 4 and 5, where zero-potential coefficients are given only on some semi-infinite lines and at certain points.

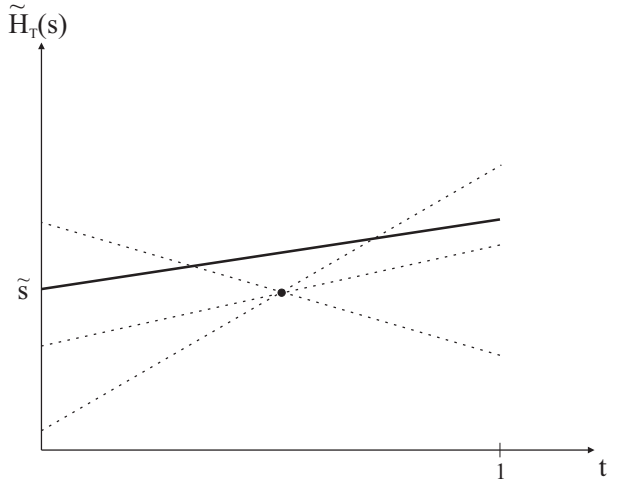

Figure 8: The illustration of the proof concerning α.

3 Stability of striped phases

In this Section[1] we consider two strongly correlated quantum systems, described by Falicov–Kimball-like Hamiltonians on a square lattice, extended by direct short-range interactions between the immobile particles. In the first system hopping particles are spinless fermions while in the second one they are hardcore bosons. Ground-state phase diagrams of the both systems in the strong-coupling regime and at half-filling are constructed rigorously. Two main conclusions are drawn. Firstly, short-range interactions in quantum gases are sufficient for the appearance of charge stripe-ordered phases. By varying the intensity of a direct nearest-neighbor interaction between the immobile particles, the both systems can be driven from a phase-separated state (the segregated phase) to a crystalline state (the chessboard phase) and these transitions occur necessarily via charge-stripe phases: via a diagonal striped phase in the case of fermions and via vertical (horizontal) striped phases in the case of hardcore bosons. Secondly, the phase diagrams of the two systems (mobile fermions or mobile hardcore bosons) are definitely different. However, if the strongest effective interaction in the fermionic case gets frustrated gently, then the phase diagram becomes similar to that of the bosonic case.

3.1 Introducing the modifications to the Falicov–Kimball model

The task is to generate the physical situation, where the striped phases appear, in the framework of Falicov–Kimball model. For technical reasons, our analysis is restricted to the case of half-filling, where the well-defined expansion can be written. However, it is now well established (proven) [26, 60] that, in the fermion spinless Falicov–Kimball model the phase-separated state, the segregated phase, is stable only off the half-filling. Thus, an additional interaction is needed to stabilize the segregated phase at half-filling.

In the regime of singly occupied sites and for strong-coupling, the strongest effective interaction in the Hubbard model is the Heisenberg antiferromagnetic interaction. Doping of holes can be seen as means to weaken the strong tendency toward antiferromagnetic ordering and to make possible a phase separated state with hole-reach and electron-reach regions. Under similar conditions, in the spinless Falicov–Kimball model an analogous role is played by the Ising-like n.n. repulsive interaction between the immobile particles that favors a chessboard-like ordering. The effect of weakening of the strong tendency toward chessboard ordering can be achieved by an extra Ising-like n.n. interaction that compensates the strongest repulsive interaction, and consequently permits the system to reach a phase-separated state, the segregated phase. On varying, in a suitable interval of values, the corresponding interaction constant, which is our control parameter, we can study how the both systems "evolve" from the crystalline chessboard phase to the segregated one.

Here, we would like to make a remark concerning physical interpretations of our extended Falicov–Kimball model. The classical spin models, like those studied in [21, 22] can be considered as classical effective models of crystallization that contain the necessary "ingredients" of such models. Namely, in these models there are two competing interactions, one favoring phase separation into macroscopic regions, which are either empty or completely filled with particles, the other favoring periodic arrangements of particles.

[1] This section is based on [28].

Our extended Falicov–Kimball model, with hopping fermions, can be thought of as a microscopic quantum model of crystallization. In this case, the necessary "ingredients" are: the tendency towards crystalline orders, coming from the kinetic energy of itinerant electrons and from the screened (in our case on site) electron-ion Coulomb interaction, a kind of Van der Walls attractive forces, favoring phase separated state, and finally the hard-core repulsion provided by the underlying lattice and the Pauli principle.

In what follows, the modified Hamiltonian reads:

$$H = H_{FK} + V, \tag{73}$$

where H_{FK} is given by (1), and a direct Ising-like interaction V between the immobile particles is of the form

$$V = \frac{W}{8} \sum_{\langle x,y \rangle_1} s_x s_y - \frac{\tilde{\varepsilon}}{16} \sum_{\langle x,y \rangle_2} s_x s_y. \tag{74}$$

Here W stands for an intensity of direct n.n. interaction between ions. We also include a subsidiary direct interaction between the immobile particles, an Ising-like n.n.n. interaction with intensity $\tilde{\varepsilon}$, much weaker than the n.n. interaction. This interaction can reinforce or frustrate the n.n. interaction, depending on the sign of its interaction constant. It appears that on varying W, the systems (fermion or boson) characterized by different values of n.n.n. interactions, may undergo different sequences of transitions between the chessboard phase and the segregated one. We find, in particular, that if we set appropriate values of the n.n.n. interaction in the fermion system and in the boson one, then the both systems settle in the same phases, for typical values of the control parameter. On the other hand, the n.n.n. interaction enables us to demonstrate that the ground-state phase diagrams in the cases of mobile fermions and mobile hardcore bosons are definitely different.

To simplify the model, we consider the case where only n.n. hopping is nonzero and does not depend on direction. So we put $t_h = t_v = t$, and $t_+ = t_- = 0$. We are interesting in investigation of the ground-state phase diagrams of our systems, so the grand-canonical formalism is used. We use the expansion (43) which was obtained in the strong-coupling regime and at half-filling. In this case, with the expansion terms up to order four shown explicitly, it reads:

$$\begin{aligned} E_S^{fermion}(\mu) &= -\frac{\mu}{2} \sum_x s_x + \left[\frac{t^2}{4} - \frac{9t^4}{16} + \frac{W}{8} \right] \sum_{\langle x,y \rangle_1} s_x s_y + \left[\frac{3t^4}{16} - \frac{\tilde{\varepsilon}}{16} \right] \sum_{\langle x,y \rangle_2} s_x s_y + \\ &+ \frac{t^4}{8} \sum_{\langle x,y \rangle_3} s_x s_y + \frac{t^4}{16} \sum_{P_2} (5 s_P + 1) + R^{(4)}, \end{aligned} \tag{75}$$

for fermions, and

$$\begin{aligned} E_S^{boson}(\mu) &= -\frac{\mu}{2} \sum_x s_x + \left[\frac{t^2}{4} - \frac{5t^4}{16} + \frac{W}{8} \right] \sum_{\langle x,y \rangle_1} s_x s_y + \left[\frac{5t^4}{16} - \frac{\tilde{\varepsilon}}{16} \right] \sum_{\langle x,y \rangle_2} s_x s_y + \\ &+ \frac{t^4}{8} \sum_{\langle x,y \rangle_3} s_x s_y - \frac{t^4}{16} \sum_{P_2} (5 + s_P) + \tilde{R}^{(4)}, \end{aligned} \tag{76}$$

for hardcore bosons, up to a term independent of the ion configuration and the chemical potentials. The remainders $R^{(4)}$, $\tilde{R}^{(4)}$, are independent of the chemical potential μ and the parameters W and $\tilde{\varepsilon}$, and collect those terms of the expansion that are proportional to t^{2m}, with $m = 3, 4, \ldots$.

Due to the convergence of the expansions (75) and (76), it is possible to establish rigorously a part of the phase diagram (that is the ground-state configurations of ions are determined everywhere in the (μ_e, μ_i)-plane, except some small regions), by determining the phase diagram of the expansion truncated at the order k, that is according to the k-th order effective Hamiltonians $(E_S^{fermion})^{(k)}(\mu)$ and $(E_S^{boson})^{(k)}(\mu)$. In order to construct a phase diagram according to a k-th order effective Hamiltonian, we use the m-potential method.

3.2 Zeroth- and second-order effective interactions — phase diagram

As was discussed above, up to the second order the effective Hamiltonians for fermions and hardcore bosons are the same. Hence, the discussion that follows applies to the both cases, and the common effective Hamiltonians are denoted as $E_S^{(0)}(\mu)$, $E_S^{(2)}(\mu)$.

In the zeroth order,

$$\begin{aligned} E_S^{(0)}(\mu) &= -\frac{\mu}{2}\sum_x (s_x+1) + \frac{W}{8}\sum_{\langle x,y\rangle_1} s_x s_y - \frac{\tilde{\varepsilon}}{16}\sum_{\langle x,y\rangle_2} s_x s_y \\ &= \sum_{P_2} H_{P_2}^{(0)}, \end{aligned} \tag{77}$$

where

$$H_{P_2}^{(0)} = -\frac{\mu}{8}{\sum_x}' (s_x+1) + \frac{W}{16}{\sum_{\langle x,y\rangle_1}}' s_x s_y - \frac{\tilde{\varepsilon}}{16}{\sum_{\langle x,y\rangle_2}}' s_x s_y, \tag{78}$$

and the primed sums in (78) are restricted to a plaquette P_2. For any $\tilde{\varepsilon} > 0$, the plaquette potentials $H_{P_2}^{(0)}$ are minimized by the restrictions to a plaquette P_2 of a few periodic configurations of ions on Λ. Namely, S_- — the empty configuration (S_+ — the completely filled configuration), where $s_x = -1$ at every site ($s_x = +1$ at every site), and the chessboard configurations S_{cb}^e, where $s_x = \epsilon_x$, and S_{cb}^o (where $s_x = -\epsilon_x$), with $\epsilon_x = 1$ if x belongs to the even sublattice of Λ and $\epsilon_x = -1$ otherwise. Moreover, out of the restrictions of those configurations to a plaquette P_2, $S_{-|P_2}$, $S_{+|P_2}$, $S_{cb|P_2}^e$, and $S_{cb|P_2}^o$, only four ground-state configurations on Λ can be built, which coincide with the four configurations named above. Clearly, this is due to the direct n.n.n. attractive interaction between the ions. The section of the phase diagram in the $(W, \mu, \tilde{\varepsilon})$ space by a plane with $\tilde{\varepsilon} > 0$, according to the effective Hamiltonian $E_S^{(0)}(\mu)$, is shown in Fig. 9.

In the second order,

$$\begin{aligned} E_S^{(2)}(\mu) &= -\frac{\mu}{2}\sum_x (s_x+1) + \left[\frac{t^2}{4} + \frac{W}{8}\right]\sum_{\langle x,y\rangle_1} s_x s_y - \frac{\tilde{\varepsilon}}{16}\sum_{\langle x,y\rangle_2} s_x s_y \\ &= \sum_{P_2} H_{P_2}^{(2)}, \end{aligned} \tag{79}$$

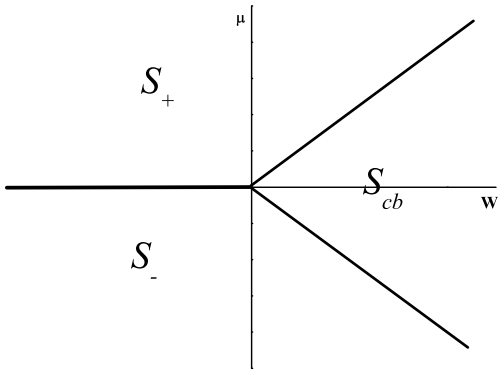

Figure 9: Ground-state phase diagram of $E_S^{(0)}(\mu)$ for fermion and hard-core boson systems.

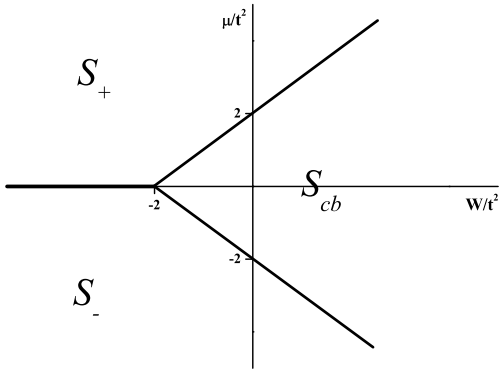

Figure 10: Ground-state phase diagram of $E_S^{(2)}(\mu)$ for fermion and hard-core boson systems.

where $H_{P_2}^{(2)}$,

$$H_{P_2}^{(2)} = -\frac{\mu}{8}\sum_x{}' (s_x+1) + \left[\frac{t^2}{8}+\frac{W}{16}\right]\sum_{\langle x,y\rangle_1}{}' s_x s_y - \frac{\tilde{\varepsilon}}{16}\sum_{\langle x,y\rangle_2}{}' s_x s_y, \tag{80}$$

and the primed sums are restricted to a plaquette P_2. Since $E_S^{(2)}$ differs from $E_S^{(0)}$ by the strength of n.n. interactions, the only effect on the phase diagram is that the coexistence lines are translated by the vector $(-2t^2,0,0)$. The section of the phase diagram in the $(W,\mu,\tilde{\varepsilon})$ space by a plane with $\tilde{\varepsilon}>0$, according to the effective Hamiltonian $E_S^{(2)}(\mu)$, is shown in Fig. 10.

3.3 Fourth-order effective interactions — phase diagram

It follows from the investigation of the phase diagram up to the second order that the degeneracy is finite, independently of the size of Λ, everywhere except the coexistence lines in the $(\tilde{\varepsilon}=0)$-plane, where it grows exponentially with $|\Lambda|$. Only there the effect of the fourth order interactions can be most significant. The meeting point of the coexistence lines in the $(\tilde{\varepsilon}=0)$-plane, where the coexistence line of S_+ and S_- sticks to the stability domain of chessboard configurations, appears to be particularly interesting. In that point, the energies of all the configurations are the same. In what follows, we shall study the phase diagrams of spinless fermions and spinless hardcore bosons up to the fourth order, in a neighborhood of radius $O(t^4)$ of the point $(-2t^2,0,0)$. In this neighborhood, it is convenient to introduce new coordinates, $(W,\mu,\tilde{\varepsilon})\to(\omega,\delta,\varepsilon)$,

$$W = -2t^2 + t^4\omega, \quad \mu = t^4\delta, \quad \tilde{\varepsilon} = t^4\varepsilon, \tag{81}$$

and a new (equivalent to $(E_S^{fermion})^{(4)}$) t-independent effective Hamiltonian, $(H_{\rm eff}^{fermion})^{(4)}$,

$$(E_S^{fermion})^{(4)}(0,\delta) = \frac{t^4}{2}(H_{\rm eff}^{fermion})^{(4)}. \tag{82}$$

Then, in the spirit of the m-potential method, we express $(H_{\rm eff}^{fermion})^{(4)}$ by the potentials $(H_T^{fermion})^{(4)}$,

$$(H_{\rm eff}^{fermion})^{(4)} = \sum_T (H_T^{fermion})^{(4)}, \tag{83}$$

where, in terms of the new variables,

$$\begin{aligned}(H_T^{fermion})^{(4)} &= -\delta\,(s_5+1) + \frac{1}{24}\left(\omega - \frac{9}{2}\right)\sum_{\langle x,y\rangle_1}'' s_x s_y + \frac{1}{32}\,(3-\varepsilon)\sum_{\langle x,y\rangle_2}'' s_x s_y + \\ &\quad \frac{1}{12}\sum_{\langle x,y\rangle_3}'' s_x s_y + \frac{1}{32}\sum_{P_2}''\,(5 s_{P_2}+1)\,. \end{aligned}\tag{84}$$

In (83) and (84), T stands for a T-plaquette of a square lattice (see Fig. 7). The double-primed sums are restricted to a T-plaquette. For bosons, we introduce $(H_{\rm eff}^{boson})^{(4)}$ and $(H_T^{boson})^{(4)}$ in the same manner as for fermions, with

$$\begin{aligned}(H_T^{boson})^{(4)} &= -\delta\,(s_5+1) + \frac{1}{24}\left(\omega - \frac{5}{2}\right)\sum_{\langle x,y\rangle_1}'' s_x s_y + \frac{1}{32}\,(5-\varepsilon)\sum_{\langle x,y\rangle_2}'' s_x s_y + \\ &\quad \frac{1}{12}\sum_{\langle x,y\rangle_3}'' s_x s_y - \frac{1}{32}\sum_{P_2}''\,(s_{P_2}+5)\,. \end{aligned}\tag{85}$$

We have to search for the lowest-energy configurations of $(E_S^{fermion})^{(4)}$ and $(E_S^{boson})^{(4)}$ among all the configurations. Consequently, the potentials $(H_T^{fermion})^{(4)}$ and $(H_T^{boson})^{(4)}$ have to be minimized over all the T-plaquette configurations. There are (up to the symmetries of H_0) 102 different T-plaquette configurations, shown in Fig. 29 in Appendix B.

Unfortunately, in contrast to the lower-order cases, the potentials $(H_T^{fermion})^{(4)}$ and $(H_T^{boson})^{(4)}$ turn out to be the m-potentials only in a small part of $(\omega,\delta,\varepsilon)$-space. This difficulty can be overcome by introducing the zero-potentials $K_T^{(4)}$, that are invariant with respect to the symmetries of H and are given by (64). Coefficients α_i, depending on $(\omega,\delta,\varepsilon)$ in general, have to be determined in the process of constructing the phase diagram, and the potentials $k_T^{(i)}$ are listed in Appendix A. We set all $\alpha_i = 0$ for $i \geqslant 6$.

Following (48), new candidates for m-potentials can be introduced,

$$(H_{\rm eff}^{fermion})^{(4)} = \sum_T \left((H_T^{fermion})^{(4)} + K_T^{(4)}\right), \tag{86}$$

with an analogous representation of $(H_{\rm eff}^{boson})^{(4)}$, and now the task is to minimize the potentials $(H_T^{fermion})^{(4)} + K_T^{(4)}$ and $(H_T^{boson})^{(4)} + K_T^{(4)}$ over all the T-plaquette configurations.

In our study of the ground-state phase diagrams we limit ourselves to the $(\delta = 0)$-plane, where the both considered systems are hole-particle invariant, and to the $(\varepsilon = 0)$-plane. Our analysis of the minima of the T-plaquette potentials, $(H_T^{fermion})^{(4)}$ and $(H_T^{boson})^{(4)}$ augmented by the zero-potentials $K_T^{(4)}$, shows that these planes are partitioned into a finite number of open domains $\mathcal{S}_D$, each with its unique set of periodic ground-state configurations on Λ, denoted also by $\mathcal{S}_D$. There is a finite number, independent of $|\Lambda|$, of configurations in $\mathcal{S}_D$ and they are related by the symmetries of H. The last two

statements do not apply to only one of the domains, denoted $\mathcal{S}_{d2}$, which will be described in the sequel.

The domains $\mathcal{S}_D$ are characterized as follows: at each point p ($p = (\omega, \varepsilon)$ or $p = (\omega, \delta)$) of a domain $\mathcal{S}_D$, there exist a set of coefficients $\{\alpha_i(p)\}$ such that the corresponding potentials are minimized by a set $\mathcal{S}_{TD}(p)$ of T-plaquette configurations. Moreover, from the configurations in $\mathcal{S}_{TD}(p)$ one can construct only the configurations in $\mathcal{S}_D$. The set of the restrictions to T-plaquettes of the configurations from $\mathcal{S}_D$, $\mathcal{S}_{D|T}$, is contained in each set $\mathcal{S}_{TD}(p)$ with $p \in \mathcal{S}_D$. In Table 11 of Appendix E we mark by asterisk the cases, where the set $\mathcal{S}_{TD}(p)$ contains, besides $\mathcal{S}_{D|T}$, some additional T-plaquette configurations.

Specifically, for $\delta = 0$ the ground-state phase diagrams due to the effective Hamiltonians $(H_{\rm eff}^{fermion})^{(4)}$ and $(H_{\rm eff}^{boson})^{(4)}$ are shown in Fig. 11 and Fig. 12, respectively, while the corresponding ground-state phase diagrams for $\varepsilon = 0$, in Fig. 13 and Fig. 14. In Fig. 15 we display the representatives of the sets $\mathcal{S}_D$ of ground-state configurations. That is, the remaining configurations of $\mathcal{S}_D$ can be obtained easily by applying the symmetries of H_0 to the displayed configurations. The domain $\mathcal{S}_{seg}$, having no representative in Fig. 15, consists of the two translation-invariant configurations S_+ and S_-, related by the hole-particle transformation.

Only in the domain $\mathcal{S}_{d2}$, which appears in the phase diagrams shown in Fig. 14, that is off the hole-particle symmetry plain, the situation is not that simple. In $\mathcal{S}_{d2}$ one can distinguish two classes, $\mathcal{S}_{d2a}$ and $\mathcal{S}_{d2b}$, of periodic configurations with parallelogram elementary cells. A configuration in $\mathcal{S}_{d2a}$ consists of vertical (horizontal) dimers of filled sites that form a square lattice, where the sides of the elementary squares have the length $2\sqrt{2}$ and the slope ± 1. In a configuration of $\mathcal{S}_{d2b}$, the elementary parallelograms formed by dimers have the sides of the length $2\sqrt{2}$ and the slope ± 1, and the sides of the length $\sqrt{10}$ and the slope $\pm 1/3$. Two configurations, one from $\mathcal{S}_{d2a}$ and one from $\mathcal{S}_{d2b}$, having the same kind of dimers (vertical or horizontal), can be merged together along a "defect line" of the slope ± 1 (dashed line in Fig. 15), as shown in Fig. 15, without increasing the energy. By introducing more defect lines one can construct many ground-state configurations whose number scales with the size of the lattice as $\exp(const\sqrt{\Lambda})$. While for a finite lattice all the configurations are periodic, many of them become aperiodic in the infinite volume limit.

As mentioned above, except $\mathcal{S}_{d2}$ all the other sets $\mathcal{S}_D$ contain exclusively periodic configurations. The set $\mathcal{S}_{pcb}$ (of plaquette-chessboard configurations) contains configurations built out of elementary plaquettes with filled sites, forming a square lattice according to the same rules as filled sites form a square lattice in the chessboard configurations from $\mathcal{S}_{cb}$. The remaining sets $\mathcal{S}_D$ consist of configurations that have a quasi-one-dimensional structure. That is, they are built out of completely filled and completely empty lattice lines of given slope. Such a configuration can be specified by the slope of the filled lattice lines of the representative configuration and the succession of filled (f) and empty (e) consecutive lattice lines in a period. For instance, the representative configuration of $\mathcal{S}_{d1}$ (see Fig. 15) is built out of filled lines with the slope 2 and, in the period, two consecutive filled lines are followed by two consecutive empty lines, which is denoted $(2; 2f, 2e)$. Similar description of the remaining quasi-one-dimensional configurations is given in Fig. 15.

The coefficients $\{\alpha_i\}$ for which the fourth order potentials, $(H_T^{fermion})^{(4)} + K_T^{(4)}$ and $(H_T^{boson})^{(4)} + K_T^{(4)}$, become m-potentials are given in the tables collected in the Appendix

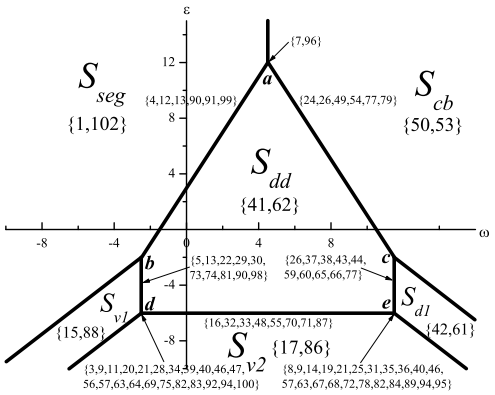

Figure 11: The $(\mu = 0)$-phase diagram of the effective Hamiltonian $(H_{\rm eff}^{fermion})^{(4)}$. The numbers in curly brackets, displayed by the symbols of open domains $\mathcal{S}_D$, denote the T-plaquette configurations that minimize the m-potential in $\mathcal{S}_D$. The numbers in curly brackets, displayed by the boundary-line segments or by the arrows pointing towards boundary segments (or their crossing points) identify the additional minimizing T-plaquette configurations. For more comments see the text. The boundary-line segments can be determined by means of their intersection points: $\mathbf{a} = (9/2, 12)$, $\mathbf{b} = (-5/2, -2)$, $\mathbf{c} = (23/2, -2)$, $\mathbf{d} = (-5/2, -6)$, $\mathbf{e} = (23/2, -6)$, and by the slope 1 of the boundary of $\mathcal{S}_{v1}$, and the slope -1 of the boundary of $\mathcal{S}_{d1}$.

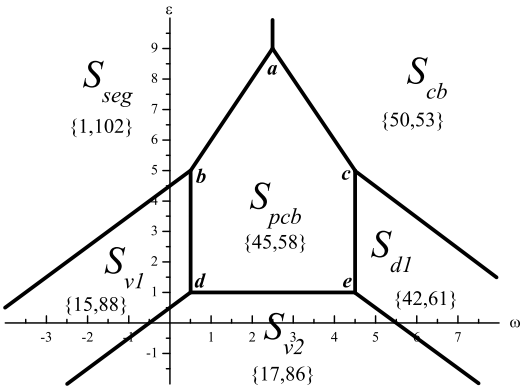

Figure 12: The $(\mu = 0)$-phase diagram of the effective Hamiltonian $(H_{\rm eff}^{boson})^{(4)}$. The boundary-line segments can be determined by means of their intersection points: $\mathbf{a} = (5/2, 9)$, $\mathbf{b} = (1/2, 5)$, $\mathbf{c} = (9/2, 5)$, $\mathbf{d} = (1/2, 1)$, $\mathbf{e} = (9/2, 1)$, and by the slope 1 of the boundary of $\mathcal{S}_{v1}$, and the slope -1 of the boundary of $\mathcal{S}_{d1}$. For more explanations see the description of Fig. 11.

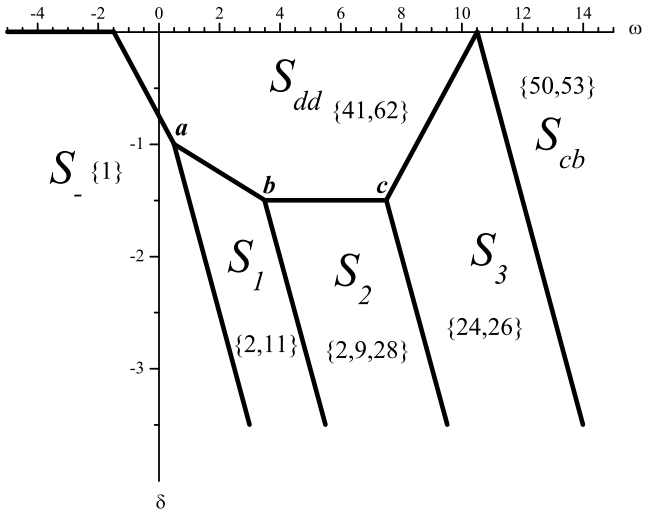

Figure 13: The ($\varepsilon = 0$)-phase diagram of the effective Hamiltonian $(H_{\rm eff}^{fermion})^{(4)}$. The boundary-line segments can be determined by means of their intersection points: $\mathbf{a} = (1/2, -1)$, $\mathbf{b} = (7/2, -3/2)$, $\mathbf{c} = (15/2, -3/2)$, and by the slope -1 of the boundaries of $\mathcal{S}_1$, $\mathcal{S}_2$, $\mathcal{S}_3$. For more comments see the description of Fig. 11.

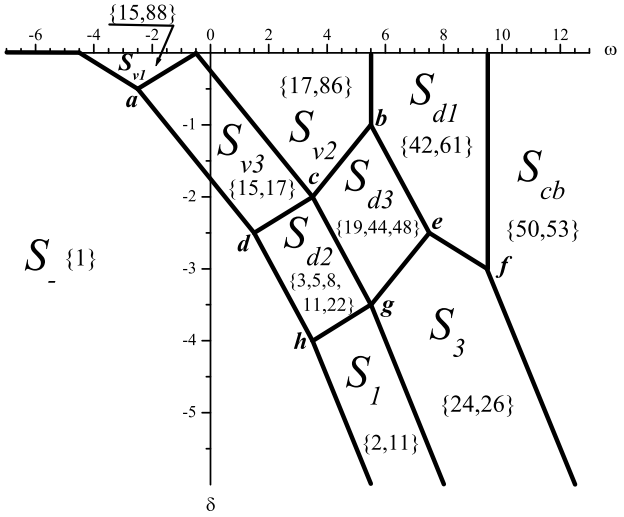

Figure 14: The ($\varepsilon = 0$)-phase diagram of the effective Hamiltonian $(H_{\rm eff}^{boson})^{(4)}$. The boundary-line segments can be determined by means of their intersection points: $\mathbf{a} = (-5/2, -1/2)$, $\mathbf{b} = (11/2, -1)$, $\mathbf{c} = (7/2, -2)$, $\mathbf{d} = (3/2, -5/2)$, $\mathbf{e} = (15/2, -5/2)$, $\mathbf{f} = (19/2, -3)$, $\mathbf{g} = (11/2, -7/2)$, $\mathbf{h} = (7/2, -4)$, and by the slope -1 of the boundaries of $\mathcal{S}_1$ and $\mathcal{S}_3$. For more comments see the description of Fig. 11

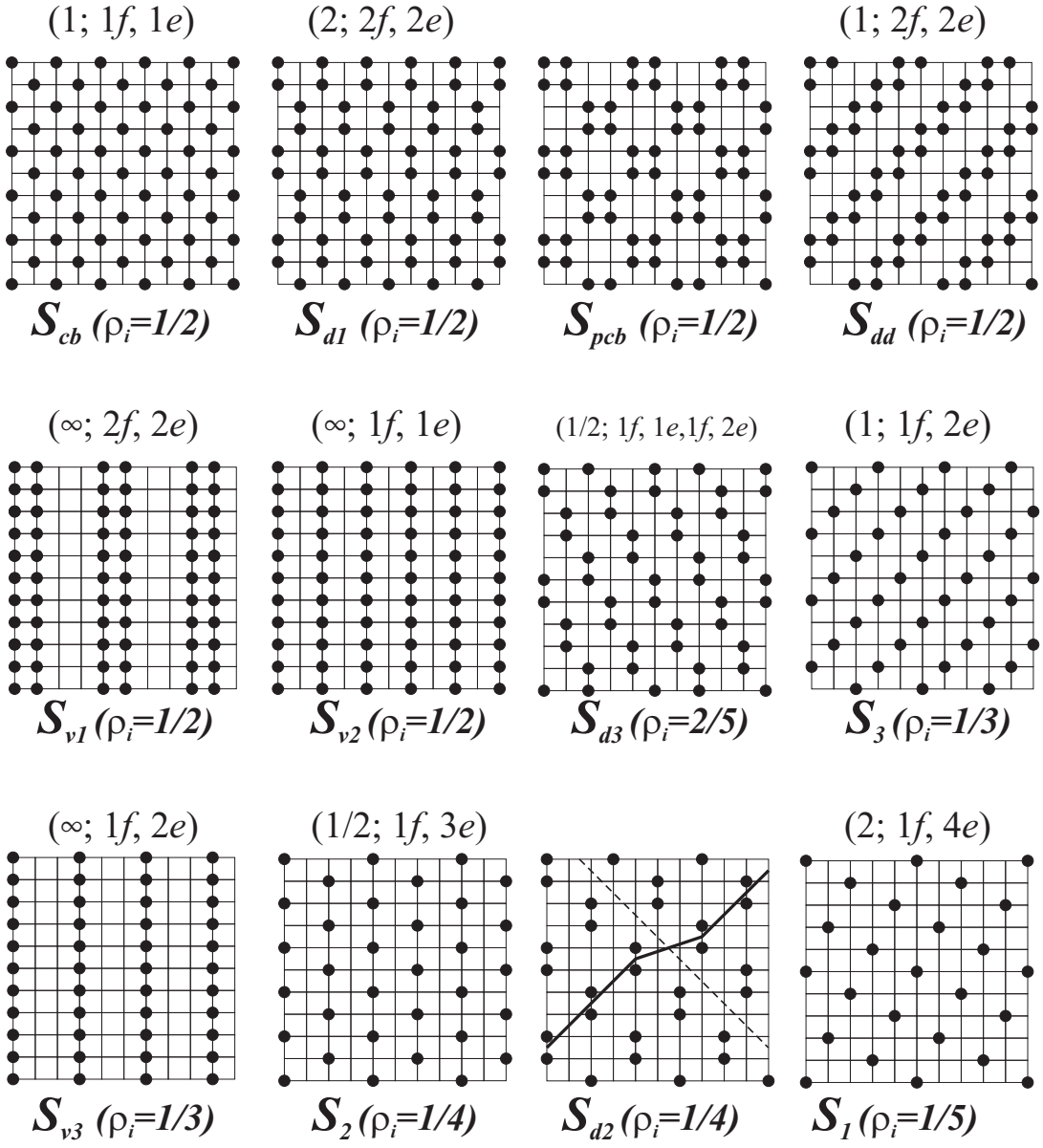

Figure 15: Representative configurations of the sets $\mathcal{S}_D$ of ground-state configurations. The remaining configurations of $\mathcal{S}_D$ can be obtained by applying the symmetries of H to the displayed configurations. As a representative configuration of $\mathcal{S}_{d2}$, we show a configuration with one defect line (the dashed line). The continuous line is a guide for the eye. For more comments see the text.

E (Tables 8–11).

Finally, a remark concerning ground-state configurations at the boundaries between the open domains $\mathcal{S}_D$ is in order. Let $\mathcal{S}_D$ and $\mathcal{S}_{D'}$ be two domains of the considered phase diagram, sharing a boundary. At this boundary, the set of the minimizing T-plaquette configurations contains always the subset $\mathcal{S}_{TD} \cup \mathcal{S}_{TD'}$, but it may contain also some additional T-plaquette configurations of minimal energy. Consequently, the set of the ground-state configurations at the boundary contains always the subset $\mathcal{S}_D \cup \mathcal{S}_{D'}$ and typically a great many of other ground-state configurations, whose number grows indefinitely with the size of the lattice. In the considered diagrams, the only exception is the boundary between $\mathcal{S}_{seg}$ and $\mathcal{S}_{cb}$, where the set of the ground-state configurations amounts exactly to $\mathcal{S}_{seg} \cup \mathcal{S}_{cb}$.

3.4 Discussion of phase diagrams

We start with a few comments concerning the phase diagrams due to the fourth order effective interactions. In the fourth order effective interaction, the parameters ω and ε control the strength of n.n. and n.n.n. interactions, respectively. The n.n. interaction is repulsive and favors the chessboard configurations if $\omega > 9/2$, for fermions ($\omega > 5/2$, for bosons). In the opposite case (attraction) it favors the S_+, S_- configurations. In turn, the n.n.n. interaction is attractive if $\varepsilon > 3$, for fermions ($\varepsilon > 5$, for bosons), and then it reinforces the tendency towards chessboard and uniform, S_+, S_-, configurations. When it becomes repulsive, it frustrates the n.n. interaction: the more negative it is the larger ω is needed to stabilize the chessboard configurations and the smaller ω is needed to stabilize the S_+, S_- configurations. Therefore, whatever the value of ε is, there is a sufficiently large ω such that $(\varepsilon, \omega) \in \mathcal{S}_{cb}$ and a sufficiently small ω such that $(\varepsilon, \omega) \in \mathcal{S}_{seg}$.

Apparently, the fourth order phase diagrams in the cases of hopping fermions and hopping bosons are quite similar if we compare the geometry of the phase boundaries and the sets of ground states. The main difference is in the domain occupying the central position: in the case of fermions the ground-state configurations are diagonal-stripe configurations, $\mathcal{S}_{dd}$, while in the case of bosons this is the set $\mathcal{S}_{pcb}$ of plaquette-chessboard configurations. These two sets of configurations are ground-state configurations of the corresponding fourth-order effective interactions with the site, n.n., and n.n.n. terms dropped, which corresponds to the points $(9/2, 3) \in \mathcal{S}_{dd}$ and $(5/2, 5) \in \mathcal{S}_{pcb}$. This means that the fourth order phase diagrams can be looked upon as the result of perturbing an Ising-like Hamiltonian, that consists of pair interactions at distance of two lattice constants and plaquette interactions, by n.n. and n.n.n. interactions. More generally, it is easy to verify that the set of ground-state configurations of the Ising-like Hamiltonian,

$$\sum_{\langle x,y\rangle_3} s_x s_y + \chi \sum_{P_2} s_{P_2}, \tag{87}$$

amount to $\mathcal{S}_{dd}$ if $\chi > 0$, and to $\mathcal{S}_{pcb}$ if $\chi < 0$. These ground states are stable with respect to perturbations by n.n. and n.n.n. interactions, if the corresponding interaction constants are in a certain vicinity of zero. Otherwise, new sets of ground states, shown in Fig. 11 and Fig. 12 emerge.

The basic question to be answered, before discussing the phase diagrams due to the complete interaction, refers to the relation between these phase diagrams and the

diagrams due to the truncated effective interactions, obtained in the previous section.

Firstly, we note, by inspection of the phase boundaries in Fig. 11 and Fig. 12, that the T-plaquette configurations $\{45, 58\}$ are missing in the phase diagram corresponding to fermion mobile particles. In turn, the T-plaquette configurations $\{41, 62\}$ are missing in the phase diagram corresponding to boson mobile particles. Consequently, the ground-state configurations of $\mathcal{S}_{pcb}$ cannot appear not only in the fourth order fermion phase diagram but also in the fermion phase diagram of the complete interaction. Similarly, the ground-state configurations of $\mathcal{S}_{dd}$ do not appear in boson phase diagrams.

Secondly, by adapting the arguments presented in [59, 40], we can demonstrate, see for instance [61], that if the remainder $R^{(4)}$ is taken into account, then there is a (sufficiently small) constant t_0 such that for $t < t_0$ the phase diagram looks the same as the phase diagram due to the effective interaction truncated at the fourth order, except some regions of width $O(t^6)$, located along the boundaries between the domains, and except the domain $\mathcal{S}_{d2}$. For $t < t_0$ and each domain $\mathcal{S}_D$, $\mathcal{S}_D \neq \mathcal{S}_{d2}$, there is a nonempty two-dimensional open domain $\mathcal{S}_D^\infty$ that is contained in the domain $\mathcal{S}_D$ and such that in $\mathcal{S}_D^\infty$ the set of ground-state configurations coincides with $\mathcal{S}_D$.

Now, consider our systems for specified particle densities, $\rho_e = \rho_i = 1/2$. According to the phase diagrams in the hole-particle symmetry plane ($\mu = \delta = 0$), shown in Fig. 11 and Fig. 12, if (ε, ω) is in $\mathcal{S}_{seg}^\infty$, then the ground state is a phase-separated state, where ion configurations are mixtures of S_+ and S_- configurations, called the segregated phase. Another phase-separated state, where the ion configurations are mixtures of S_+, S_-, S_{cb}^e, and S_{cb}^o configurations, exists at a line that is a small ($O(t^2)$) distortion of the boundary between the domains $\mathcal{S}_{seg}$ and $\mathcal{S}_{cb}$ [62]. In all the other domains $\mathcal{S}_D^\infty$ of these diagrams the ground-state phase exhibits a crystalline long-range order of ions.

By the properties of the fourth order phase diagrams, whatever the value of ε is, there is a sufficiently large ω such that the systems are in the chessboard phase ($(\varepsilon, \omega) \in \mathcal{S}_{cb}^\infty$) and a sufficiently small ω such that the systems are in the segregated phase ($(\varepsilon, \omega) \in \mathcal{S}_{seg}^\infty$). In between, the systems undergo a series of phase transitions and visit various striped phases. Consider first unbiased systems ($\varepsilon = 0$). Then, it follows from the phase diagram in Fig. 11, that the fermion system visits necessarily the diagonal striped phase, described by the configurations in $\mathcal{S}_{dd}$. In turn, the phase diagram in Fig. 12 implies that the boson system has to visit the dimerized-chessboard phase, described by the configurations in $\mathcal{S}_{d1}$, then the vertical/horizontal striped phase, described by the configurations in $\mathcal{S}_{v2}$, and after that a dimerized vertical/horizontal striped phase, described by the configurations in $\mathcal{S}_{v1}$. These scenarios are preserved, if $\varepsilon \in (-2 + O(t^2), 12 - O(t^2))$ in the fermion case, and $\varepsilon \in (-\infty, 1 - O(t^2))$ in the boson case.

Note that the same sequence of transitions, as found in the unbiased boson system, can be realized by the fermion system if ε is sufficiently small ($\varepsilon < -6 - O(t^2)$).

For somewhat larger values of ε, $\varepsilon \in (-6 + O(t^2), -2 - O(t^2))$, on its way from the chessboard phase to the segregated phase the fermion systems visits the dimerized chessboard phase, then the diagonal striped phase, and after that the dimerized vertical/horizontal striped phase. The vertical/horizontal striped phase is closer to the segregated phase than the diagonal striped phase. In case the both kinds of stripe phases (vertical/horizontal and diagonal) appear in a phase diagram, such a succession of striped phases is perhaps generic, see also [20, 63].

For sufficiently large ε, the tendency toward the chessboard and the uniform config-

urations is so strong that the both systems jump directly from the chessboard phase to the segregated phase.

Above, we have described the states of the considered systems for typical values of the control parameter ω. Only in small intervals (whose width is of the order of $O(t^2)$) of values of ω, about the transition points of the diagrams in Fig. 11 and Fig. 12, the states of the systems remain undetermined.

For completeness we present also ground-state phase diagrams of the both systems off the hole-particle symmetry plane, for $\varepsilon = 0$, see Fig. 13, 14. Away from the hole-particle symmetry plane new phases appear. In particular we find the phases described by the quasi-one-dimensional configurations $\mathfrak{S}_1$, $\mathfrak{S}_2$, and $\mathfrak{S}_3$, well known from the studies of the phase diagram of the spinless Falicov–Kimball model [40]. In the boson phase diagram, Fig. 14, there appears the domain $\mathfrak{S}_{d2}$ that is not amenable to the kind of arguments used in this thesis.

4 Influence of nearest-neighbor anisotropy on axial striped phases

In this Section[2] we show that any anisotropy of nearest-neighbor hopping eliminates the $\pi/2$-rotation degeneracy of the dimeric and axial-stripe phases and orients them in the direction of a weaker hopping. Moreover, due to the same anisotropy the obtained phase diagrams of fermions show a tendency to become similar to those of hardcore bosons.

4.1 The effective interaction up to the fourth order

We consider the model similar to (73): only a n.n. hopping is taken into account and we allow for its anisotropy. We set $t_h \equiv t$, and $t_v = \sqrt{\gamma}t$, with $0 \leq \gamma \leq 1$. In this case, up to a term independent of the ion configurations and the chemical potentials, the ground-state energy expansion (43) reads:

$$\begin{aligned}
E_S^f(\mu) &= \left(E_S^f\right)^{(4)}(\mu) + \left(R_S^f\right)^{(4)}, \\
\left(E_S^f\right)^{(4)}(\mu) &= -\frac{\mu}{2}\sum_x (s_x+1) + \left[\frac{t^2}{4} - \frac{3t^4}{16} - \frac{3}{8}\gamma t^4 + \frac{W}{8}\right]\sum_{\langle x,y\rangle_{1,h}} s_x s_y + \\
&+ \left[\gamma\frac{t^2}{4} - \frac{3}{8}\gamma t^4 - \gamma^2\frac{3t^4}{16} + \frac{W}{8}\right]\sum_{\langle x,y\rangle_{1,v}} s_x s_y + \left[\gamma\frac{3t^4}{16} - \frac{\tilde{\varepsilon}}{16}\right]\sum_{\langle x,y\rangle_2} s_x s_y + \\
&+ \frac{t^4}{8}\sum_{\langle x,y\rangle_{3,h}} s_x s_y + \gamma^2\frac{t^4}{8}\sum_{\langle x,y\rangle_{3,v}} s_x s_y + \gamma\frac{t^4}{16}\sum_{P_2}(1+5s_{P_2}),
\end{aligned} \tag{88}$$

in the case of hopping fermions, and

$$\begin{aligned}
E_S^b(\mu) &= \left(E_S^b\right)^{(4)}(\mu) + \left(R_S^b\right)^{(4)}, \\
\left(E_S^b\right)^{(4)}(\mu) &= -\frac{\mu}{2}\sum_x (s_x+1) + \left[\frac{t^2}{4} - \frac{3t^4}{16} - \frac{1}{8}\gamma t^4 + \frac{W}{8}\right]\sum_{\langle x,y\rangle_{1,h}} s_x s_y + \\
&+ \left[\gamma\frac{t^2}{4} - \frac{1}{8}\gamma t^4 - \gamma^2\frac{3t^4}{16} + \frac{W}{8}\right]\sum_{\langle x,y\rangle_{1,v}} s_x s_y + \left[\gamma\frac{5t^4}{16} - \frac{\tilde{\varepsilon}}{16}\right]\sum_{\langle x,y\rangle_2} s_x s_y + \\
&+ \frac{t^4}{8}\sum_{\langle x,y\rangle_{3,h}} s_x s_y + \gamma^2\frac{t^4}{8}\sum_{\langle x,y\rangle_{3,v}} s_x s_y - \gamma\frac{t^4}{16}\sum_{P_2}(5+s_{P_2}),
\end{aligned} \tag{89}$$

in the case of hopping hardcore bosons. As previously, the remainders, $\left(R_S^f\right)^{(4)}$ and $\left(R_S^b\right)^{(4)}$, are independent of the chemical potentials and the parameters W and $\tilde{\varepsilon}$, but in this case, they depend on γ, and collect those terms of the expansions that are proportional to t^{2m}, with $m = 3, 4, \ldots$. The expressions (88) and (89) refer to (75) and (76) for $\gamma = 1$, respectively.

In the previous Section we have obtained the ground-state phase diagrams, according to the fourth-order isotropic effective Hamiltonians ($\gamma = 1$), for hole-particle symmetric

[2]This section is based on [29].

systems ($\mu = 0$) with a weak (of fourth order) n.n.n. subsidiary interaction, and for unsymmetrical systems without the subsidiary interaction ($\tilde{\varepsilon} = 0$), see the top phase diagrams in Figs. 11-14. Second-order phase diagrams of the isotropic case consist exclusively of phases whose configurations are invariant with respect to $\pi/2$-rotations, with *macroscopic degeneracies* (i.e. the number of configurations grows exponentially with the number of sites) at the boundaries of phase domains. Stripe phases, whose configurations are not invariant with respect to $\pi/2$-rotations, appear on perturbing the second-order phase diagrams by the fourth-order isotropic interactions. Here, we would like to observe the influence of a weak anisotropy of n.n. hopping on these stripe phases. Since we are working with truncated effective Hamiltonians, we have to assign an order to the deviation of the anisotropy parameter γ from the value 1 (corresponding to the isotropic case). Therefore, we introduce an anisotropy order, a, and a new anisotropy parameter, β_a:

$$\gamma = 1 - \beta_a t^a. \tag{90}$$

The orders of the deviations can be neither too small, not to modify the second-order effective Hamiltonians, nor too high, to effect the considered effective Hamiltonian of the highest order. Since here, the highest order of the effective Hamiltonians is $k = 4$, the weakest admissible deviation from the isotropic case corresponds to the highest anisotropy order $a = 2$. Then, we can consider an intermediate deviation, i.e. $0 < a < 2$. The strongest deviation, i.e. $a = 0$, is not admissible, since it modifies the second-order effective Hamiltonians.

4.2 The smallest deviation from the isotropic case

In the sequel, we drop the arguments of ground-state energies, that is we set $\left(E_S^f\right)^{(4)}(\mu) \equiv \left(E_S^f\right)^{(4)}$, etc. In the case of the smallest deviation from the isotropic case the fourth-order effective Hamiltonian for fermions reads:

$$\left(E_S^f\right)^{(4)} = \left(E_S^f\right)^{(4)}\Big|_{\gamma=1} - \beta_2 \frac{t^4}{4} \sum_{\langle x,y\rangle_{1,v}} s_x s_y, \tag{91}$$

while for hardcore bosons only the first term, representing the isotropic fourth-order effective Hamiltonian, has to be changed properly.

Apparently, the effective Hamiltonians of order zero and two are isotropic, and there is no difference between the cases of hopping fermions and hopping bosons (see Figs. 9, 10). To observe the effect of the fourth-order anisotropy term of (91) the construction of the fourth-order diagrams has to be carried out again. As in the isotropic case, this is facilitated by introducing new variables, ω, δ, and ε given by (81), and rewriting the fourth order effective Hamiltonian in the form,

$$\left(E_S^f\right)^{(4)} = \frac{t^4}{2} \sum_T \left(H_T^f\right)^{(4)}, \tag{92}$$

where

$$\left(H_T^f\right)^{(4)} = \left(H_T^f\right)^{(4)}\Big|_{\gamma=1} - \frac{\beta_2}{12} \sum_{\langle x,y\rangle_{1,v}}'' s_x s_y, \tag{93}$$

with analogous expressions in the bosonic case, and with the isotropic potentials $\left(H_T^f\right)^{(4)}\Big|_{\gamma=1}$, $\left(H_T^b\right)^{(4)}\Big|_{\gamma=1}$ given by (84) and (85), respectively.

We would like to get an idea of the phase diagram in the space of the four energy parameters $(\omega, \varepsilon, \beta_2, \delta)$, that appear in the Hamiltonian. Due to the fact that the domains occupied by the phases are polyhedral sets, this goal can be achieved by studying phase diagrams in two-dimensional hyperplanes. Of particular interest are those hyperplanes that result from intersecting the four-dimensional space by hyperplanes $\delta = 0$ and $\beta_2 = const$, and by hyperplanes $\varepsilon = 0$ and $\beta_2 = const$. A collection of such sections for suitable values of β_2, forming a finite increasing from zero sequence, enable us to observe how the anisotropy effects our system if it is hole-particle symmetric and if it is not, respectively.

Specifically, in Fig. 16 we show phase diagrams in the hole-particle-symmetric case, while in the absence of the hole-particle symmetry, the phase diagrams are shown in Fig. 17 – for fermions, and in Fig. 18 – for bosons.

The phases that appear in these phase diagrams can conveniently be described in terms of the phases found in ground-state phase diagrams of the isotropic systems, with Hamiltonian H given by (73) (see Fig. 15). The phases of anisotropic systems, considered here, either coincide with or are simple modifications of the isotropic phases. In fact, in Fig. 15 only representative configurations of the phases of isotropic systems are displayed. The remaining configurations can be obtained by means of the spatial symmetry operations of isotropic Hamiltonian, like translations and rotations by $\pi/2$. The numbers in curly brackets, placed by the symbols of phases, stand for the numbers of the T-plaquette configurations (according to Fig. 30) that are obtained by restricting the configurations of a phase to a T-plaquette. By the same symbols as the phases we denote also their domains.

Among the phases of isotropic systems, we can distinguish a class of *dimeric phases*, $\mathfrak{S}_{d1}$, ..., $\mathfrak{S}_{d4}$, and a class of *axial-stripe phases*, $\mathfrak{S}_{v1}$, $\mathfrak{S}_{v2}$, and $\mathfrak{S}_{v3}$. The configurations of dimeric phases consist of isolated pairs of n.n. occupied sites (in the sequel called *the dimers*). In the configurations of axial-stripe phases, the ions fill completely some, parallel to one of the axes, lattice lines, so that a periodic pattern of *stripes* is formed. Out of the dimeric or axial-stripe configurations of Fig. 15, only those with dimers or stripes, respectively, oriented vertically appear in the phase diagrams of anisotropic systems. Such a restricted phases are marked in anisotropic phase diagrams by the additional superscript, v.

In comparison with the isotropic phase, a new domain $\mathfrak{S}_{d4}$ appears in the phase diagrams shown in Fig. 17. Similarly to $\mathfrak{S}_{d2}$, its degeneracy grows indefinitely with the size of the lattice. This phase consists of three classes of periodic configurations of dimers. In the class $\mathfrak{S}_{d4a}$, the elementary cell can be chosen as a parallelogram whose two sides of length 3 are parallel to dimers (which are vertical or horizontal). If the dimers are oriented vertically, then the other two sides have the slope $1/2$ and the length $\sqrt{5}$. By reflecting an elementary cell of $\mathfrak{S}_{d4a}$ in a lattice line passing through its side that is parallel to dimers, we obtain an elementary cell of the class $\mathfrak{S}_{d4b}$. In the third class, $\mathfrak{S}_{d4c}$, an elementary cell can be chosen as a rhomb formed by the centers of dimers, with the sides of length $\sqrt{10}$. Two configurations, one from $\mathfrak{S}_{d4a}$ and one from $\mathfrak{S}_{d4b}$, having the same kind of dimers (vertical or horizontal), can be merged together along a "defect line"

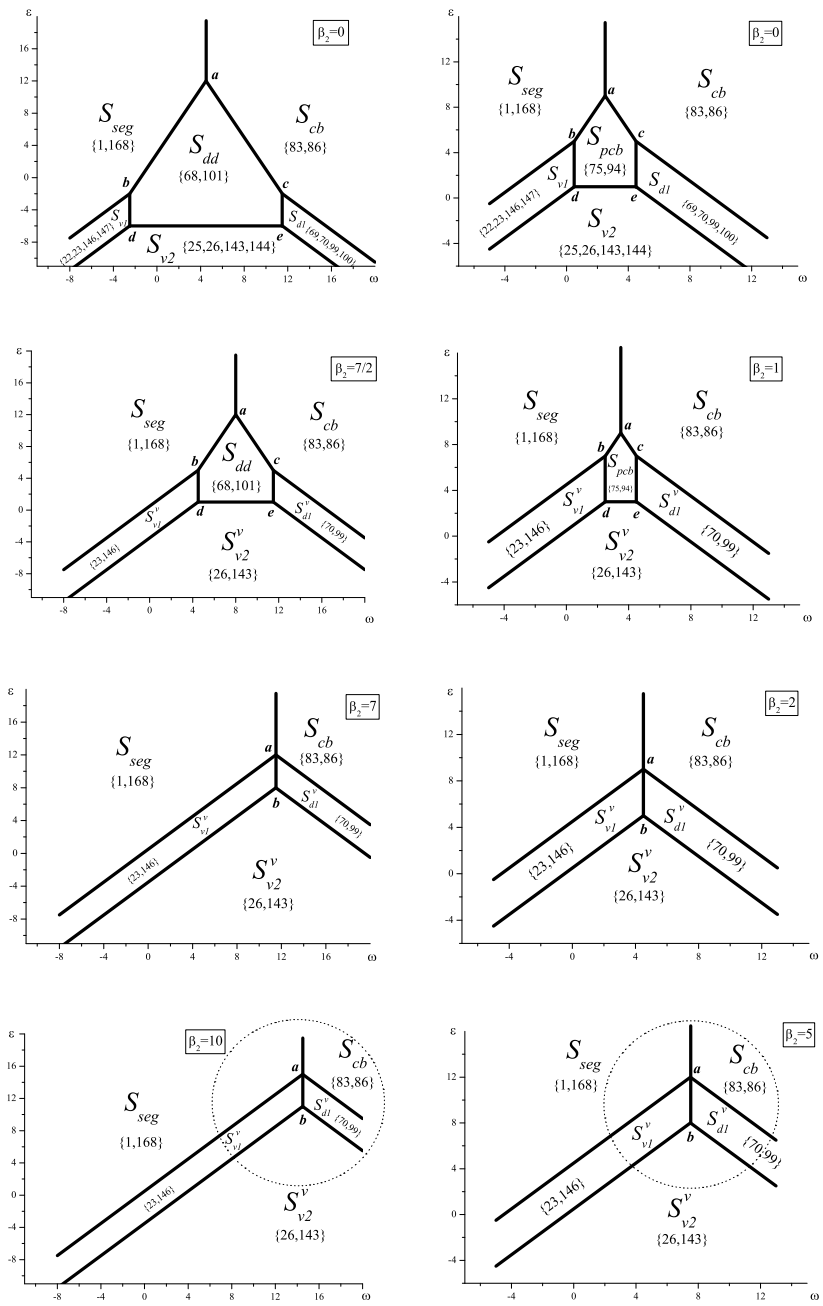

Figure 16: The case of the weakest anisotropy and of hole-particle symmetric systems ($\mu = 0$). Phase diagrams of $\left(H_T^f\right)^{(4)}$ (given by (93)) — left column, and $\left(H_T^b\right)^{(4)}$ — right column, for an increasing sequence of values of β_2. The representative ion configurations of the displayed phases are shown in Fig. 15 (for more comments see text). For fermions, the critical value is $\beta_2 = 7$, while for bosons it is $\beta_2 = 2$. The equations defining the boundary lines of the phase domains are given in Tab. 1 and Tab. 2 of Appendix D, while the corresponding zero-potential coefficients $\{\alpha_i\}$ — in Tab. 12 – Tab. 19 of Appendix E. In the bottom diagrams, the regions surrounded by dotted circles, are reconsidered in the case of an intermediate anisotropy.

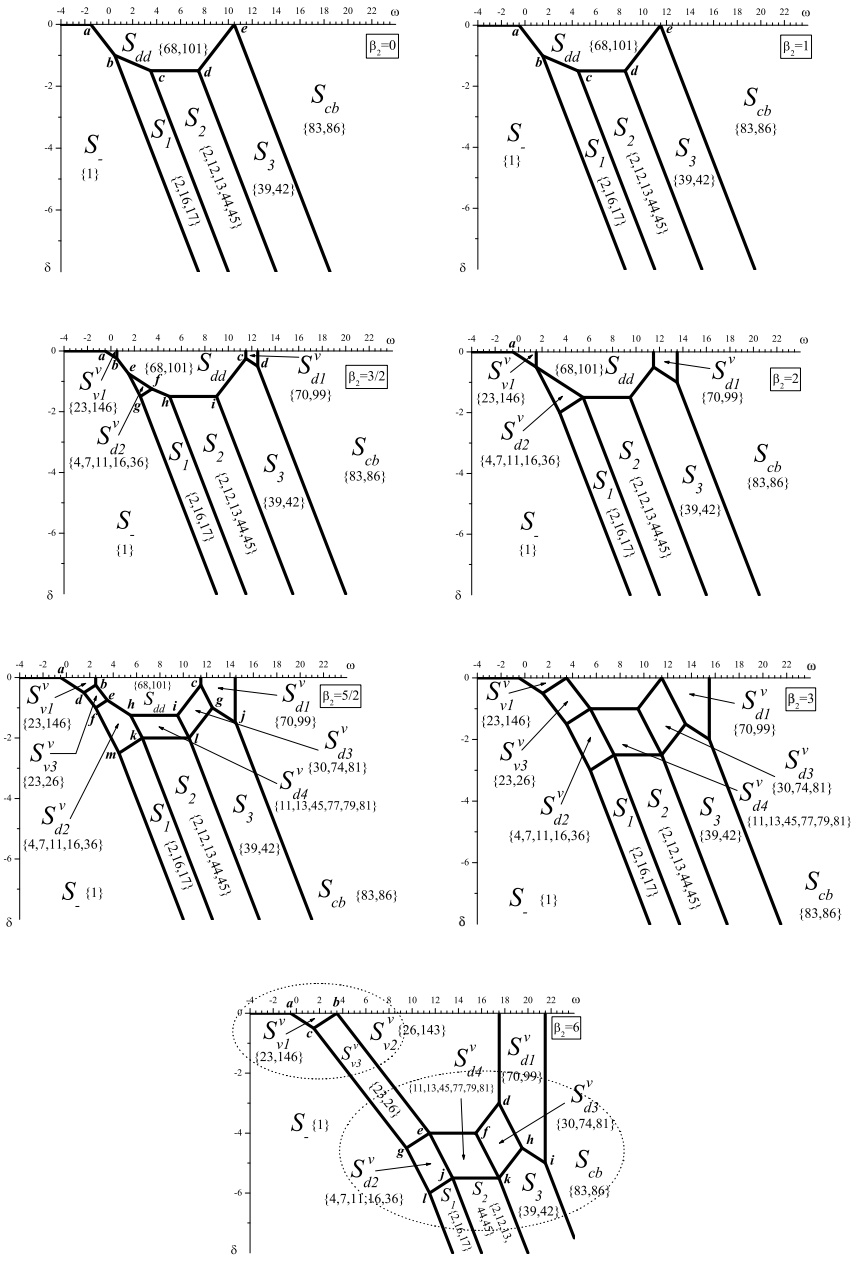

Figure 17: The case of the weakest anisotropy, off the hole-particle symmetry, with $\varepsilon = 0$. The phase diagram of $\left(H_T^f\right)^{(4)}$ (given by (93)) for an increasing sequence of values of β_2. The representative ion configurations of the displayed phases are shown in Fig. 15 (for more comments see text). The critical values are: $\beta_2 = 1$, $\beta_2 = 2$, and $\beta_2 = 3$. In the blank region of the phase diagram for the critical $\beta_2 = 3$, the following T-plaquette configurations have the minimal energy: 26,52,53,68,81,88,101,116,117,143 (see Fig. 30). By means of these T-plaquette configurations one can construct $\mathcal{S}^v_{v2}$, $\mathcal{S}_{dd}$, and many other configurations. The equations defining the boundary lines of the phase domains are given in Tab. 3 of Appendix D, while the corresponding zero-potential coefficients $\{\alpha_i\}$ — in Tab. 20 – Tab. 26 of Appendix E. In the bottom diagram, the regions surrounded by dotted ellipses are reconsidered in the case of an intermediate anisotropy.

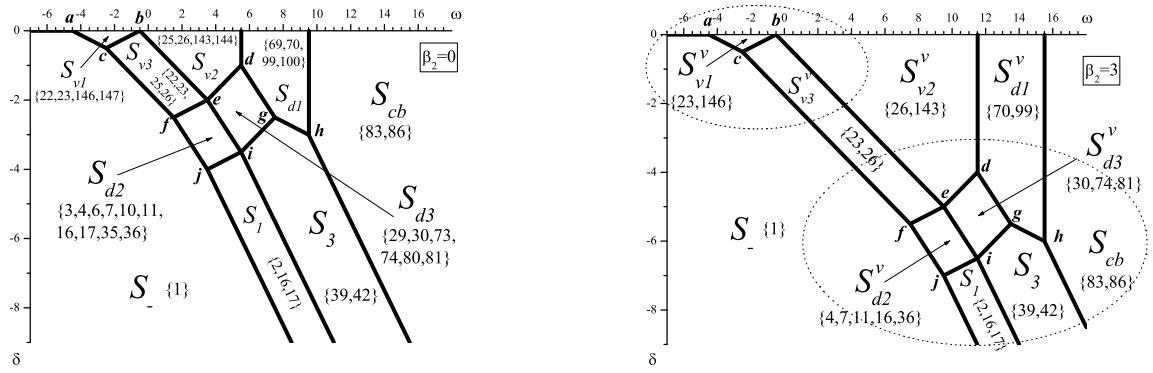

Figure 18: The case of the weakest anisotropy, off the hole-particle symmetry, with $\varepsilon = 0$. The phase diagram of $(H_T^b)^{(4)}$ (given by (93)); the isotropic diagram ($\beta_2 = 0$) and the anisotropic diagram ($\beta_2 = 3$). The representative ion configurations of the displayed phases are shown in Fig. 15 (for more comments see text). Here, no critical values have been detected. The equations defining the boundary lines of the phase domains are given in Tab. 4 of Appendix D, while the corresponding zero-potential coefficients $\{\alpha_i\}$ — in Tab. 27 and Tab. 28 of Appendix E. In the right diagram, the regions surrounded by dotted ellipses are reconsidered in the case of an intermediate anisotropy.

parallel to dimers (dashed line in Fig. 19) without increasing the energy. In this way, a numerous family of configurations can be constructed, with the number of configurations growing like $\exp(const\sqrt{\Lambda})$.

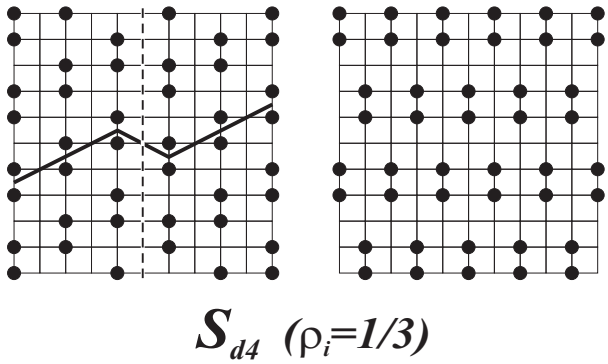

Figure 19: The representative configurations of the set $\mathcal{S}^v_{d4}$ whose degeneracy grows like $\exp(const\sqrt{\Lambda})$. The left configuration is an example of configurations with defect lines. Here, there is one defect line (the dashed line, the continuous line is a guide for the eye): the vertical lattice line separating a periodic configuration of vertical dimers from its vertical translate by one lattice constant. The right configuration is a periodic configuration of dimers. For more comments see text.

It follows from the polyhedral shape of the phase domains, that the set of values of β_2 is partitioned into open intervals, where the boundary lines of phase domains do not change their direction, only their distance to the origin varies in an affine way. The boundary points of these open intervals are special values of the anisotropy for the phase diagrams, and in the sequel we call them *the critical values*. As a critical value of anisotropy is approached, some boundary lines merge into a line or a point, which results in disappearance of some phase domains. And vice versa, some points and lines break off, creating new phase domains.

In particular, in the hole-particle symmetric case it can be inferred from (Fig. 16) that at least up to $\beta_2 = 10$ – for hopping fermions, and at least up to $\beta_2 = 5$ – for hardcore

bosons, there is only one critical value of β_2. For fermions, it amounts to $\beta_2 = 7$, where the phase $\mathfrak{S}_{dd}$ disappears, while for hardcore bosons it is $\beta_2 = 2$, where the phase $\mathfrak{S}_{pcb}$ disappears.

Off the hole-particle symmetry, for bosons, there are no critical values of β_2, at least up to $\beta_2 = 3$. On the other hand, for fermions and for $\beta_2 \leq 6$ there are as many as three critical values of β_2. In increasing order, the first is $\beta_2 = 1$, where the phases $\mathfrak{S}^v_{v1}$, $\mathfrak{S}^v_{d1}$, and $\mathfrak{S}^v_{d2}$ appear. The second is $\beta_2 = 2$, where the phases $\mathfrak{S}^v_{d3}$, $\mathfrak{S}^v_{d4}$, and $\mathfrak{S}^v_{v3}$ appear. And the last one is $\beta_2 = 3$, where $\mathfrak{S}_{dd}$ is replaced by $\mathfrak{S}^v_{v2}$.

If there are no more critical values of the anisotropy parameter β_2, the shape of the fourth-order phase diagrams for any value β_2 larger than the greatest considered in Figs. 16, 17, 18 remains the same. On increasing the anisotropy parameter, the diagrams undergo only some translations. To verify whether for the values of β_2 larger than those considered in this section new critical values do appear, we proceed to investigating stronger, i.e. intermediate, deviations from the isotropic case.

4.3 The intermediate deviation from the isotropic case

Now, the fourth-order effective Hamiltonian for fermions assumes the form:

$$\left(E^f_S\right)^{(4)} = \left(E^f_S\right)^{(4)}\Big|_{\gamma=1} - \beta_2 \frac{t^{2+a}}{4} \sum_{\langle x,y\rangle_{1,v}} s_x s_y, \tag{94}$$

and for hardcore bosons an analogous formula holds true. Obviously, the phase diagrams in the zeroth and second orders remain the same as in the isotropic case, described above. Therefore, we proceed to constructing the phase diagram in next order, which is $(2+a)$-order with $0 < a < 2$, and the corresponding effective Hamiltonian reads:

$$E^{(2+a)}_S = E^{(2)}_S - \beta_2 \frac{t^{2+a}}{4} \sum_{\langle x,y\rangle_{1,v}} s_x s_y, \tag{95}$$

where $E^{(2)}_S$ stands for the, common for fermions and bosons, second-order effective Hamiltonian. For the reasons given in the previous subsection, we consider a neighborhood of the point $W = -2t^2$, $\mu = 0$, $\tilde{\varepsilon} = 0$, where the energies of all the configurations are equal. In this neighborhood it is convenient to introduce new variables, δ', ε', and ω',

$$\mu = t^{2+a}\delta', \qquad \tilde{\varepsilon} = t^{2+a}\varepsilon', \qquad W = -2t^2 + t^{2+a}\omega', \tag{96}$$

and rewrite the expansion up to the order $2+a$:

$$\begin{aligned} E^{(2+a)}_S &= \frac{t^{2+a}}{2}\left\{-\delta' \sum_x (s_x + 1) + \frac{\omega'}{4} \sum_{\langle x,y\rangle_1} s_x s_y - \frac{\varepsilon'}{8} \sum_{\langle x,y\rangle_2} s_x s_y - \frac{\beta_a}{2} \sum_{\langle x,y\rangle_{1,v}} s_x s_y\right\} \\ &= \frac{t^{2+a}}{2} \sum_{P_2} H^{(2+a)}_{P_2}, \end{aligned} \tag{97}$$

where

$$H^{(2+a)}_{P_2} = -\frac{\delta'}{4} \sum_x{}' (s_x + 1) + \frac{\omega'}{8} \sum_{\langle x,y\rangle_1}{}' s_x s_y - \frac{\varepsilon'}{8} \sum_{\langle x,y\rangle_2}{}' s_x s_y - \frac{\beta_a}{4} \sum_{\langle x,y\rangle_{1,v}}{}' s_x s_y. \tag{98}$$

The summations in the primed sums run over a plaquette P_2. The plaquette potentials $H_{P_2}^{(2+a)}$ have to be minimized over all the plaquette configurations. As in the previous case, we are interested in phase diagrams of hole-particle symmetric systems ($\delta' = 0$) or unsymmetrical systems with $\varepsilon' = 0$. It turns out that for such energy parameters and plaquette configurations the potentials $H_{P_2}^{(2+a)}$ are m-potentials. The resulting phase diagrams are shown in Fig. 20 and Fig. 21. We note that each of the points **a**: $\omega' = \beta_a$,

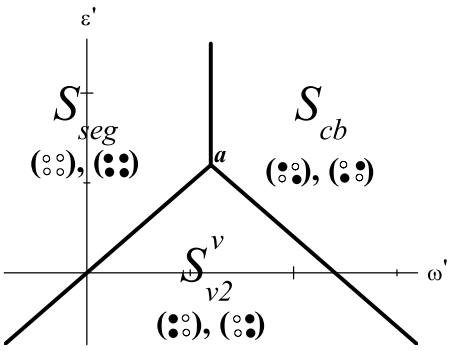

Figure 20: The case of an intermediate anisotropy ($0 < a < 2$) and of hole-particle symmetric systems ($\mu = 0$). The phase diagram (common for hopping fermion and hardcore boson systems) of $H_{P_2}^{(2+a)}$. The coordinates of point **a** are $\omega' = \beta_a$, $\varepsilon' = \beta_a$. The boundary lines of $\mathbb{S}_{v_2}^{v}$, from left to right, are: $\varepsilon' = \omega'$ and $\varepsilon' = -\omega' + 2\beta_a$. The boundary between $\mathbb{S}_{seg}$ and $\mathbb{S}_{cb}$ is $\omega' = \beta_a$.

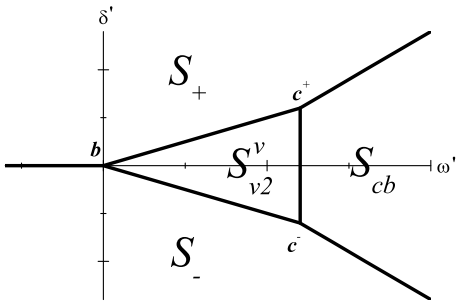

Figure 21: The case of an intermediate anisotropy ($0 < a < 2$), off the hole-particle symmetry, with $\varepsilon' = 0$. The phase diagram (common for hopping fermion and hardcore boson systems) of $H_{P_2}^{(2+a)}$. In the (ω', δ')-plane, $\mathbf{b} = (0, 0)$, $\mathbf{c}^+ = (2\beta_a, \beta_a)$, $\mathbf{c}^- = (2\beta_a, -\beta_a)$. The boundary lines of $\mathbb{S}_-$, from left to right, are: $\delta' = 0$, $\delta' = -\frac{\omega'}{2}$ and $\delta' = -\omega' + \beta_a$. The boundary lines of $\mathbb{S}_+$ are obtained by changing $\delta' \to -\delta'$.

$\varepsilon' = \beta_a$, **b**: $\omega' = 0$, $\delta' = 0$, $\mathbf{c}^-$: $\omega' = 2\beta_a$, $\delta' = -\beta_a$, and $\mathbf{c}^+$: $\omega' = 2\beta_a$, $\delta' = \beta_a$, is the coexistence point of three periodic phases. That is, the only plaquette configurations minimizing the potential $H_{P_2}^{(2+a)}$ at such a point are those obtained by restricting the configurations of coexisting phases to a plaquette (these plaquette configurations are shown in Fig. 20)

Now, following our recursive procedure of constructing phase diagrams to some order, we are ready to investigate the effect of fourth-order interactions. As in earlier steps, it is enough to consider neighborhoods of the coexistence points **a**, **b**, and $\mathbf{c}^-$ of Figs. 20, 21 (the diagram in a neighborhood of $\mathbf{c}^+$ can be obtained from that around $\mathbf{c}^-$ by a symmetry operation).

A. A neighborhood of a

Here $\delta' = 0$, hence the systems are hole-particle invariant. A convenient change of variables is:

$$\omega' = \beta_a + t^{2-a}\omega, \qquad \varepsilon' = \beta_a + t^{2-a}\varepsilon. \tag{99}$$

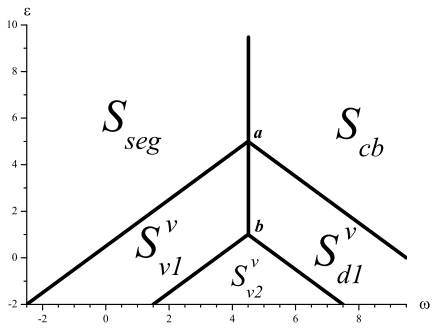

Figure 22: The case of an intermediate anisotropy ($0 < a < 2$) and of hole-particle symmetric systems ($\mu = 0$). The phase diagram of $\left(E^f_S\right)^{(4)}$ in a neighborhood of point **a** ($\omega' = \beta_a$, $\varepsilon' = \beta_a$) (see formula (100)). The equations defining the boundary lines of the phase domains are given in Tab. 5 of Appendix D.

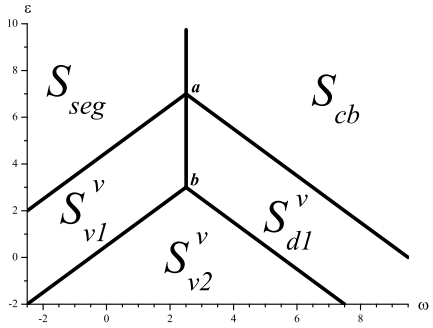

Figure 23: The case of an intermediate anisotropy ($0 < a < 2$) and of hole-particle symmetric systems ($\mu = 0$). The phase diagram of $\left(E^b_S\right)^{(4)}$ in a neighborhood of point **a** ($\omega' = \beta_a$, $\varepsilon' = \beta_a$) (see formula (100)). The equations defining the boundary lines of the phase domains are given in Tab. 5 of Appendix D.

In these variables, the fourth-order effective Hamiltonian reads:

$$\left(E^f_S\right)^{(4)} = \frac{t^{2+a}}{2} \sum_{P_2} H^{(2+a)}_{P_2}\Big|_{\substack{\delta'=0 \\ \varepsilon'=\omega'=\beta_a}} + \frac{t^4}{2} \sum_{T} \left(H^f_T\right)^{(4)}\Big|_{\gamma=1}, \tag{100}$$

with a similar formula for hard-core bosons, where

$$H^{(2+a)}_{P_2}\Big|_{\substack{\delta'=0 \\ \varepsilon'=\omega'=\beta_a}} = \frac{\beta_a}{8} \left(\sum_{\langle x,y\rangle_{1,h}}{}' s_x s_y - \sum_{\langle x,y\rangle_{1,v}}{}' s_x s_y - \sum_{\langle x,y\rangle_{2}}{}' s_x s_y \right). \tag{101}$$

In the previous order, it has been established that the only plaquette configurations minimizing $H^{(2+a)}_{P_2}\Big|_{\substack{\delta'=0 \\ \varepsilon'=\omega'=\beta_a}}$ are the ones obtained by restricting to a plaquette P_2 the periodic configurations $\mathcal{S}_+$, $\mathcal{S}_-$, $\mathcal{S}_{cb}$, and $\mathcal{S}^v_{v2}$. Let us denote this set of plaquette configurations by $\mathcal{S}^{\mathbf{a}}_{P_2}$. Consequently, the minimization of the fourth-order potentials $\left(H^f_T\right)^{(4)}\Big|_{\gamma=1}$, $\left(H^b_T\right)^{(4)}\Big|_{\gamma=1}$, should be carried out only over the set $\mathcal{S}^{\mathbf{a}}_T$ of those T-plaquette configurations whose restriction to a plaquette P_2 belongs to $\mathcal{S}^{\mathbf{a}}_{P_2}$. The configurations of the set $\mathcal{S}^{\mathbf{a}}_T$ are displayed in Fig. 31. It appears that on the set $\mathcal{S}^{\mathbf{a}}_T$, the potentials $\left(H^f_T\right)^{(4)}\Big|_{\gamma=1}$, $\left(H^b_T\right)^{(4)}\Big|_{\gamma=1}$, are m-potentials. The obtained phase diagrams, independent of the anisotropy parameter β_a, are shown in Fig. 22 and Fig. 23.

B. A neighborhood of b

Here the system is not hole-particle symmetric and $\varepsilon' = 0$. A convenient change of variables is:

$$\omega' = t^{2-a}\omega, \qquad \delta' = t^{2-a}\delta. \tag{102}$$

Then, the fourth-order effective Hamiltonian takes the form,

$$\left(E_S^f\right)^{(4)} = \frac{t^{2+a}}{2}\sum_{P_2} H_{P_2}^{(2+a)}\Big|_{\substack{\delta'=0\\ \varepsilon'=\omega'=0}} + \frac{t^4}{2}\sum_T \left(H_T^f\right)^{(4)}\Big|_{\gamma=1}, \tag{103}$$

where

$$H_{P_2}^{(2+a)}\Big|_{\substack{\delta'=0\\ \varepsilon'=\omega'=0}} = -\frac{\beta_a}{4}{\sum_{\langle x,y\rangle_{1,v}}}' s_x s_y \tag{104}$$

with a similar formula for hard-core bosons. The minimum of $H_{P_2}^{(2+a)}\Big|_{\substack{\delta'=0\\ \varepsilon'=\omega'=0}}$ is attained at the configurations belonging to $\mathfrak{S}_{P_2}^{\mathbf{b}}$, i.e. the plaquette configurations obtained by restricting the periodic configurations $\mathfrak{S}_+$, $\mathfrak{S}_-$, and $\mathfrak{S}_{v2}^v$ to a plaquette P_2. Let $\mathfrak{S}_T^{\mathbf{b}}$ be the corresponding set of T-plaquette configurations (there are no vertical pairs of n.n. sites occupied by one ion). This set is shown in Fig. 32. Here the potentials $\left(H_T^f\right)^{(4)}\Big|_{\gamma=1}$ are not the m-potentials. The obtained phase diagrams are shown in Figs. 24, 25.

C. A neighborhood of $\mathbf{c}^-$

Here the system is not hole-particle symmetric and $\varepsilon' = 0$. A convenient change of variables is:

$$\omega' = 2\beta_a + t^{2-a}\omega, \qquad \delta' = -\beta_a + t^{2-a}\delta. \tag{105}$$

The fourth-order effective Hamiltonian reads:

$$\left(E_S^f\right)^{(4)} = \frac{t^{2+a}}{2}\sum_{P_2} H_{P_2}^{(2+a)}\Big|_{\substack{\varepsilon'=0\\ \delta'=-\beta_a,\omega'=2\beta_a}} + \frac{t^4}{2}\sum_T \left(H_T^f\right)^{(4)}\Big|_{\gamma=1} \tag{106}$$

with a similar formula for hard-core bosons, where

$$H_{P_2}^{(2+a)}\Big|_{\substack{\varepsilon'=0\\ \delta'=-\beta_a,\omega'=2\beta_a}} = \frac{\beta_a}{4}{\sum_{\langle x,y\rangle_{1,h}}}' (s_x + s_y + s_x s_y + 1) \tag{107}$$

The potentials $H_{P_2}^{(2+a)}\Big|_{\substack{\varepsilon'=0\\ \delta'=-\beta_a,\omega'=2\beta_a}}$ are minimized by restrictions to a plaquette P_2 of periodic configurations $\mathfrak{S}_-$, $\mathfrak{S}_{cb}$, and $\mathfrak{S}_{v2}^v$, that constitute the set $\mathfrak{S}_{P_2}^{c^-}$. The corresponding set $\mathfrak{S}_T^{c^-}$ of T-plaquette configurations consists of configurations where no horizontal pair of n.n. sites is occupied by two ions (see Fig. 33). Here the potentials $\left(H_T^f\right)^{(4)}\Big|_{\gamma=1}$ are not the m-potentials. The corresponding phase diagrams are shown in Fig. 26 and Fig. 27.

4.4 Discussion of the phase diagrams and conclusions

In previous subsection, we have obtained phase diagrams according to the truncated effective Hamiltonians of fourth order, with an intermediate anisotropy of hopping. These diagrams have been constructed to see what happens to the fourth-order phase diagrams with the weakest anisotropy if the anisotropy parameter β_2 grows beyond the values taken

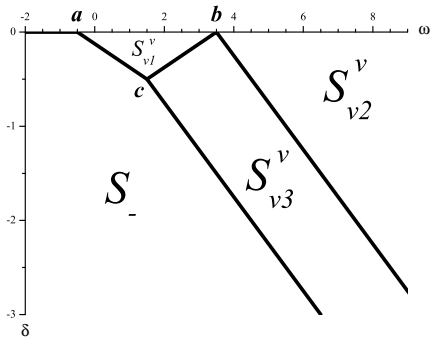

Figure 24: The case of an intermediate anisotropy ($0 < a < 2$), off the hole-particle symmetry, with $\varepsilon' = 0$. The phase diagram of $\left(E^f_S\right)^{(4)}$ in a neighborhood of point **b** ($\omega' = 0$, $\delta' = 0$), see formula (103). The equations defining the boundary lines of the phase domains are given in Tab. 6 of Appendix D, while the corresponding zero-potential coefficients $\{\alpha_i\}$ in Tab. 29 of Appendix E.

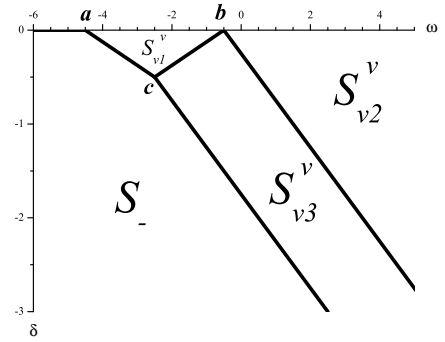

Figure 25: The case of an intermediate anisotropy ($0 < a < 2$), off the hole-particle symmetry, with $\varepsilon' = 0$. The phase diagram of $\left(E^b_S\right)^{(4)}$ in a neighborhood of point **b** ($\omega' = 0$, $\delta' = 0$)), see formula (103). The equations defining the boundary lines of the phase domains are given in Tab. 6 of Appendix D, while the corresponding zero-potential coefficients $\{\alpha_i\}$ in Tab. 30 of Appendix E.

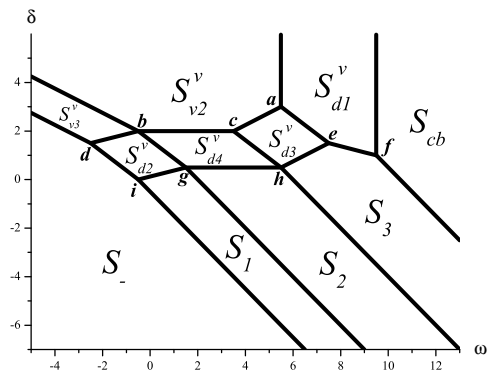

Figure 26: The case of an intermediate anisotropy ($0 < a < 2$), off the hole-particle symmetry, with $\varepsilon' = 0$. The phase diagram of $\left(E^f_S\right)^{(4)}$ in a neighborhood of point $\mathbf{c}^-$ ($\omega' = 2\beta_a$, $\delta' = -\beta_a$), see formula (106). The equations defining the boundary lines of the phase domains are given in Tab. 7 of Appendix D, while the corresponding zero-potential coefficients $\{\alpha_i\}$ in Tab. 31 of Appendix E.

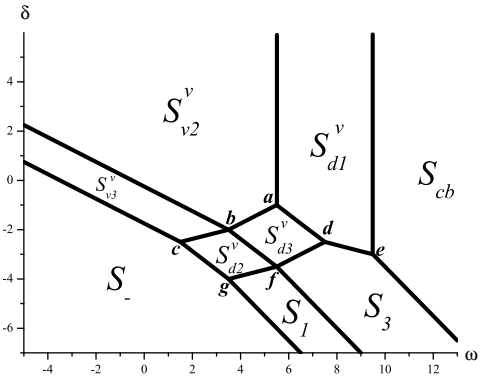

Figure 27: The case of an intermediate anisotropy ($0 < a < 2$), off the hole-particle symmetry, with $\varepsilon' = 0$. The phase diagram of $\left(E^b_S\right)^{(4)}$ in a neighborhood of point $\mathbf{c}^-$ ($\omega' = 2\beta_a$, $\delta' = -\beta_a$), see formula (106). The equations defining the boundary lines of the phase domains are given in Tab. 7 of Appendix D, while the corresponding zero-potential coefficients $\{\alpha_i\}$ in Tab. 32 of Appendix E.

into account in subsection 4.2. Let us consider firstly the diagrams in a neighborhood of point **a**. Apparently, up to a rescaling the phase diagram in Fig. 22 looks the same as the part in the dotted circle of the fermionic phase diagram in Fig. 16. Similarly, up to a rescaling the phase diagram in Fig. 23 looks the same as the the part in the dotted circle of the bosonic phase diagram in Fig. 16. The same remarks apply to the phase diagrams in neighborhoods of points **b** and $\mathbf{c}^-$. The phase diagram in Fig. 24 reproduces the part in the upper dotted ellipse in Fig. 17, while the diagram in Fig. 25 – the part in the upper dotted ellipse in Fig. 18. Then, the phase diagram in Fig. 26 reproduces the part in the lower dotted ellipse in Fig. 17, while the diagram in Fig. 27 – the part in the lower dotted ellipse in Fig. 18. Therefore, we conclude that in the case of the weakest anisotropy in the fourth-order effective Hamiltonians, we have determined all the critical values of the anisotropy parameter β_2. For the both kinds of hopping particles, if β_2 exceeds the greatest critical value, the obtained phase diagram undergoes only a translation (varying with β_2).

Now, the basic question to be answered is concerned with the relation between these fourth-order phase diagrams and the phase diagrams of quantum systems described by Hamiltonians H, given by (73). By adapting the arguments presented in Refs. [59, 40], we can demonstrate, see for instance Ref. [61], that if the remainders, $\left(R_S^f\right)^{(4)}$ and $\left(R_S^b\right)^{(4)}$, are taken into account, then there is a sufficiently small t_0 such that for $t < t_0$ the phase diagrams of quantum systems look the same as the phase diagrams according to the effective Hamiltonians truncated at the fourth order, except some narrow regions, of width $O(t^2)$ (at the diagrams displayed above), located along the phase-domains boundaries, and except the domains $\mathfrak{S}_{d2}^v$ and $\mathfrak{S}_{d4}^v$. For $t < t_0$ and for each domain $\mathfrak{S}_D$, which is different from $\mathfrak{S}_{d2}^v$ and $\mathfrak{S}_{d4}^v$, there is a nonempty two-dimensional open domain $\mathfrak{S}_D^\infty$ that is contained in the domain $\mathfrak{S}_D$ and such that in $\mathfrak{S}_D^\infty$ the set of ground-state configurations coincides with $\mathfrak{S}_D$. Moreover, in comparison with the critical values of the anisotropy parameter β_2, determined according to the fourth-order effective Hamiltonians, the corresponding critical values of the quantum systems described by Hamiltonians H differ by $O(t^2)$, i.e. for a quantum system $\gamma = 1 - \beta_2 t^2 + O(t^4)$.

Remarkably, in the fourth-order the hole-particle symmetric phase diagrams of fermions and of hardcore bosons are geometrically similar. That is, a phase diagram of hard core bosons, with any $\beta_2 \geq 0$, can be obtained from a phase diagram of fermions, with $\beta_2 \geq 5$, by the translation whose vector reads: $\omega = -7$, $\varepsilon = -3$, and $\beta_2 = -5$. The existence of this translation vector is related to the fact that for both kinds of systems there is one critical value of the anisotropy parameter. Additionally, for fermions with $\beta_2 < 7$, it is necessary to replace the phase $\mathfrak{S}_{dd}$ in the central domain by $\mathfrak{S}_{pcb}$. Off the hole-particle symmetry, the relation between the bosonic and fermionic phase diagrams is not that close. For fermions, there are three critical values of β_2, while for hardcore bosons there is no critical values. Thus, the system with hopping hardcore bosons is less sensitive to the anisotropy of hopping, than the system with hopping fermions. Nevertheless, if $\varepsilon = 0$, then the phase diagrams of both kinds of systems are topologically similar, except that in the bosonic phase diagrams the phases $\mathfrak{S}_{d3}^v$ and $\mathfrak{S}_2$ are missing. However, we know from Ref. [61] that this deficiency can be removed by switching on the n.n.n. interactions with negative ε.

In the fourth-order effective Hamiltonians (91), the weakest anisotropy of n.n. hopping

assumes the form of a fourth-order attractive n.n. interaction in vertical direction (i.e. the direction of a weaker hopping). This interaction favors n.n pairs of occupied or empty sites that are oriented vertically. As a result, the dimeric and axial-stripe phases oriented vertically are stabilized for any value of the anisotropy parameter β_2, while $\mathbb{S}_{pcb}$ and $\mathbb{S}_{dd}$ are replaced by $\mathbb{S}^{v}_{v2}$ above a critical value of β_2. Note however, that at any higher order $2k$, $k = 3, 4 \ldots$ the weakest anisotropy of n.n. hopping will cause the same effects, in the effective Hamiltonians as well as in the corresponding phase diagrams. This implies that in the quantum systems described by H, arbitrary small anisotropy of n.n. hopping orients the dimeric and axial-stripe phases in the direction of a weaker hopping.

5 Influence of next-nearest-neighbor anisotropy on diagonally-striped phases

In the previous Section the influence of n.n. anisotropy of hopping intensity on axial striped phases, was investigated. At the regime where stripes are stable, we have proved rigorously that for both systems, of hopping fermions and hard-core bosons, an arbitrarily small anisotropy of n.n. hopping orients the axial striped phases in the direction of a weaker hopping. The analogous, arising naturally, question is how the anisotropy of the next-nearest-neighbor (n.n.n.) hopping influences the degeneracy of diagonal-striped phases. To answer this question, we investigate the influence of n.n.n. hopping on the phase $\mathcal{S}_{dd}$ (Fig. 11), whose stability was proved for fermions in Section 3.

In this Section[3] we introduce a next-nearest-neighbor hopping, small enough not to destroy the striped structure and examine rigorously how the presence of the next-nearest-neighbor hopping anisotropy reduces the $\pi/2$-rotation degeneracy of the diagonal-striped phase. The effect appears to be similar to that in the case of anisotropy of the nearest-neighbor hopping: the stripes are oriented in the direction of the weaker next-nearest-neighbor hopping.

5.1 The effective interaction up to the fourth order

We consider our model in the case when only next-nearest-neighbor hopping is anisotropic, and nearest-neighbor hopping amplitude remains the same in different directions, i.e. $t_h = t_v = t$. For simplicity $\tilde{\varepsilon} = 0$. In this case, the ground-state energy expansion (43) with the expansion terms up to the fourth order, i.e. $a + b + c \leqslant 4$, reads:

$$
\begin{aligned}
E_S(\mu) =& E_S^{(4)}(\mu) + R^{(4)},\\
E_S^{(4)}(\mu) =& -\left[\frac{\mu}{2} + \frac{3}{4}t^2(t_+ + t_-)\right]\sum_x s_x +\\
&+\left[\frac{1}{4}t^2 - \frac{9}{16}t^4 - \frac{1}{16}t^2\left(3t_+^2 + 10t_+t_- + 3t_-^2\right) + \frac{W}{8}\right]\sum_{\langle x,y\rangle_1} s_x s_y +\\
&+\left[\frac{1}{4}t_+^2 + \frac{3}{16}t^4 - \frac{3}{8}t^2\left(2t_+^2 + t_+t_-\right) - \frac{3}{16}t_+^4 - \frac{3}{8}t_+^2t_-^2\right]\sum_{\langle x,y\rangle_{2,+}} s_x s_y +\\
&+\left[\frac{1}{4}t_-^2 + \frac{3}{16}t^4 - \frac{3}{8}t^2\left(2t_-^2 + t_+t_-\right) - \frac{3}{16}t_-^4 - \frac{3}{8}t_+^2t_-^2\right]\sum_{\langle x,y\rangle_{2,-}} s_x s_y +\\
&+\left[\frac{1}{8}t^4 - \frac{1}{8}t^2t_+t_- + \frac{3}{16}t_+^2t_-^2\right]\sum_{\langle x,y\rangle_3} s_x s_y + \frac{3}{16}t^2t_+^2\sum_{\langle x,y\rangle_{4,+}} s_x s_y + \frac{3}{16}t^2t_-^2\sum_{\langle x,y\rangle_{4,-}} s_x s_y +\\
&+\frac{1}{8}t_+^4\sum_{\langle x,y\rangle_{5,+}} s_x s_y + \frac{1}{8}t_-^4\sum_{\langle x,y\rangle_{5,-}} s_x s_y + \frac{3}{8}t^2t_+\sum_{P_1^+} s_{P_1^+} + \frac{3}{8}t^2t_-\sum_{P_1^-} s_{P_1^-} +\\
&+\frac{5}{16}\left[t^4 + 2t^2t_+t_-\right]\sum_{P_2} s_{P_2} + \frac{5}{16}t_+^2t_-^2\sum_{P_3} s_{P_3} + \frac{5}{16}t^2t_+t_-\sum_{P_4} s_{P_4} +
\end{aligned}
$$

[3]This section is based on [30].

$$+\frac{5}{16}t^2t_+^2\sum_{P_5^+}s_{P_5^+}+\frac{5}{16}t^2t_-^2\sum_{P_5^-}s_{P_5^-}. \tag{108}$$

The remainder $R^{(4)}$ is independent of the chemical potentials and W, and collects all the terms proportional to $t^at_+^bt_-^c$, with $a+b+c=5,6,\ldots$. The above expansion is absolutely convergent for sufficiently small t, t_+ and t_-, uniformly in Λ. In the special case of $t_+=t_-=t'$ and $W=0$ it was obtained in [64].

In Section 3, we have obtained the phase diagram of the isotropic model without n.n.n. hopping, i.e. for $t_+=t_-=0$. Here, our aim is to determine the influence of the n.n.n.-hopping anisotropy on the diagonal-striped phase $\mathcal{S}_{dd}$ (see Fig. 11). For this job, the value of the n.n.n.-hopping intensities, t_+, t_-, cannot be too large, in order to preserve the phase diagram up to 4th order. On the other hand, the n.n.n.-hopping intensities cannot be too small, in order to appear in the fourth-order effective Hamiltonian. In an attempt to satisfy the both requirements, we choose the smallest n.n.n.-hopping intensities t_+, t_-, i.e. such that they do not appear in the expansion terms of order smaller than four: $t_+=a_+t^2$ and $t_-=a_-t^2$. In this case, the effective Hamiltonian assumes the form:

$$\begin{aligned}E_S^{(4)}(\mu)=&-\left[\frac{1}{2}\mu+\frac{3}{4}t^4(a_++a_-)\right]\sum_x s_x+\left[\frac{1}{4}t^2-\frac{9}{16}t^4+\frac{W}{8}\right]\sum_{\langle x,y\rangle_1}s_xs_y+\\&+\left[\frac{1}{4}t^4a_+^2+\frac{3}{16}t^4\right]\sum_{\langle x,y\rangle_{2,+}}s_xs_y+\left[\frac{1}{4}t^4a_-^2+\frac{3}{16}t^4\right]\sum_{\langle x,y\rangle_{2,-}}s_xs_y+\\&+\frac{1}{8}t^4\sum_{\langle x,y\rangle_3}s_xs_y+\frac{3}{8}t^4a_+\sum_{P_1^+}s_{P_1^+}+\frac{3}{8}t^4a_-\sum_{P_1^-}s_{P_1^-}+\frac{5}{16}t^4\sum_{P_2}s_{P_2},\end{aligned} \tag{109}$$

i.e. the second requirement is satisfied. To answer the question concerning the influence of anisotropy of n.n.n. hopping on the degeneracy of the phase $\mathcal{S}_{dd}$, there is no need to consider the whole phase diagram. For $t_+=t_-=0$, we fix a point, well inside the domain of the diagonal-striped phase S_{dd}, say $\mu=0$ and $W=-2t^2+9/2t^4$, i.e. $\omega=9/2$ (see Fig. 11). Then, with the fixed point in (μ,W)-plain, we introduce a n.n.n. hopping which does not change the ground-state configurations. Calculations show that $\mathcal{S}_{dd}$ has the minimal energy for $a=|a_+|=|a_-|$, where $-1/4\leqslant a\leqslant 1/4$ (we suppose that the difference between a_+ and a_- is not large, so they are of the same sign). Therefore, with our choice of n.n.n.-hopping intensities, the first of the above two requirements can also be satisfied. Eventually, we fix the values of n.n.n.-hopping intensities: $a_+=1/8$, $a_-=\gamma a_+$, with γ varying about 1 (say, $0\leqslant\gamma\leqslant 2$).

Since all the energy parameters, except the parameter γ of n.n.n.-hopping anisotropy, have been fixed, the effective Hamiltonian (109) depends only on γ. In the following subsection, we examine how n.n.n.-hopping anisotropy, $\gamma\neq 1$, influences the degeneracy of the diagonal-striped phase $\mathcal{S}_{dd}$.

5.2 Diagonally-striped phase versus n.n.n.-hopping anisotropy

For technical reasons (see paragraph 2.4.5), it is convenient to deal with such energies of configurations that are affine functions of the parameters of the effective Hamiltonian. However, the effective Hamiltonian (109) contains the terms proportional to γ and γ^2. To

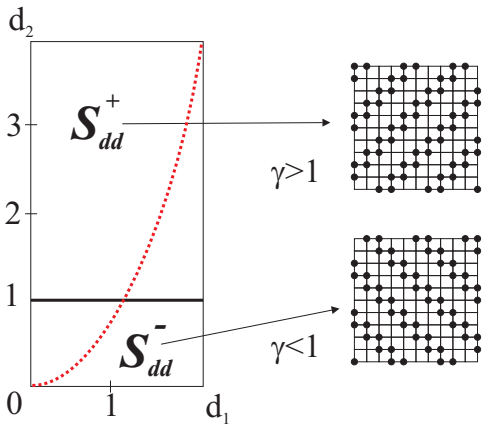

Figure 28: The phase diagram of $E^{(4)}(d_1, d_2)$, with $0 \leqslant d_1 \leqslant 2$ and $0 \leqslant d_2 \leqslant 4$. The rectangle breaks down into two regions: above $d_2 = 1$ the configurations $\mathcal{S}^+_{dd}$ are the ground-state configurations, while $\mathcal{S}^+_{dd}$ are replaced by $\mathcal{S}^-_{dd}$ below $d_2 = 1$. The dashed line represents the condition $d_2 = d_1^2$. The representative configurations (up to translations) of $\mathcal{S}^+_{dd}$, $\mathcal{S}^-_{dd}$ are shown on the right.

get rid of nonlinearities, we replace γ and γ^2 by two independent parameters d_1 and d_2, respectively, with d_1, d_2 varying in the rectangle $0 \leq d_1 \leq 2$ and $0 \leq d_2 \leq 4$, in which the Hamiltonian is affine. After constructing the phase diagram in (d_1, d_2)-plane, we restrict it to the $d_2 = d_1^2$ curve.

To compare the energies of configurations, we rewrite $E^{(4)}_S(d_1, d_2)$ as the sum,

$$E^{(4)}_S(d_1, d_2) = \frac{t^4}{2} \sum_T H^{(4)}_T, \tag{110}$$

over T-plaquettes. The potential $H^{(4)}_T$ is of the form:

$$\begin{aligned} H^{(4)}_T \;=\; & -\frac{3}{16}(d_1+1)\, s_5 + \frac{49}{512}{\sum_{\langle x,y\rangle_{2,+}}}'' s_x s_y + \frac{1}{32}\left(\frac{1}{16}d_2 + 3\right){\sum_{\langle x,y\rangle_{2,-}}}'' s_x s_y + \frac{1}{12}{\sum_{\langle x,y\rangle_3}}'' s_x s_y + \\ & + \frac{3}{128}{\sum_{P_1^+}}'' s_{P_1^+} + \frac{3}{128} d_1 {\sum_{P_1^-}}'' s_{P_1^-} + \frac{5}{32}{\sum_{P_2}}'' s_{P_2}, \end{aligned} \tag{111}$$

where s_5 is the central site of a T-plaquette (Fig. 7).

Unfortunately, the potential (111) is not an m-potential in the rectangle of considered values of d_1 and d_2. Therefore, we introduce appropriate zero-potentials given in Appendix A. In order to obtain the phase diagram, we have to compare the energies of all the possible T-plaquette configurations. The zero-potential coefficients α needed for this are given in Tab. 33 in the Appendix. We provide their values only at certain generating points, since we can assume that the coefficients α are affine functions of parameters (d_1, d_2).

The phase diagram of $E^{(4)}$ is shown in Fig. 28. The rectangle of considered points (d_1, d_2) breaks down into two domains. In the lower one, where $\gamma < 1$ and $t_- < t_+$, it is the phase $\mathcal{S}^-_{dd}$, with stripes being parallel to the direction of t_--hopping, that is stable.

The analogous situation is in the upper domain, where $\gamma > 1$ and $t_- > t_+$: the stable phase, $\mathbb{S}^+_{dd}$, consists of stripes oriented along t_+-hopping. At $\gamma = 1$, we have the isotropic phase $\mathbb{S}_{dd}$ whose configurations consist of $\mathbb{S}^+_{dd}$ and $\mathbb{S}^-_{dd}$.

So we see that, at least for the truncated effective Hamiltonian, switching on of a n.n.n.-hopping anisotropy reduces the rotational degeneracy of diagonal-striped phases: they become oriented in the direction of the weaker hopping.

This result is similar to that described in Section 4, where the influence of n.n.-hopping anisotropy on axial-striped phases was investigated. In that case, not only for a truncated effective Hamiltonian but also for the corresponding quantum one, it was proved that for any nonzero value of n.n.-hopping anisotropy the rotational degeneracy of axial-striped phases is reduced by making them oriented along the direction of the weaker n.n. hopping. Now in turn, the natural question is whether the conclusions we arrived at, concerning n.n.n.-hopping anisotropy, hold true for the quantum model, described by Hamiltonian (73). Applying the arguments presented in [40, 59], it could be demonstrated, that the stable phases of the obtained above phase diagram remain stable for the model (73), but in some smaller domains. That is, if the remainder $R^{(4)}$ is taken into account, then there exist such a small t_0, that for $t < t_0$ the phase diagram looks the same for the quantum model, excepting of some narrow regions (of width $O(t)$ in the scale of the fourth-order phase diagram shown in Fig. 28), located along the phase-boundary lines. In our case that means that the breaking of the rotational symmetry occurs for $\gamma = 1 + O(t)$, when the n.n.n.-hopping intensities are $O(t^2)$. Unfortunately, we cannot claim that any non-zero n.n.n.-hopping anisotropy reduces the rotational degeneracy of the quantum model, as it was the case for n.n. hopping (see Section 4). Here it seems, at least for small n.n.n.-hopping intensities, that there is certain critical value of $|\gamma - 1|$, above which the degeneracy of phase $\mathbb{S}_{dd}$ is reduced.

6 Conclusions

In Sections 3 and 4, we have succeeded in constructing ground-state phase diagrams of some classical (i.e. diagonal in some basis) Hamiltonians, in the whole range of parameters (coupling constants, chemical potentials). These Hamiltonians have been derived as effective Hamiltonians in certain orders of quantum Hamiltonians (termed the extended Falicov–Kimball Hamiltonians), in the strong-coupling regime. In other words, we have proved that the considered classical Hamiltonians can be expressed by m-potentials, for arbitrary value of parameters. Such Hamiltonians are sometimes referred to as frustrationless. It should be emphasized however, that, a priori, nothing guarantees that the method we used here will "produce" any phase diagram: one can fail to construct m-potentials or they might not exist.

Those ground-state phase diagrams of effective Hamiltonians constitute the basic input of the quantum extension of the Pirogov–Sinai theory of phase diagrams, developed in [57]. This theory enables us to claim that not only the periodic ground states of effective classical Hamiltonians are also ground states of the corresponding quantum Hamiltonians, but that, at sufficiently low temperatures, to each periodic ground-state phase there corresponds a thermodynamic phase characterized by the same kind of long-range order. The above mentioned properties of periodic ground-states of effective Hamiltonians are referred to as stability with respect to higher-order effective interactions and to small thermal fluctuations.

Several basic problems concerning striped phases in a system of strongly correlated electrons were considered. First of all, we addressed the problem of the stability of charge-stripe phases versus the phase separated state — the segregated phase, in strongly-interacting systems of fermions or hardcore bosons. There are numerous works devoted to this problem, where it is studied, by approximate methods, in the framework of models relevant for experiments. Unfortunately, due to tiny energy differences involved, it is difficult to settle this problem by means of approximate methods, which bias the calculated energies with hardly controllable errors of various nature. We have studied simple models, that by many physicists can be considered less realistic, but which, in return, are amenable to a rigorous analysis. Our models are described by extended Falicov–Kimball Hamiltonians, with hopping particles being spinless fermions or hardcore bosons. The ground-state phase diagrams of these models have been constructed rigorously in the regime of strong coupling and half-filling. In the both cases, of fermions and hardcore bosons, we have found transitions from a crystalline chessboard phase to the segregated phase via striped phases.

After the stability of striped phases had been proven, both system (with the hopping particles being either spinless fermions or hardcore bosons) have been studied in order to show rigorously the influence of nearest-neighbor and next-nearest-neighbor hopping anisotropy on phase diagrams. In the case of nearest-neighbor hopping only, two main conclusions have been drawn. Firstly, arbitrary small anisotropy of nearest-neighbor hopping orients the dimeric and axial-stripe phases in the direction of a weaker hopping. Secondly, even a weak anisotropy of hopping reveals a tendency of fermionic phase diagrams to become similar to the bosonic ones.

In the case of next-nearest-neighbor hopping we have shown that a weak anisotropy of the next-nearest-neighbor hopping reduces the degeneracy of a diagonal-striped phase,

it orients the stripes in the direction of the weaker next-nearest-neighbor hopping.

Acknowledgments

The author is deeply indebted to Prof. Janusz Jędrzejewski for his unstinting support over years.

The author thanks Łukasz Andrzejewski and Paweł Musiał for their comments on the manuscript.

The author is grateful to the University of Wrocław for Scientific Research Grant 2479/W/IFT, and to the Institute of Theoretical Physics for financial support. The Max Born Scholarship is gratefully acknowledged.

References

[1] J.M. Tranquada, D.J. Buttrey, V. Sachan, and J.E. Lorenzo, *Simultaneous Ordering of Holes and Spins in $La_2NiO_{4.125}$*, Phys. Rev. Lett. **73**, 1003 (1994)

[2] J.M. Tranquada, B.J. Sternlieb, J.D. Axe, Y. Nakamura, and S. Uchida, *Evidence for stripe correlations of spins and holes in copper oxide superconductors*, Nature (London) **375**, 561 (1995)

[3] K. Kern, H. Niehus, A. Schatz, P. Zeppenfeld, J. Goerge, and G. Comsa, *Long-Range Spatial Self-Organization in the Adsorbate-Induced Restructuring of Surfaces: $Cu\{110\} - (2 \times 1)O$*, Phys. Rev. Lett. **67**, 855 (1991)

[4] M. Seul and R. Wolfe, *Evolution of disorder in magnetic stripe domains. I. Transverse instabilities and disclination unbinding in lamellar patterns*, Phys. Rev. A **46**, 7519 (1992); M. Seul and R. Wolfe, *volution of disorder in two-dimensional stripe patterns: "smectic" instabilities and disclination unbinding*, Phys. Rev. Lett. **68**, 2460 (1992); R. Allenspach, M. Stampanoni, and A. Bischof, *Magnetic domains in thin epitaxial $Co/Au(111)$ films*, Phys. Rev. Lett. **65**, 3344 (1990); R. Allenspach and A. Bischof, *Magnetization direction switching in $Fe/Cu(100)$ epitaxial films: temperature and thickness dependence*, Phys. Rev. Lett. **69**, 3385 (1992)

[5] G. Malescio and G. Pellicane, *Stripe phases from isotropic repulsive interactions*, Nature Materials **2**, 97 (2003)

[6] K. Sasaki, *Lattice gas model for striped structures of adatom rows on surfaces*, Surf. Sci. **318**, L1230 (1994)

[7] I. Booth, A. B. MacIsaac, J. P. Whitehead, K. De'Bell, *Domain Structures in Ultrathin Magnetic Films*, Phys. Rev. Lett. **75**, 950 (1995); J. Arlett, J. P. Whitehead, A. B. MacIsaac, K. De'Bell, *Phase diagram for the striped phase in the two-dimensional dipolar Ising model*, Phys. Rev. B **54**, 3394 (1996); A. D. Stoycheva and S. J. Singer, *Stripe melting in a two-dimensional system with competing interactions*, Phys. Rev. Lett. **84**, 4657 (2000)

[8] A.W. Sandvik, S. Daul, R.R.P. Singh, and D.J. Scalapino, *Striped Phase in a Quantum XY Model with Ring Exchange*, Phys. Rev. Lett. **89**, 247201 (2002)

[9] B. Spivak, *Phase separation in the two-dimensional electron liquid in MOSFET's*, Phys. Rev. B **67**, 125205 (2003); B. Spivak and S. A. Kivelson, *Phases intermediate between a two-dimensional electron liquid and Wigner crystal*, Phys. Rev. B **70**, 155114 (2004)

[10] D. Poilblanc and T.M. Rice, *Charged solitons in the Hartree-Fock approximation to the large-U Hubbard model*, Phys. Rev. B **39**, 9749 (1989)

[11] J. Zaanen and O. Gunnarsson, *Charged magnetic domain lines and the magnetism of high-T_c oxides*, Phys. Rev. B **40**, 7391 (1989)

[12] K. Machida, *Magnetism in La_2CuO_4 based compounds*, Physica C **158**, 192 (1989)

[13] M. Kato, K. Machida, H. Nakanishi, and M. Fujita, *Soliton lattice modulation of incommensurate spin density wave in two dimensional Hubbard model — a mean field study*, J. Phys. Soc. Jpn., **59**, 1047 (1990)

[14] A.M. Oleś, *Stripe phases in high-temperature superconductors*, Acta Physica Polonica B **31**, 2963 (2000)

[15] S.R. White and D.J. Scalapino, *Density Matrix Renormalization Group Study of the Striped Phase in the 2D t–J Model*, Phys. Rev. Lett. **80**, 1272 (1998)

[16] S.R. White and D.J. Scalapino, *Energetics of Domain Walls in the 2D t–J Model*, Phys. Rev. Lett. **81**, 3227 (1998)

[17] J. M. Tipper and K. J. E. Vos, *Formation of stripes and incommensurate peaks in the orthorombic phase of underdoped* $La_{2-x}Sr_xCuO_4$, Phys. Rev. B **67**, 144511 (2003)

[18] V.J. Emery, S.A. Kivelson, and J.M. Tranquada, *Stripe phases in high-temperature superconductors*, Proc. Natl. Acad. Sci. USA **96**, 8814 (1999)

[19] N.G. Zhang and C.L. Henley, *Stripes and holes in a two-dimensional model of spinless fermions or hardcore bosons*, Phys. Rev. B **68**, 014506 (2003)

[20] R. Lemański, J.K. Freericks, and G. Banach, *Stripe Phases in the Two-Dimensional Falicov–Kimball Model*, Phys. Rev. Lett. **89**, 196403 (2002)

[21] U. Löw, V. J. Emery, K. Fabricius, and S. A. Kivelson, *Study of an Ising model with competing long- and short-range interactions*, Phys. Rev. Lett. **72**, 1918 (1994)

[22] D. Valdez-Balderas and D. Stroud, *Superconductivity versus phase separation, stripes, and checkerboard ordering: a two-dimensional Monte Carlo study*, Phys. Rev. B **72**, 214501 (2005)

[23] C. Buhler, S. Yunoki, and A. Moreo, *Magnetic Domains and Stripes in a Spin-Fermion Model for Cuprates*, Phys. Rev. Lett. **84**, 2690 (2000)

[24] R. Lemański, J.K. Freericks, and G. Banach, *Charge Stripes due to Electron Correlations in the Two-Dimensional Spinless Falicov–Kimball Model*, J. Stat. Phys. **116**, 699 (2004)

[25] C.L. Henley and N.G. Zhang, *Spinless fermions and charged stripes at the strong-coupling limit*, Phys. Rev. B **63**, 233107 (2001)

[26] J.K.Freericks, E.H. Lieb, and D. Ueltschi, *Phase separation due to quantum mechanical correlations*, Phys. Rev. Lett. **88**, 106401 (2002).

[27] M. Raczkowski, B. Normand, and A. M. Oleś, *Vertical and diagonal stripes in the extended Hubbard model*, Phys. Stat. Sol. (b) **236**, 376 (2003)

[28] V. Derzhko, J. Jędrzejewski, *Formation of charge-stripe phases in a system of spinless fermions or hardcore bosons*, Physica A **349**, 511 (2005).

[29] V. Derzhko, J. Jędrzejewski, *Charge-stripe phases versus a weak anisotropy of nearest-neighbor hopping*, arXiv:cond-mat/0509698.

[30] V. Derzhko, *Influence of anisotropic next-nearest-neighbor hopping on diagonal charge-striped phases*, arXiv:cond-mat/0511557.

[31] J. Hubbard, Proc. Roy. Soc. London A **276**, 238 (1963); **277**, 237 (1964); **281**, 401 (1964).

[32] M. C. Gutzwiller, *Correlation of electrons in a narrow s band*, Phys. Rev. **137**, A1726 (1965).

[33] L.M. Falicov and J.C. Kimball, *Simple model for semiconductor-metal transitions: SmB_6 and transition-metal oxides*, Phys. Rev. Lett. **22**, 997 (1969).

[34] T. Kennedy and E. H. Lieb, *An itinerant electron model with crystalline or magnetic long range order*, Physica A **138**, 320 (1986).

[35] E. H. Lieb, *A model for crystallization: a variation on the Hubbard model*, Physica A **140**, 240 (1986)

[36] J. K. Freericks, V. Zlatić, *Exact dynamical mean-field theory of the Falicov-Kimball model*, Rev. Mod. Phys. **75**, 1333 (2003)

[37] H. Čenčariková, P. Farkašovský, *The influence of correlated hopping on the ground-state properties of the two-dimensional Falicov–Kimball model*, Phys. Stat. Sol. (b) **242**, 2061 (2005)

[38] P. Farkašovský, H. Čenčariková, N. Tomašovičová, *Ground-states of the three-dimensional Falicov–Kimball model*, Eur. J. Phys. B **45**, 479 (2005)

[39] P. Farkašovský, *Ground-state properties of the Falicov-Kimball model in one and two dimensions*, Eur. J. Phys. B **20**, 209 (2001)

[40] C. Gruber, N. Macris, A. Messager, D. Ueltschi, *Ground states and flux configurations of the two-dimensional Falicov–Kimball model*, J. Stat. Phys. **86**, 57 (1997).

[41] Z. Gajek, R. Lemański, *Correlated hopping in the 1D Falicov–Kimball model*, Acta Phys. Polon. B **32**, 3473 (2001)

[42] J. Wojtkiewicz, R. Lemański, *Ground states of the Falicov–Kimball model with correlated hopping*, Phys. Rev. B **64**, 233103 (2001)

[43] J. Wojtkiewicz, R. Lemański, *2D Falicov–Kimball model with correlated hopping in the large U limit*, Acta Phys. Polon. B **32**, 3467 (2001)

[44] U. Brandt, A. Fledderjohann, and G. Hülsenbeck, *New phases in a spin-1/2 Falicov-Kimball model*, Z. Phys. B 81, 409 (1990).

[45] U. Brandt, A. Fledderjohann, *Existence of a phase transition in a spin-1/2 Falicov-Kimball model*, Z. Phys. B 87 (1992) 111.

[46] R. Lemański, J. Wojtkiewicz, *Ground states of the spin-1/2 Falicov–Kimball model*, Phys. Stat. Sol. (b) **236**, 408 (2003)

[47] R. Lemański, *Model of charge and magnetic order formation in itinerant electron system*, Phys. Rev. B **71**, 035107 (2005)

[48] J. Jędrzejewski and R. Lemański, *Falicov–Kimball models of collective phenomena in solids (a concise guide)*, Acta Phys. Pol. B **32**, 3243 (2001).

[49] A. Messager and S. Miracle-Solé, *Low temperature states in the Falicov–Kimball model*, Rev. Math. Phys. **8**, 271 (1996).

[50] C. Gruber, J. Jędrzejewski and P. Lemberger, *Ground States of the Spinless Falicov–Kimball Model. II*, J. Stat. Phys. **66**, 913 (1992).

[51] C. Gruber and N. Macris, *The Falicov–Kimball model: a review of exact results and extensions*, Helv. Phys. Acta **69**, 850 (1996).

[52] C. Gruber, *Falicov–Kimball models: a partial review of the ground states problem*, arXiv:cond-mat/9811299

[53] C. Gruber and D. Ueltschi, *The Falicov–Kimball model*, arXiv:math-ph/0502041 (2005).

[54] N. Datta, R. Fernández, J. Fröhlich, *Low-temperature Phase Diagrams of quantum lattice systems. I. Stability for quantum pertrubations of classical systems with finitely-many ground states*, J. Stat. Phys. **84**, 455 (1996).

[55] N. Datta, R. Fernández, J. Fröhlich, L. Rey-Bellet, *Low-temperature Phase Diagrams of quantum lattice systems. II. Convergent pertrubation expansions and stability in systems with infenite degeneracy*, Helv. Phys. Acta. **69**, 752 (1996).

[56] J. Fröhlich, L. Rey-Bellet, *Low-temperature Phase Diagrams of quantum lattice systems. III. Examples*, Helv. Phys. Acta. **69**, 821 (1996).

[57] N. Datta, R. Fernández, J. Fröhlich, *Effective Hamiltonians and phase diagrams for tight-binding models*, J. Stat. Phys. **96**, 545 (1999).

[58] J. Slawny, *Low-temperature properties of classical lattice systems: phase transitions and phase diagrams*, in: C. Domb, J. Lebowitz (Eds.), Phase Transitions and Critical Phenomena, vol. 11, Academic Press, London, New York, 1985.

[59] Tom Kennedy, *Some rigorous results on the ground states of the Falicov–Kimball model*, Rev. Math. Phys. **6**, 901 (1994).

[60] J.K.Freericks, E.H. Lieb, and D. Ueltschi, *Segregation in the Falicov–Kimball model*, Commun. Math. Phys. **227**, 243 (2002).

[61] V. Derzhko and J. Jędrzejewski, *From phase separation to long-range order in a system of interacting electrons*, Physica A **328**, 449 (2003)

[62] T. Kennedy, *Phase separation in the neutral Falicov–Kimball model*, J. Stat. Phys. **91**, 829 (1998)

[63] C. Morais Smith, Yu.A. Dimashko, N. Hasselmann, and A.O. Caldeira, *Dynamics of stripes in doped antiferromagnets*, Phys. Rev. B **58**, 453 (1998)

[64] J. Wojtkiewicz, *Phase diagram of the two-dimensional t-t' Falicov-Kimball model*, arXiv:cond-mat/0310043.

Appendix A

Here we present T-block zero-potentials in the isotropic case (considered in Section 3), which are invariant with respect to $\pi/2$-rotations and reflections.

$$
\begin{aligned}
k_T^{(1)}(s) =& s_1 + s_3 + s_7 + s_9 - 4s_5,\\
k_T^{(2)}(s) =& s_2 + s_4 + s_6 + s_8 - 4s_5;\\
k_T^{(3)}(s) =& s_1s_2 + s_2s_3 + s_3s_6 + s_6s_9 + s_8s_9 + s_7s_8 + s_4s_7 + s_1s_4\\
&- 2s_2s_5 - 2s_5s_6 - 2s_5s_8 - 2s_4s_5,\\
k_T^{(4)}(s) =& s_1s_5 + s_3s_5 + s_5s_9 + s_5s_7 - s_2s_4 - s_4s_8 - s_8s_6 - s_2s_6,\\
k_T^{(5)}(s) =& s_1s_3 + s_3s_9 + s_7s_9 + s_1s_7 - 2s_4s_6 - 2s_2s_8;\\
k_T^{(6)}(s) =& s_1s_2s_3 + s_3s_6s_9 + s_7s_8s_9 + s_1s_4s_7 - 2s_4s_5s_6 - 2s_2s_5s_8,\\
k_T^{(7)}(s) =& s_1s_2s_5 + s_4s_5s_7 + s_5s_8s_9 + s_3s_5s_6 + s_2s_3s_5 + s_1s_4s_5 + s_5s_7s_8 + s_5s_6s_9\\
&- 2s_1s_2s_4 - 2s_4s_7s_8 - 2s_6s_8s_9 - 2s_2s_3s_6,\\
k_T^{(8)}(s) =& s_1s_2s_5 + s_4s_5s_7 + s_5s_8s_9 + s_3s_5s_6 + s_2s_3s_5 + s_1s_4s_5 + s_5s_7s_8 + s_5s_6s_9\\
&- 2s_2s_4s_5 - 2s_4s_5s_8 - 2s_5s_6s_8 - 2s_2s_5s_6,\\
k_T^{(9)}(s) =& s_1s_2s_6 + s_2s_4s_7 + s_4s_8s_9 + s_3s_6s_8 + s_6s_7s_8 + s_2s_6s_9 + s_2s_3s_4 + s_1s_4s_8\\
&- s_3s_4s_5 - s_1s_5s_8 - s_5s_6s_7 - s_2s_5s_9 - s_4s_5s_9 - s_3s_5s_8 - s_1s_5s_6 - s_2s_5s_7,\\
k_T^{(10)}(s) =& s_1s_2s_7 + s_4s_7s_9 + s_3s_8s_9 + s_1s_3s_6 + s_2s_3s_9 + s_1s_3s_4 + s_1s_7s_8 + s_6s_7s_9\\
&- s_1s_2s_8 - s_4s_6s_7 - s_2s_8s_9 - s_3s_4s_6 - s_2s_3s_8 - s_1s_4s_6 - s_2s_7s_8 - s_4s_6s_9,\\
k_T^{(11)}(s) =& s_1s_3s_5 + s_1s_5s_7 + s_5s_7s_9 + s_3s_5s_9 - s_2s_4s_8 - s_4s_6s_8 - s_2s_6s_8 - s_2s_4s_6;\\
k_T^{(12)}(s) =& s_1s_2s_4s_7 + s_4s_7s_8s_9 + s_3s_6s_8s_9 + s_1s_2s_3s_6 + s_2s_3s_6s_9 + s_1s_2s_3s_4\\
&+ s_1s_4s_7s_8 + s_6s_7s_8s_9 - s_1s_2s_5s_8 - s_4s_5s_6s_7 - s_2s_5s_8s_9 - s_3s_4s_5s_6\\
&- s_2s_3s_5s_8 - s_1s_4s_5s_6 - s_2s_5s_7s_8 - s_4s_5s_6s_9,\\
k_T^{(13)}(s) =& s_1s_2s_3s_5 + s_1s_4s_5s_7 + s_5s_7s_8s_9 + s_3s_5s_6s_9 - s_2s_4s_5s_8 - s_4s_5s_6s_8\\
&- s_2s_5s_6s_8 - s_2s_4s_5s_6,\\
k_T^{(14)}(s) =& s_1s_2s_4s_8 + s_4s_6s_7s_8 + s_2s_6s_8s_9 + s_2s_3s_4s_6 + s_2s_3s_6s_8 + s_1s_2s_4s_6\\
&+ s_2s_4s_7s_8 + s_4s_6s_8s_9 - s_1s_2s_5s_7 - s_4s_5s_7s_9 - s_3s_5s_8s_9 - s_1s_3s_5s_6\\
&- s_2s_3s_5s_9 - s_1s_3s_4s_5 - s_1s_5s_7s_8 - s_5s_6s_7s_9;\\
k_T^{(15)}(s) =& s_4s_6s_7s_8s_9 + s_2s_3s_6s_8s_9 + s_1s_2s_3s_4s_6 + s_1s_2s_4s_7s_8 - s_4s_5s_6s_7s_9\\
&- s_2s_3s_5s_8s_9 - s_1s_3s_4s_5s_6 - s_1s_2s_5s_7s_8,\\
k_T^{(16)}(s) =& s_3s_5s_6s_8s_9 + s_1s_4s_5s_7s_8 + s_1s_2s_3s_5s_6 + s_1s_2s_4s_5s_7 + s_4s_5s_7s_8s_9\\
&+ s_5s_6s_7s_8s_9 + s_2s_3s_5s_6s_9 + s_1s_2s_3s_4s_5 - s_4s_5s_6s_8s_9 - s_2s_3s_5s_6s_8\\
&- s_1s_2s_4s_5s_6 - s_2s_4s_5s_7s_8 - s_2s_3s_4s_5s_6 - s_1s_2s_4s_5s_8 - s_4s_5s_6s_7s_8\\
&- s_2s_5s_6s_8s_9.
\end{aligned}
$$

In the case of n.n. hopping anisotropy (considered in Section 4), the zero-potentials

invariant with respect to π-rotations and reflections are of the form:

$$
\begin{aligned}
k_{\mathrm{T}}^{(1)} =& s_1 + s_3 + s_7 + s_9 - 4s_5,\\
k_{\mathrm{T}}^{(2)} =& s_2 + s_8 - 2s_5,\\
k_{\mathrm{T}}^{(3)} =& s_4 + s_6 - 2s_5;\\
k_{\mathrm{T}}^{(4)} =& s_1s_2 + s_2s_3 + s_7s_8 + s_8s_9 - 2s_4s_5 - 2s_5s_6,\\
k_{\mathrm{T}}^{(5)} =& s_1s_4 + s_3s_6 + s_4s_7 + s_6s_9 - 2s_2s_5 - 2s_5s_8,\\
k_{\mathrm{T}}^{(6)} =& s_1s_5 + s_3s_5 + s_5s_9 + s_5s_7 - s_2s_4 - s_4s_8 - s_8s_6 - s_2s_6,\\
k_{\mathrm{T}}^{(7)} =& s_1s_3 + s_7s_9 - 2s_4s_6,\\
k_{\mathrm{T}}^{(8)} =& s_1s_7 + s_3s_9 - 2s_2s_8;\\
k_{\mathrm{T}}^{(9)} =& s_1s_2s_4 + s_6s_8s_9 + s_2s_3s_6 + s_4s_7s_8 - s_2s_4s_5 - s_5s_6s_8 - s_2s_5s_6 - s_4s_5s_8,\\
k_{\mathrm{T}}^{(10)} =& s_1s_2s_5 + s_5s_8s_9 + s_2s_3s_5 + s_5s_7s_8 - s_2s_4s_5 - s_5s_6s_8 - s_2s_5s_6 - s_4s_5s_8,\\
k_{\mathrm{T}}^{(11)} =& s_4s_5s_7 + s_3s_5s_6 + s_5s_6s_9 + s_1s_4s_5 - s_2s_4s_5 - s_5s_6s_8 - s_2s_5s_6 - s_4s_5s_8,\\
k_{\mathrm{T}}^{(12)} =& s_1s_2s_3 + s_7s_8s_9 - 2s_4s_5s_6,\\
k_{\mathrm{T}}^{(13)} =& s_1s_4s_7 + s_3s_6s_9 - 2s_2s_5s_8,\\
k_{\mathrm{T}}^{(14)} =& s_1s_2s_6 + s_4s_8s_9 + s_2s_3s_4 + s_6s_7s_8 - s_3s_4s_5 - s_5s_6s_7 - s_1s_5s_6 - s_4s_5s_9,\\
k_{\mathrm{T}}^{(15)} =& s_2s_4s_7 + s_3s_6s_8 + s_2s_6s_9 + s_1s_4s_8 - s_1s_5s_8 - s_2s_5s_9 - s_3s_5s_8 - s_2s_5s_7,\\
k_{\mathrm{T}}^{(16)} =& s_1s_2s_7 + s_3s_8s_9 + s_2s_3s_9 + s_1s_7s_8 - s_1s_2s_8 - s_2s_8s_9 - s_2s_3s_8 - s_2s_7s_8,\\
k_{\mathrm{T}}^{(17)} =& s_4s_7s_9 + s_1s_3s_6 + s_6s_7s_9 + s_1s_3s_4 - s_4s_6s_7 - s_3s_4s_6 - s_4s_6s_9 - s_1s_4s_6,\\
k_{\mathrm{T}}^{(18)} =& s_1s_3s_5 + s_5s_7s_9 - s_4s_6s_8 - s_2s_4s_6,\\
k_{\mathrm{T}}^{(19)} =& s_1s_5s_7 + s_3s_5s_9 - s_2s_4s_8 - s_2s_6s_8;\\
k_{\mathrm{T}}^{(20)} =& s_1s_2s_4s_7 + s_3s_6s_8s_9 + s_2s_3s_6s_9 + s_1s_4s_7s_8 - s_1s_2s_5s_8 - s_2s_5s_8s_9 - s_2s_3s_5s_8 - s_2s_5s_7s_8,\\
k_{\mathrm{T}}^{(21)} =& s_4s_7s_8s_9 + s_1s_2s_3s_6 + s_6s_7s_8s_9 + s_1s_2s_3s_4 - s_4s_5s_6s_7 - s_3s_4s_5s_6 - s_4s_5s_6s_9 - s_1s_4s_5s_6,\\
k_{\mathrm{T}}^{(22)} =& s_1s_2s_3s_5 + s_5s_7s_8s_9 - s_4s_5s_6s_8 - s_2s_4s_5s_6,\\
k_{\mathrm{T}}^{(23)} =& s_1s_4s_5s_7 + s_3s_5s_6s_9 - s_2s_4s_5s_8 - s_2s_5s_6s_8,\\
k_{\mathrm{T}}^{(24)} =& s_1s_2s_4s_8 + s_2s_6s_8s_9 + s_2s_3s_6s_8 + s_2s_4s_7s_8 - s_1s_2s_5s_7 - s_3s_5s_8s_9 - s_2s_3s_5s_9 - s_1s_5s_7s_8,\\
k_{\mathrm{T}}^{(25)} =& s_4s_6s_7s_8 + s_2s_3s_4s_6 + s_4s_6s_8s_9 + s_1s_2s_4s_6 - s_4s_5s_7s_9 - s_1s_3s_5s_6 - s_5s_6s_7s_9 - s_1s_3s_4s_5;\\
k_{\mathrm{T}}^{(26)} =& s_2s_3s_5s_8s_9 + s_1s_2s_5s_7s_8 - s_2s_3s_6s_8s_9 - s_1s_2s_4s_7s_8,\\
k_{\mathrm{T}}^{(27)} =& s_4s_5s_6s_7s_9 + s_1s_3s_4s_5s_6 - s_4s_6s_7s_8s_9 - s_1s_2s_3s_4s_6,\\
k_{\mathrm{T}}^{(28)} =& s_2s_3s_5s_6s_8 + s_2s_4s_5s_7s_8 + s_1s_2s_4s_5s_8 + s_2s_5s_6s_8s_9\\
&- s_3s_5s_6s_8s_9 - s_1s_2s_4s_5s_7 - s_1s_4s_5s_7s_8 - s_2s_3s_5s_6s_9,\\
k_{\mathrm{T}}^{(29)} =& s_4s_5s_6s_8s_9 + s_1s_2s_4s_5s_6 + s_4s_5s_6s_7s_8 + s_2s_3s_4s_5s_6\\
&- s_1s_2s_3s_5s_6 - s_4s_5s_7s_8s_9 - s_1s_2s_3s_4s_5 - s_5s_6s_7s_8s_9.
\end{aligned}
$$

In Section 4, it is sufficient to consider only first nine zero-potentials, i.e. we put $\alpha_i = 0$

for $i \geqslant 10$.

In the case of n.n. and n.n.n. hopping anisotropy (considered in Section 5), the zero-potentials invariant with respect to π-rotations are of the form:

Here the zero-potentials, in the case considered in Section 5, are presented:

$$
\begin{aligned}
k_{\mathrm{T}}^{(1)} =& s_1 + s_9 - 2s_5,\\
k_{\mathrm{T}}^{(2)} =& s_2 + s_8 - 2s_5,\\
k_{\mathrm{T}}^{(3)} =& s_3 + s_7 - 2s_5,\\
k_{\mathrm{T}}^{(4)} =& s_4 + s_6 - 2s_5;\\
k_{\mathrm{T}}^{(5)} =& s_1s_2 + s_8s_9 - s_4s_5 - s_5s_6,\\
k_{\mathrm{T}}^{(6)} =& s_2s_3 + s_7s_8 - s_4s_5 - s_5s_6,\\
k_{\mathrm{T}}^{(7)} =& s_1s_4 + s_6s_9 - s_2s_5 - s_5s_8,\\
k_{\mathrm{T}}^{(8)} =& s_3s_6 + s_4s_7 - s_2s_5 - s_5s_8,\\
k_{\mathrm{T}}^{(9)} =& s_2s_4 + s_6s_8 - s_3s_5 - s_5s_7,\\
k_{\mathrm{T}}^{(10)} =& s_2s_6 + s_4s_8 - s_1s_5 - s_5s_9,\\
k_{\mathrm{T}}^{(11)} =& s_1s_3 + s_7s_9 - 2s_4s_6,\\
k_{\mathrm{T}}^{(12)} =& s_1s_7 + s_3s_9 - 2s_2s_8;\\
k_{\mathrm{T}}^{(13)} =& s_1s_2s_5 + s_5s_8s_9 - s_2s_3s_6 - s_4s_7s_8,\\
k_{\mathrm{T}}^{(14)} =& s_2s_5s_6 + s_4s_5s_8 - s_2s_3s_6 - s_4s_7s_8,\\
k_{\mathrm{T}}^{(15)} =& s_1s_4s_5 + s_5s_6s_9 - s_2s_3s_6 - s_4s_7s_8,\\
k_{\mathrm{T}}^{(16)} =& s_2s_3s_5 + s_5s_7s_8 - s_1s_2s_4 - s_6s_8s_9,\\
k_{\mathrm{T}}^{(17)} =& s_3s_5s_6 + s_4s_5s_7 - s_1s_2s_4 - s_6s_8s_9,\\
k_{\mathrm{T}}^{(18)} =& s_2s_4s_5 + s_5s_6s_8 - s_1s_2s_4 - s_6s_8s_9,\\
k_{\mathrm{T}}^{(19)} =& s_1s_5s_6 + s_4s_5s_9 - s_1s_2s_6 - s_4s_8s_9,\\
k_{\mathrm{T}}^{(20)} =& s_2s_3s_4 + s_6s_7s_8 - s_3s_4s_5 - s_5s_6s_7,\\
k_{\mathrm{T}}^{(21)} =& s_2s_4s_7 + s_3s_6s_8 - s_2s_5s_7 - s_3s_5s_8,\\
k_{\mathrm{T}}^{(22)} =& s_1s_4s_8 + s_2s_6s_9 - s_2s_5s_9 - s_1s_5s_8,\\
k_{\mathrm{T}}^{(23)} =& s_1s_2s_3 + s_7s_8s_9 - 2s_4s_5s_6,\\
k_{\mathrm{T}}^{(24)} =& s_1s_4s_7 + s_3s_6s_9 - 2s_2s_5s_8,\\
k_{\mathrm{T}}^{(25)} =& s_1s_2s_7 + s_3s_8s_9 - s_2s_3s_8 - s_2s_7s_8,\\
k_{\mathrm{T}}^{(26)} =& s_1s_3s_6 + s_4s_7s_9 - s_1s_4s_6 - s_4s_6s_9,\\
k_{\mathrm{T}}^{(27)} =& s_3s_4s_6 + s_4s_6s_7 - s_1s_3s_4 - s_6s_7s_9,\\
k_{\mathrm{T}}^{(28)} =& s_1s_2s_8 + s_2s_8s_9 - s_1s_7s_8 - s_2s_3s_9,\\
k_{\mathrm{T}}^{(29)} =& s_1s_3s_5 + s_5s_7s_9 - s_2s_4s_6 - s_4s_6s_8,\\
k_{\mathrm{T}}^{(30)} =& s_1s_5s_7 + s_3s_5s_9 - s_2s_4s_8 - s_2s_6s_8;
\end{aligned}
$$

$$
\begin{aligned}
k_{\mathrm{T}}^{(31)} =& s_1s_2s_4s_5 + s_5s_6s_8s_9 - s_2s_3s_5s_6 - s_4s_5s_7s_8,\\
k_{\mathrm{T}}^{(32)} =& s_1s_2s_4s_7 + s_3s_6s_8s_9 - s_2s_3s_5s_8 - s_2s_5s_7s_8,\\
k_{\mathrm{T}}^{(33)} =& s_1s_4s_7s_8 + s_2s_3s_6s_9 - s_1s_2s_5s_8 - s_2s_5s_8s_9,\\
k_{\mathrm{T}}^{(34)} =& s_1s_2s_3s_6 + s_4s_7s_8s_9 - s_1s_4s_5s_6 - s_4s_5s_6s_9,\\
k_{\mathrm{T}}^{(35)} =& s_1s_2s_3s_4 + s_6s_7s_8s_9 - s_3s_4s_5s_6 - s_4s_5s_6s_7,\\
k_{\mathrm{T}}^{(36)} =& s_1s_2s_3s_5 + s_5s_7s_8s_9 - s_2s_4s_5s_6 - s_4s_5s_6s_8,\\
k_{\mathrm{T}}^{(37)} =& s_1s_4s_5s_7 + s_3s_5s_6s_9 - s_2s_4s_5s_8 - s_2s_5s_6s_8,\\
k_{\mathrm{T}}^{(38)} =& s_1s_2s_4s_8 + s_2s_6s_8s_9 - s_1s_5s_7s_8 - s_2s_3s_5s_9,\\
k_{\mathrm{T}}^{(39)} =& s_2s_3s_6s_8 + s_2s_4s_7s_8 - s_1s_2s_5s_7 - s_3s_5s_8s_9,\\
k_{\mathrm{T}}^{(40)} =& s_2s_3s_4s_6 + s_4s_6s_7s_8 - s_1s_3s_4s_5 - s_5s_6s_7s_9,\\
k_{\mathrm{T}}^{(41)} =& s_1s_2s_4s_6 + s_4s_6s_8s_9 - s_1s_3s_5s_6 - s_4s_5s_7s_9;\\
k_{\mathrm{T}}^{(42)} =& s_1s_2s_3s_4s_6 + s_4s_6s_7s_8s_9 - s_1s_3s_4s_5s_6 - s_4s_5s_6s_7s_9,\\
k_{\mathrm{T}}^{(43)} =& s_1s_2s_5s_7s_8 + s_2s_3s_5s_8s_9 - s_1s_2s_4s_7s_8 - s_2s_3s_6s_8s_9,\\
k_{\mathrm{T}}^{(44)} =& s_1s_2s_4s_5s_7 + s_3s_5s_6s_8s_9 - s_2s_3s_5s_6s_8 - s_2s_4s_5s_7s_8,\\
k_{\mathrm{T}}^{(45)} =& s_1s_2s_4s_5s_8 + s_2s_5s_6s_8s_9 - s_1s_4s_5s_7s_8 - s_2s_3s_5s_6s_9,\\
k_{\mathrm{T}}^{(46)} =& s_1s_2s_3s_5s_6 + s_4s_5s_7s_8s_9 - s_1s_2s_4s_5s_6 - s_4s_5s_6s_8s_9,\\
k_{\mathrm{T}}^{(47)} =& s_1s_2s_3s_4s_5 + s_5s_6s_7s_8s_9 - s_2s_3s_4s_5s_6 - s_4s_5s_6s_7s_8.
\end{aligned}
$$

In Section 5, it is sufficient to consider only first nine zero-potentials, i.e. we put $\alpha_i = 0$ for $i \geqslant 10$.

Appendix B

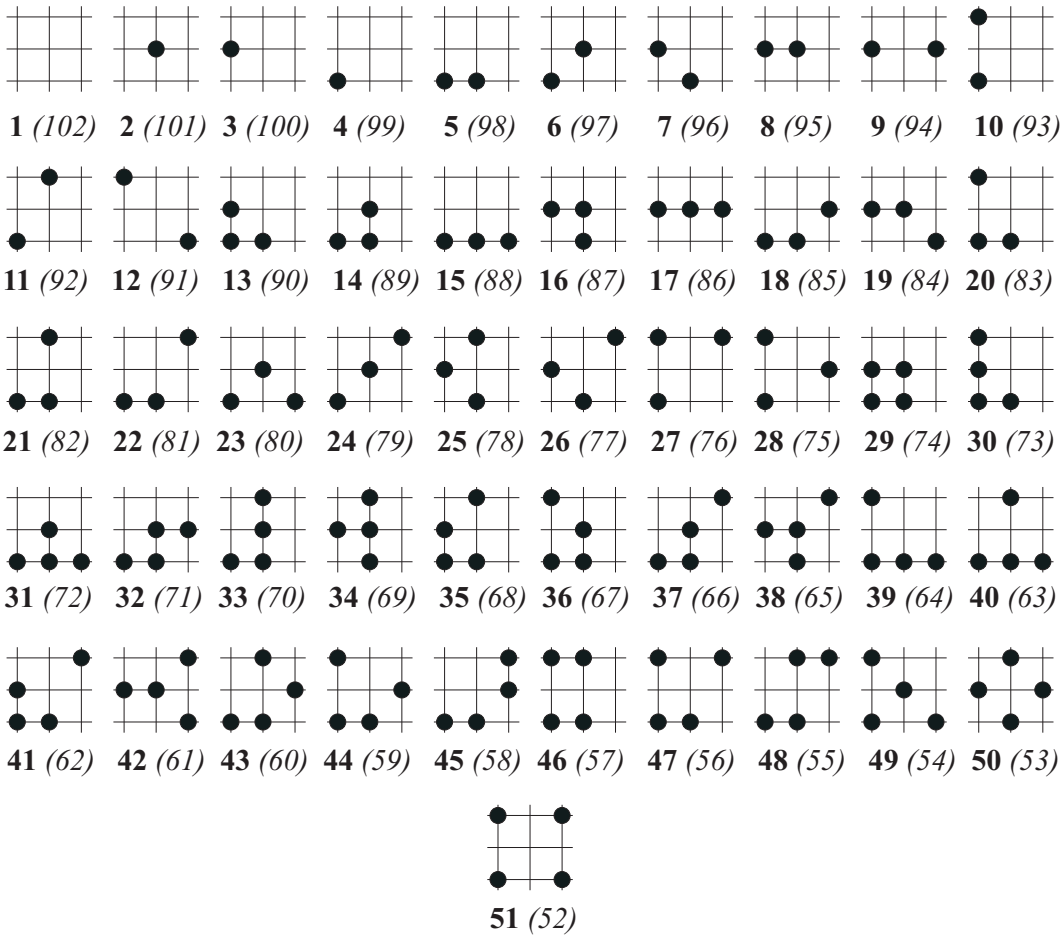

Figure 29: All the T-plaquette configurations, over which the potentials (84) and (85) are minimized, up to the symmetries of H (in the isotropic case of n.n. hopping only). The configurations that can be obtained from the displayed ones by the hole-particle transformation are not shown, only the numbers assigned to them are given in brackets.

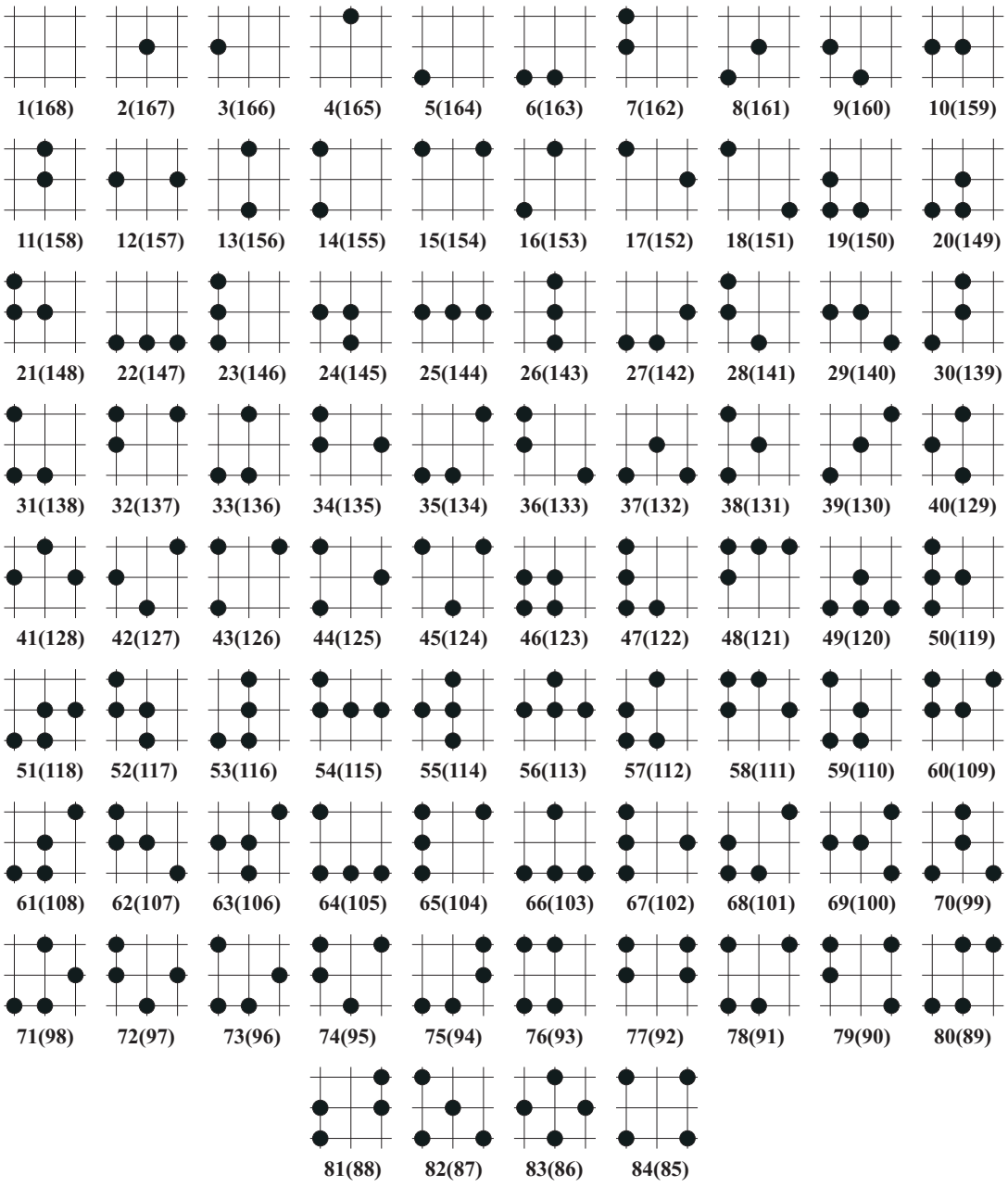

Figure 30: All the T-plaquette configurations in the case of anisotropic interactions of n.n. hopping, up to rotations by π and reflections in lattice lines parallel to the axes. The configurations that can be obtained from the displayed ones by the hole-particle transformation are not shown, only the numbers assigned to them are given in the brackets.

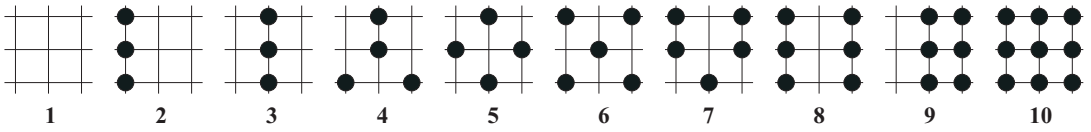

Figure 31: All the admissible T-plaquette configurations, up to rotations by π, that are used in constructing the fourth-order phase diagram in a neighborhood of point **a** of Fig. 20, i.e. the elements of $\mathcal{S}_T^{\mathbf{a}}$.

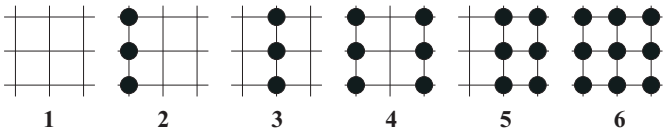

Figure 32: All the admissible T-plaquette configurations that are used in constructing the fourth-order phase diagram, up to rotations by π, in a neighborhood of point **b** of Fig. 21, i.e. the elements of $\mathcal{S}_T^{\mathbf{b}}$ (the vertical n.n. pairs that are occupied by one ion are forbidden).

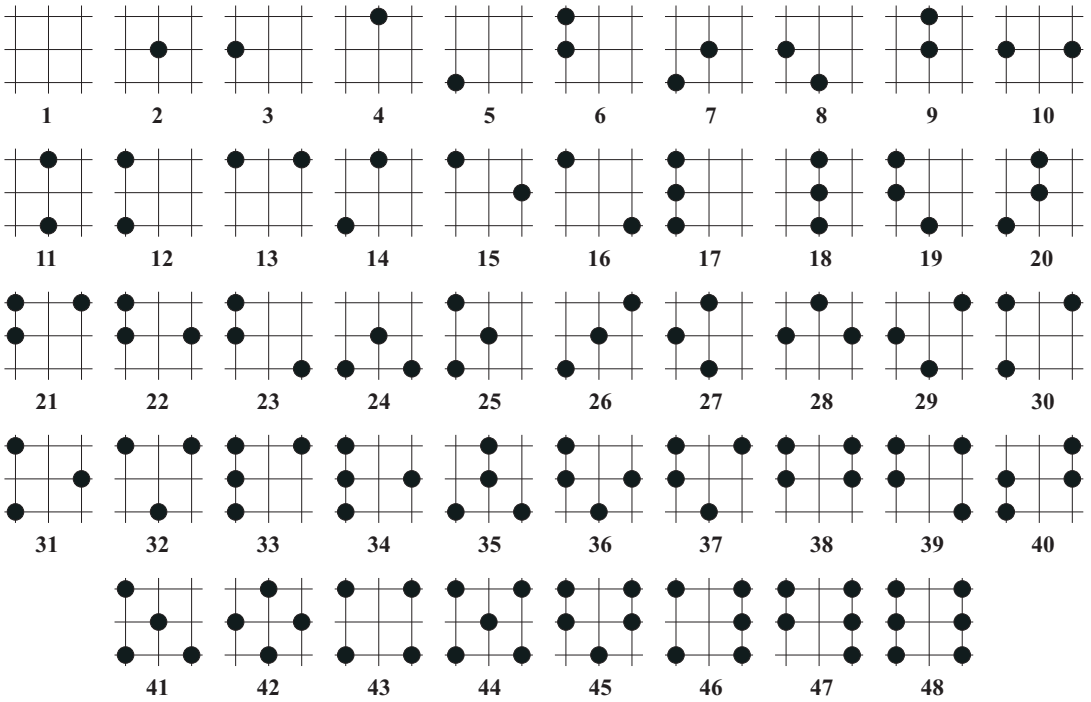

Figure 33: All the admissible T-plaquette configurations, up to rotations by π and reflections in lattice lines parallel to the axes, that are used in constructing the fourth-order phase diagram in a neighborhood of point $\mathbf{c}^-$ of Fig. 21, i.e. the elements of $\mathcal{S}_T^{\mathbf{c}^-}$ (the horizontal n.n. pairs that are occupied by two ions are forbidden).

Appendix C

In this section, at each point $p = (\omega, \varepsilon)$ we give the sets $\{\alpha_i(p)\}$ of the zero-potential coefficients α_i that we used to construct the four phase diagrams, presented in the previous section. Specifically, for each of the four phase diagrams we define a partition, called α-partition, of the (ω, ε)-plane (see Figs. 34–37 displayed below and Tables 8–11 in Appendix E) into sets that differ, in general, from the domains $\mathcal{S}_D$. To each set of such a partition we assign a set $\{(a_i, b_i, c_i)\}$ of triplets of rational numbers, such that the coefficients $\alpha_i(p)$ (with p in the considered set) are affine functions of the form $a_i\omega + b_i\varepsilon + c_i$. We have not been able to find one set $\{(a_i, b_i, c_i)\}$, that turns the fourth order potentials into m-potentials in the whole (ω, ε)-plane. We have not also succeeded in assigning to each domain $\mathcal{S}_D$ an exactly one set $\{(a_i, b_i, c_i)\}$. The same remarks apply to the (ω, δ)-plane.

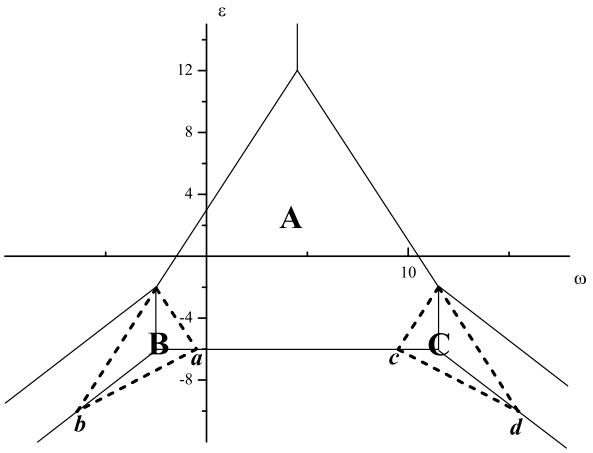

Figure 34: The sets **A**, **B**, **C**, whose boundaries are marked with dashed lines, used in Table 8 to define the α-partition of the fourth order phase diagram in the case of fermions and for $\delta = 0$.The dashed-line segments are determined by their intersection points: $\mathbf{a} = (-1/2, -6)$, $\mathbf{b} = (-13/2, -10)$, $\mathbf{c} = (19/2, -6)$, $\mathbf{d} = (31/2, -10)$. The coordinates of the remaining points can be read from Fig. 11.

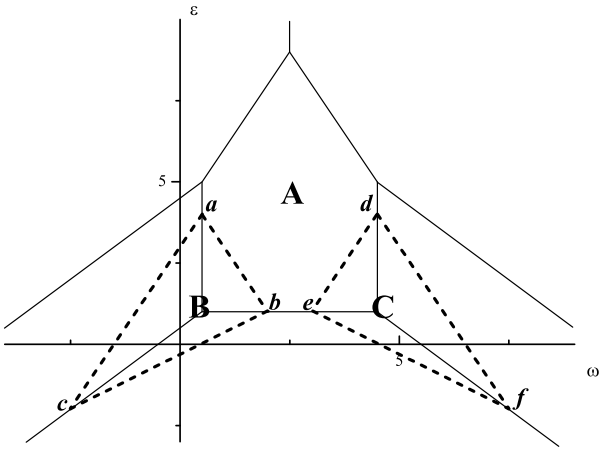

Figure 35: The sets **A**, **B**, **C**, whose boundaries are marked with dashed lines, used in Table 9 to define the α-partition of the fourth order phase diagram in the case of hardcore bosons and for $\delta = 0$. The dashed-line segments are determined by their intersection points: $\mathbf{a} = (1/2, 4)$, $\mathbf{b} = (2, 1)$, $\mathbf{c} = (-5/2, -2)$, $\mathbf{d} = (9/2, 4)$, $\mathbf{e} = (3, 1)$, $\mathbf{f} = (15/2, -2)$.

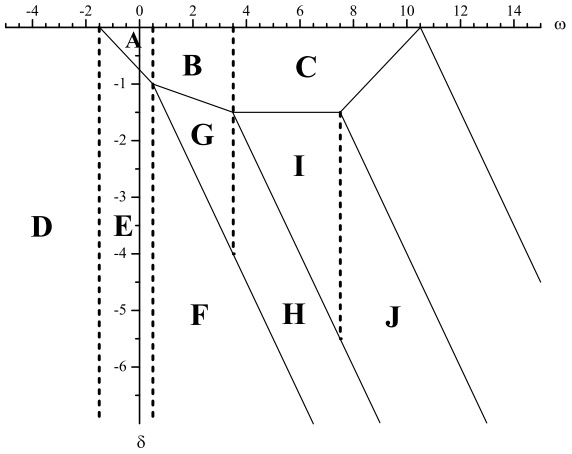

Figure 36: The sets **A,B**,..., whose boundaries are marked with dashed and continuous lines (the continuous lines are the boundaries of the phase diagram), used in Table 10 to define the α-partition of the fourth order phase diagram in the case of fermions and for $\varepsilon = 0$.

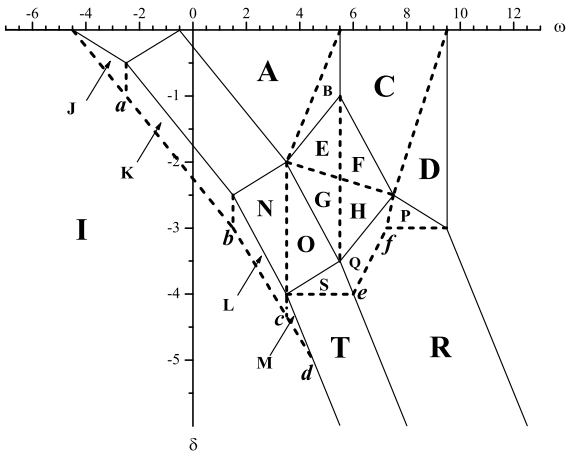

Figure 37: The sets **A,B**,..., whose boundaries are marked with dashed and continuous lines (the continuous lines are the boundaries of the phase diagram), used in Table 11 to define the α-partition of the fourth order phase diagram in the case of hardcore bosons and for $\varepsilon = 0$. The dashed-line segments are determined by their intersection points: $\mathbf{a} = (-5/2, -1)$, $\mathbf{b} = (3/2, -3)$, $\mathbf{c} = (7/2, -13/3)$, $\mathbf{d} = (9/2, -5)$, $\mathbf{e} = (6, -4)$, $\mathbf{f} = (29/4, -3)$.

Appendix D

Here we provide equations of line boundaries between the phase domains, and coordinates of the crossing points of the line boundaries that appear in the phase diagrams presented in Section 4. The symbols like $\mathbb{S}_1|\mathbb{S}_2$ stand for the line boundary between the phases $\mathbb{S}_1$ and $\mathbb{S}_2$, etc.

Table 1: Domain boundaries of the phase diagrams for fermions, shown in Fig. 16.

Lines	$0 < \beta_2 \leqslant 7$	$7 \leqslant \beta_2 \leqslant 10$
$\mathbb{S}_{seg}\|\mathbb{S}_{cb}$	$\omega = \beta_2 + \frac{9}{2}$	
$\mathbb{S}_{seg}\|\mathbb{S}_{dd}$	$\varepsilon = 2\omega - 2\beta_2 + 3$	—
$\mathbb{S}_{dd}\|\mathbb{S}_{cb}$	$\varepsilon = -2\omega + 2\beta_2 + 21$	—
$\mathbb{S}_{seg}\|\mathbb{S}^v_{v1}$	$\varepsilon = \omega + \frac{1}{2}$	
$\mathbb{S}^v_{d1}\|\mathbb{S}_{cb}$	$\varepsilon = -\omega + 2\beta_2 + \frac{19}{2}$	
$\mathbb{S}^v_{v1}\|\mathbb{S}_{dd}$	$\omega = 2\beta_2 - \frac{5}{2}$	—
$\mathbb{S}_{dd}\|\mathbb{S}^v_{d1}$	$\omega = \frac{23}{2}$	—
$\mathbb{S}^v_{v2}\|\mathbb{S}_{dd}$	$\varepsilon = 2\beta_2 - 6$	—
$\mathbb{S}^v_{v1}\|\mathbb{S}^v_{v2}$	$\varepsilon = \omega - \frac{7}{2}$	
$\mathbb{S}^v_{v2}\|\mathbb{S}^v_{d1}$	$\varepsilon = -\omega + 2\beta_2 + \frac{11}{2}$	
$\mathbb{S}^v_{v1}\|\mathbb{S}^v_{d1}$	—	$\omega = \beta_2 + \frac{9}{2}$

Points	$0 < \beta_2 \leqslant 7$	$7 \leqslant \beta_2 \leqslant 10$
a	$\left(\beta_2 + \frac{9}{2}, 12\right)$	$\left(\beta_2 + \frac{9}{2}, \beta_2 + 5\right)$
b	$\left(2\beta_2 - \frac{5}{2}, 2\beta_2 - 2\right)$	$\left(\beta_2 + \frac{9}{2}, \beta_2 + 1\right)$
c	$\left(\frac{23}{2}, 2\beta_2 - 2\right)$	—
d	$\left(2\beta_2 - \frac{5}{2}, 2\beta_2 - 6\right)$	—
e	$\left(\frac{23}{2}, 2\beta_2 - 6\right)$	—

Table 2: Domain boundaries of the phase diagrams for hardcore bosons, shown in Fig. 16.

Lines	$0 < \beta_2 \leqslant 2$	$2 < \beta_2 \leqslant 5$
$\mathbb{S}_{seg}\|\mathbb{S}_{cb}$	$\omega = \beta_2 + \frac{5}{2}$	
$\mathbb{S}_{seg}\|\mathbb{S}_{pcb}$	$\varepsilon = 2\omega - 2\beta_2 + 4$	—
$\mathbb{S}_{pcb}\|\mathbb{S}_{cb}$	$\varepsilon = -2\omega + 2\beta_2 + 14$	—
$\mathbb{S}_{seg}\|\mathbb{S}^v_{v1}$	$\varepsilon = \omega + \frac{9}{2}$	
$\mathbb{S}^v_{d1}\|\mathbb{S}_{cb}$	$\varepsilon = -\omega + 2\beta_2 + \frac{19}{2}$	
$\mathbb{S}^v_{v1}\|\mathbb{S}_{pcb}$	$\omega = 2\beta_2 + \frac{1}{2}$	—
$\mathbb{S}_{pcb}\|\mathbb{S}^v_{d1}$	$\omega = \frac{9}{2}$	—
$\mathbb{S}^v_{v2}\|\mathbb{S}_{pcb}$	$\varepsilon = 2\beta_2 + 1$	—
$\mathbb{S}^v_{v1}\|\mathbb{S}^v_{v2}$	$\varepsilon = \omega + \frac{1}{2}$	
$\mathbb{S}^v_{v2}\|\mathbb{S}^v_{d1}$	$\varepsilon = -\omega + 2\beta_2 + \frac{11}{2}$	
$\mathbb{S}^v_{v1}\|\mathbb{S}^v_{d1}$	—	$\omega = \beta_2 + \frac{5}{2}$

Points	$0 < \beta_2 \leqslant 2$	$2 < \beta_2 \leqslant 5$
a	$\left(\beta_2 + \frac{5}{2}, 9\right)$	$\left(\beta_2 + \frac{5}{2}, \beta_2 + 7\right)$
b	$\left(2\beta_2 + \frac{1}{2}, 2\beta_2 + 5\right)$	$\left(\beta_2 + \frac{5}{2}, \beta_2 + 3\right)$
c	$\left(\frac{9}{2}, 2\beta_2 + 5\right)$	—
d	$\left(2\beta_2 + \frac{1}{2}, 2\beta_2 + 1\right)$	—
e	$\left(\frac{9}{2}, 2\beta_2 + 1\right)$	—

Table 3: Domain boundaries of the phase diagrams shown in Fig. 17.

Lines	$0 < \beta_2 \leqslant 1$	$1 < \beta_2 \leqslant 2$	$2 < \beta_2 \leqslant 3$	$3 < \beta_2 \leqslant 6$
$\mathbb{S}_+ \vert \mathbb{S}_-$	$\delta = 0$			
$\mathbb{S}_{dd} \vert \mathbb{S}_-$	$\delta = -\frac{\omega}{2} + \frac{\beta_2}{2} - \frac{3}{4}$		—	
$\mathbb{S}_{dd} \vert \mathbb{S}_1$	$\delta = -\frac{\omega}{6} + \frac{\beta_2}{6} - \frac{11}{12}$		—	
$\mathbb{S}_{dd} \vert \mathbb{S}_2$	$\delta = -\frac{3}{2}$		—	
$\mathbb{S}_{dd} \vert \mathbb{S}_3$	$\delta = \frac{\omega}{2} - \frac{\beta_2}{2} - \frac{21}{4}$		—	
$\mathbb{S}_- \vert \mathbb{S}_1$	$\delta = -\omega + \beta_2 - \frac{1}{2}$			
$\mathbb{S}_1 \vert \mathbb{S}_2$	$\delta = -\omega + \beta_2 + 2$			
$\mathbb{S}_2 \vert \mathbb{S}_3$	$\delta = -\omega + \beta_2 + 6$			
$\mathbb{S}_3 \vert \mathbb{S}_{cb}$	$\delta = -\omega + \beta_2 + \frac{21}{2}$			
$\mathbb{S}_- \vert \mathbb{S}^v_{v1}$	—	$\delta = -\frac{\omega}{4} - \frac{1}{8}$		
$\mathbb{S}^v_{d2} \vert \mathbb{S}_{dd}$	—	$\delta = -\frac{\omega}{4} + \frac{\beta_2}{2} - \frac{9}{8}$		—
$\mathbb{S}^v_{d2} \vert \mathbb{S}_-$	—	$\delta = -\frac{3\omega}{4} + \frac{\beta_2}{2} - \frac{3}{8}$		
$\mathbb{S}^v_{d2} \vert \mathbb{S}_1$	—	$\delta = \frac{\omega}{4} - \frac{3\beta_2}{2} + \frac{1}{8}$		
$\mathbb{S}^v_{d1} \vert \mathbb{S}_3$	—	$\delta = -\frac{\omega}{4} - \frac{\beta_2}{2} + \frac{27}{8}$		
$\mathbb{S}^v_{v1} \vert \mathbb{S}_{dd}$	—	$\omega = 2\beta_2 - \frac{5}{2}$		—
$\mathbb{S}^v_{d1} \vert \mathbb{S}_{dd}$	—	$\omega = \frac{23}{2}$		—
$\mathbb{S}^v_{d1} \vert \mathbb{S}_{cb}$	—	$\omega = 2\beta_2 + \frac{19}{2}$		
$\mathbb{S}^v_{v3} \vert \mathbb{S}^v_{v1}$	—		$\delta = \frac{\omega}{4} - \frac{7}{8}$	
$\mathbb{S}^v_{v3} \vert \mathbb{S}_{dd}$	—		$\delta = -\frac{\omega}{2} + \frac{3\beta_2}{2} - \frac{11}{4}$	—
$\mathbb{S}^v_{v3} \vert \mathbb{S}_-$	—		$\delta = -\frac{\omega}{2} + \frac{1}{4}$	
$\mathbb{S}^v_{v3} \vert \mathbb{S}^v_{d2}$	—		$\delta = \frac{\omega}{4} - \frac{3\beta_2}{2} + \frac{17}{8}$	
$\mathbb{S}^v_{d4} \vert \mathbb{S}^v_{d2}$	—		$\delta = -\frac{3\omega}{4} + \frac{\beta_2}{2} + \frac{13}{8}$	
$\mathbb{S}^v_{d4} \vert \mathbb{S}_{dd}$	—		$\delta = \frac{\beta_2}{2} - \frac{5}{2}$	—
$\mathbb{S}^v_{d4} \vert \mathbb{S}_2$	—		$\delta = -\beta_2 + \frac{1}{2}$	
$\mathbb{S}^v_{d4} \vert \mathbb{S}^v_{d3}$	—		$\delta = -\frac{3\omega}{4} + \frac{\beta_2}{2} + \frac{37}{8}$	
$\mathbb{S}^v_{d3} \vert \mathbb{S}_{dd}$	—		$\delta = \frac{\omega}{2} + \frac{\beta_2}{2} - \frac{29}{4}$	—
$\mathbb{S}^v_{d3} \vert \mathbb{S}_3$	—		$\delta = \frac{\omega}{2} - 2\beta_2 - \frac{9}{4}$	
$\mathbb{S}^v_{d3} \vert \mathbb{S}^v_{d1}$	—		$\delta = -\frac{3\omega}{4} + \frac{\beta_2}{2} + \frac{57}{8}$	
$\mathbb{S}^v_{v2} \vert \mathbb{S}^v_{v3}$	—			$\delta = -\frac{\omega}{2} + \frac{7}{4}$
$\mathbb{S}^v_{v2} \vert \mathbb{S}^v_{d4}$	—			$\delta = -\beta_2 + 2$
$\mathbb{S}^v_{v2} \vert \mathbb{S}^v_{d3}$	—			$\delta = \frac{\omega}{2} - 2\beta_2 + \frac{1}{4}$
$\mathbb{S}^v_{v2} \vert \mathbb{S}^v_{d1}$	—			$\omega = 2\beta_2 + \frac{11}{2}$

Points	$0 < \beta_2 \leqslant 1$	$1 < \beta_2 \leqslant 2$	$2 < \beta_2 \leqslant 3$	$3 < \beta_2 \leqslant 6$
a	$\left(\beta_2 - \frac{3}{2}, 0\right)$	$\left(-\frac{1}{2}, 0\right)$		
b	$\left(\beta_2 + \frac{1}{2}, -1\right)$	$\left(2\beta_2 - \frac{5}{2}, -\frac{\beta_2}{2} + \frac{1}{2}\right)$	$\left(2\beta_2 - \frac{5}{2}, \frac{\beta_2}{2} - \frac{3}{2}\right)$	$\left(\frac{7}{2}, 0\right)$
c	$\left(\beta_2 + \frac{7}{2}, -\frac{3}{2}\right)$	$\left(\frac{23}{2}, -\frac{\beta_2}{2} + \frac{1}{2}\right)$	$\left(\frac{23}{2}, \frac{\beta_2}{2} - \frac{3}{2}\right)$	$\left(\frac{3}{2}, -\frac{1}{2}\right)$
d	$\left(\beta_2 + \frac{15}{2}, -\frac{3}{2}\right)$	$\left(2\beta_2 + \frac{19}{2}, -\beta_2 + 1\right)$	$\left(\frac{3}{2}, -\frac{1}{2}\right)$	$\left(2\beta_2 + \frac{11}{2}, -\beta_2 + 3\right)$
e	$\left(\beta_2 + \frac{21}{2}, 0\right)$	$\left(\frac{3}{2}, \frac{\beta_2}{2} - \frac{3}{2}\right)$	$\left(4\beta_2 - \frac{13}{2}, -\frac{\beta_2}{2} + \frac{1}{2}\right)$	$\left(2\beta_2 - \frac{1}{2}, -\beta_2 + 2\right)$
f	—	$\left(4\beta_2 - \frac{5}{2}, -\frac{\beta_2}{2} - \frac{1}{2}\right)$	$\left(2\beta_2 - \frac{5}{2}, -\beta_2 + \frac{3}{2}\right)$	$\left(2\beta_2 + \frac{7}{2}, -\beta_2 + 2\right)$
g	—	$\left(2\beta_2 - \frac{1}{2}, -\beta_2\right)$	$\left(2\beta_2 + \frac{15}{2}, -\beta_2 + \frac{3}{2}\right)$	$\left(2\beta_2 - \frac{5}{2}, -\beta_2 + \frac{3}{2}\right)$
h	—	$\left(\beta_2 + \frac{7}{2}, -\frac{3}{2}\right)$	$\left(\frac{11}{2}, \frac{\beta_2}{2} - \frac{5}{2}\right)$	$\left(2\beta_2 + \frac{15}{2}, -\beta_2 + \frac{3}{2}\right)$
i	—	$\left(\beta_2 + \frac{15}{2}, -\frac{3}{2}\right)$	$\left(\frac{19}{2}, \frac{\beta_2}{2} - \frac{5}{2}\right)$	$\left(2\beta_2 + \frac{19}{2}, -\beta_2 + 1\right)$
j	—		$\left(2\beta_2 + \frac{19}{2}, -\beta_2 + 1\right)$	$\left(2\beta_2 + \frac{3}{2}, -\beta_2 + \frac{1}{2}\right)$
k	—		$\left(2\beta_2 + \frac{3}{2}, -\beta_2 + \frac{1}{2}\right)$	$\left(2\beta_2 + \frac{11}{2}, -\beta_2 + \frac{1}{2}\right)$
l	—		$\left(2\beta_2 + \frac{11}{2}, -\beta_2 + \frac{1}{2}\right)$	$\left(2\beta_2 - \frac{1}{2}, -\beta_2\right)$
m	—		$\left(2\beta_2 - \frac{1}{2}, -\beta_2\right)$	—

Table 4: Domain boundaries of the phase diagrams shown in Fig. 18.

Lines	$0 < \beta_2 \leqslant 3$
$\mathcal{S}_-\vert\mathcal{S}_+$	$\delta = 0$
$\mathcal{S}_-\vert\mathcal{S}^v_{v1}$	$\delta = -\frac{\omega}{4} - \frac{9}{8}$
$\mathcal{S}^v_{v1}\vert\mathcal{S}^v_{v3}$	$\delta = \frac{\omega}{4} + \frac{1}{8}$
$\mathcal{S}^v_{v3}\vert\mathcal{S}^v_{v2}$	$\delta = -\frac{\omega}{2} - \frac{1}{4}$
$\mathcal{S}_-\vert\mathcal{S}^v_{v3}$	$\delta = -\frac{\omega}{2} - \frac{7}{4}$
$\mathcal{S}^v_{v3}\vert\mathcal{S}^v_{d2}$	$\delta = \frac{\omega}{4} - \frac{3\beta_2}{2} - \frac{23}{8}$
$\mathcal{S}^v_{d2}\vert\mathcal{S}^v_{d3}$	$\delta = -\frac{3\omega}{4} + \frac{\beta_2}{2} + \frac{5}{8}$
$\mathcal{S}_-\vert\mathcal{S}^v_{d2}$	$\delta = -\frac{3\omega}{4} + \frac{\beta_2}{2} - \frac{11}{8}$
$\mathcal{S}^v_{d2}\vert\mathcal{S}_1$	$\delta = \frac{\omega}{4} - \frac{3\beta_2}{2} - \frac{39}{8}$
$\mathcal{S}^v_{v2}\vert\mathcal{S}^v_{d3}$	$\delta = \frac{\omega}{2} - 2\beta_2 - \frac{15}{4}$
$\mathcal{S}^v_{d3}\vert\mathcal{S}_3$	$\delta = \frac{\omega}{2} - 2\beta_2 - \frac{25}{4}$
$\mathcal{S}^v_{d3}\vert\mathcal{S}^v_{d1}$	$\delta = -\frac{3\omega}{4} + \frac{\beta_2}{2} + \frac{25}{8}$
$\mathcal{S}^v_{d1}\vert\mathcal{S}_3$	$\delta = -\frac{\omega}{4} - \frac{\beta_2}{2} - \frac{5}{8}$
$\mathcal{S}^v_{v2}\vert\mathcal{S}^v_{d1}$	$\omega = 2\beta_2 + \frac{11}{2}$
$\mathcal{S}^v_{d1}\vert\mathcal{S}_{cb}$	$\omega = 2\beta_2 + \frac{19}{2}$
$\mathcal{S}_-\vert\mathcal{S}_1$	$\delta = -\omega + \beta_2 - \frac{1}{2}$
$\mathcal{S}_1\vert\mathcal{S}_3$	$\delta = -\omega + \beta_2 + 2$
$\mathcal{S}_3\vert\mathcal{S}_{cb}$	$\delta = -\omega + \beta_2 + \frac{13}{2}$

Points	$0 < \beta_2 \leqslant 3$
a	$\left(-\frac{9}{2}, 0\right)$
b	$\left(-\frac{1}{2}, 0\right)$
c	$\left(-\frac{5}{2}, -\frac{1}{2}\right)$
d	$\left(2\beta_2 + \frac{11}{2}, -\beta_2 - 1\right)$
e	$\left(2\beta_2 + \frac{7}{2}, -\beta_2 - 2\right)$
f	$\left(2\beta_2 + \frac{3}{2}, -\beta_2 - \frac{5}{2}\right)$
g	$\left(2\beta_2 + \frac{15}{2}, -\beta_2 - \frac{5}{2}\right)$
h	$\left(2\beta_2 + \frac{19}{2}, -\beta_2 - 3\right)$
i	$\left(2\beta_2 + \frac{11}{2}, -\beta_2 - 7/2\right)$
j	$\left(2\beta_2 + \frac{7}{2}, -\beta_2 - 4\right)$

Table 5: Domain boundaries of the phase diagrams shown in Fig. 22 and Fig. 23.

Lines	fermions	bosons
$\mathbb{S}_{seg}\|\mathbb{S}_{cb}$	$\omega = \frac{9}{2}$	$\omega = \frac{5}{2}$
$\mathbb{S}^v_{v1}\|\mathbb{S}^v_{d1}$	$\omega = \frac{9}{2}$	$\omega = \frac{5}{2}$
$\mathbb{S}^v_{v1}\|\mathbb{S}_{seg}$	$\varepsilon = \omega + \frac{1}{2}$	$\varepsilon = \omega + \frac{9}{2}$
$\mathbb{S}^v_{d1}\|\mathbb{S}_{cb}$	$\varepsilon = -\omega + \frac{19}{2}$	
$\mathbb{S}^v_{v2}\|\mathbb{S}^v_{v1}$	$\varepsilon = \omega - \frac{7}{2}$	$\varepsilon = \omega + \frac{1}{2}$
$\mathbb{S}^v_{v2}\|\mathbb{S}^v_{d1}$	$\varepsilon = -\omega + \frac{11}{2}$	

Points	fermions	bosons
a	$\left(\frac{9}{2}, 5\right)$	$\left(\frac{5}{2}, 7\right)$
b	$\left(\frac{9}{2}, 1\right)$	$\left(\frac{5}{2}, 3\right)$

Table 6: Domain boundaries of the phase diagrams shown in Fig. 24 and Fig. 25.

Lines	fermions	bosons
$\mathbb{S}_-\|\mathbb{S}_+$	$\delta = 0$	
$\mathbb{S}^v_{v1}\|\mathbb{S}_-$	$\delta = -\frac{\omega}{4} - \frac{1}{8}$	$\delta = -\frac{\omega}{4} - \frac{9}{8}$
$\mathbb{S}^v_{v1}\|\mathbb{S}^v_{v3}$	$\delta = \frac{\omega}{4} - \frac{7}{8}$	$\delta = \frac{\omega}{4} + \frac{1}{8}$
$\mathbb{S}^v_{v3}\|\mathbb{S}_-$	$\delta = -\frac{\omega}{2} + \frac{1}{4}$	$\delta = -\frac{\omega}{2} - \frac{7}{4}$
$\mathbb{S}^v_{v3}\|\mathbb{S}^v_{v2}$	$\delta = -\frac{\omega}{2} + \frac{7}{4}$	$\delta = -\frac{\omega}{2} - \frac{1}{4}$

Points	fermions	bosons
a	$\left(-\frac{1}{2}, 0\right)$	$\left(-\frac{9}{2}, 0\right)$
b	$\left(\frac{7}{2}, 0\right)$	$\left(-\frac{1}{2}, 0\right)$
c	$\left(\frac{3}{2}, -\frac{1}{2}\right)$	$\left(-\frac{5}{2}, -\frac{1}{2}\right)$

Table 7: Domain boundaries of the phase diagrams shown in Fig. 26 and Fig. 27.

Lines	fermions	bosons
$\mathbb{S}^v_{v3}\|\mathbb{S}_-$	$\delta=-\frac{\omega}{2}+\frac{1}{4}$	$\delta=-\frac{\omega}{2}-\frac{7}{4}$
$\mathbb{S}^v_{v3}\|\mathbb{S}^v_{v2}$	$\delta=-\frac{\omega}{2}+\frac{7}{4}$	$\delta=-\frac{\omega}{2}-\frac{1}{4}$
$\mathbb{S}^v_{v3}\|\mathbb{S}^v_{d2}$	$\delta=\frac{\omega}{4}+\frac{17}{8}$	$\delta=\frac{\omega}{4}-\frac{23}{8}$
$\mathbb{S}^v_{d2}\|\mathbb{S}_-$	$\delta=-\frac{3\omega}{4}-\frac{3}{8}$	$\delta=-\frac{3\omega}{4}-\frac{11}{8}$
$\mathbb{S}^v_{d2}\|\mathbb{S}^v_{d4}$	$\delta=-\frac{3\omega}{4}+\frac{13}{8}$	—
$\mathbb{S}^v_{d2}\|\mathbb{S}^v_{d3}$	—	$\delta=-\frac{3\omega}{4}+\frac{5}{8}$
$\mathbb{S}^v_{d2}\|\mathbb{S}_1$	$\delta=\frac{\omega}{4}+\frac{1}{8}$	$\delta=\frac{\omega}{4}-\frac{39}{8}$
$\mathbb{S}^v_{d4}\|\mathbb{S}^v_{v2}$	$\delta=2$	—
$\mathbb{S}^v_{d4}\|\mathbb{S}_2$	$\delta=\frac{1}{2}$	—
$\mathbb{S}^v_{d4}\|\mathbb{S}^v_{d3}$	$\delta=-\frac{3\omega}{4}+\frac{37}{8}$	—
$\mathbb{S}^v_{d3}\|\mathbb{S}^v_{v2}$	$\delta=\frac{\omega}{2}+\frac{1}{4}$	$\delta=\frac{\omega}{2}-\frac{15}{4}$
$\mathbb{S}^v_{d3}\|\mathbb{S}_3$	$\delta=\frac{\omega}{2}-\frac{9}{4}$	$\delta=\frac{\omega}{2}-\frac{25}{4}$
$\mathbb{S}^v_{d3}\|\mathbb{S}^v_{d1}$	$\delta=-\frac{3\omega}{4}+\frac{57}{8}$	$\delta=-\frac{3\omega}{4}+\frac{25}{8}$
$\mathbb{S}^v_{d1}\|\mathbb{S}_3$	$\delta=-\frac{\omega}{4}+\frac{27}{8}$	$\delta=-\frac{\omega}{4}-\frac{5}{8}$
$\mathbb{S}^v_{d1}\|\mathbb{S}^v_{v2}$	$\omega=\frac{11}{2}$	
$\mathbb{S}^v_{d1}\|\mathbb{S}_{cb}$	$\omega=\frac{19}{2}$	
$\mathbb{S}_-\|\mathbb{S}_1$	$\delta=-\omega-\frac{1}{2}$	
$\mathbb{S}_1\|\mathbb{S}_2$	$\delta=-\omega+2$	—
$\mathbb{S}_1\|\mathbb{S}_3$	—	$\delta=-\omega+2$
$\mathbb{S}_2\|\mathbb{S}_3$	$\delta=-\omega+6$	—
$\mathbb{S}_3\|\mathbb{S}_{cb}$	$\delta=-\omega+\frac{21}{2}$	$\delta=-\omega+\frac{13}{2}$

Points	fermions	bosons
a	$\left(\frac{11}{2},3\right)$	$\left(\frac{11}{2},-1\right)$
b	$\left(-\frac{1}{2},2\right)$	$\left(\frac{7}{2},-2\right)$
c	$\left(\frac{7}{2},2\right)$	$\left(\frac{3}{2},-\frac{5}{2}\right)$
d	$\left(-\frac{5}{2},\frac{3}{2}\right)$	$\left(\frac{15}{2},-\frac{5}{2}\right)$
e	$\left(\frac{15}{2},\frac{3}{2}\right)$	$\left(\frac{19}{2},-3\right)$
f	$\left(\frac{19}{2},1\right)$	$\left(\frac{11}{2},-\frac{7}{2}\right)$
g	$\left(\frac{3}{2},\frac{1}{2}\right)$	$\left(\frac{7}{2},-4\right)$
h	$\left(\frac{11}{2},\frac{1}{2}\right)$	—
i	$\left(-\frac{1}{2},0\right)$	—

Appendix E

Table 8: The case of isotropic n.n. hopping only. The set of zero-potential coefficients $\{\alpha_i\}$ in the case of fermions and for $\delta = 0$. In the first column the sets of the α-partition are specified. For more comments see the text in Appendix C.

	α_1	α_2	α_3	α_4	α_5
$\mathbf{A}$	0	0	$-\frac{\omega}{96}+\frac{3}{64}$	0	$-\frac{1}{48}$
$\mathcal{S}_{dd}\cap\mathbf{B}$	0	0	$-\frac{5\omega}{192}-\frac{\varepsilon}{64}-\frac{3}{128}$	$\frac{\omega}{32}+\frac{\varepsilon}{32}+\frac{9}{64}$	$\frac{\omega}{64}+\frac{\varepsilon}{64}+\frac{19}{384}$
$\mathcal{S}_{v1}\cap\mathbf{B}$	0	0	$\frac{\omega}{192}-\frac{\varepsilon}{64}+\frac{7}{128}$	$-\frac{\omega}{32}+\frac{\varepsilon}{32}-\frac{1}{64}$	$-\frac{\omega}{64}+\frac{\varepsilon}{64}-\frac{11}{384}$
$\mathcal{S}_{v2}\cap\mathbf{B}$	0	0	$-\frac{5\omega}{192}+\frac{\varepsilon}{64}+\frac{21}{128}$	$\frac{\omega}{32}-\frac{\varepsilon}{32}-\frac{15}{64}$	$\frac{\omega}{64}-\frac{\varepsilon}{64}-\frac{53}{384}$
$\mathcal{S}_{dd}\cap\mathbf{C}$	0	0	$-\frac{5\omega}{192}+\frac{\varepsilon}{64}+\frac{33}{128}$	$-\frac{\omega}{32}+\frac{\varepsilon}{32}+\frac{27}{64}$	$-\frac{\omega}{64}+\frac{\varepsilon}{64}+\frac{73}{384}$
$\mathcal{S}_{v2}\cap\mathbf{C}$	0	0	$-\frac{5\omega}{192}-\frac{\varepsilon}{64}+\frac{9}{128}$	$-\frac{\omega}{32}-\frac{\varepsilon}{32}+\frac{3}{64}$	$-\frac{\omega}{64}-\frac{\varepsilon}{64}+\frac{1}{384}$
$\mathcal{S}_{d1}\cap\mathbf{C}$	0	0	$\frac{\omega}{192}+\frac{\varepsilon}{64}-\frac{13}{128}$	$\frac{\omega}{32}+\frac{\varepsilon}{32}-\frac{19}{64}$	$\frac{\omega}{64}+\frac{\varepsilon}{64}-\frac{65}{384}$

Table 9: The case of isotropic n.n. hopping only. The set of zero-potential coefficients $\{\alpha_i\}$ in the case of hardcore bosons and for $\delta = 0$. In the first column the sets of the α-partition are specified. For more comments see the text in Appendix C.

	α_1	α_2	α_3	α_4	α_5
$\mathbf{A}$	0	0	$-\frac{\omega}{96}+\frac{5}{192}$	0	$-\frac{1}{48}$
$\mathcal{S}_{pcb}\cap\mathbf{B}$	0	0	$-\frac{\omega}{24}-\frac{\varepsilon}{64}+\frac{23}{192}$	$\frac{\omega}{16}+\frac{7\varepsilon}{192}-\frac{37}{192}$	$\frac{\omega}{32}+\frac{5\varepsilon}{256}-\frac{91}{768}$
$\mathcal{S}_{v1}\cap\mathbf{B}$	0	0	$\frac{\omega}{192}-\frac{\varepsilon}{64}+\frac{37}{384}$	$-\frac{7\omega}{192}+\frac{7\varepsilon}{192}-\frac{55}{384}$	$-\frac{5\omega}{256}+\frac{5\varepsilon}{256}-\frac{143}{1536}$
$\mathcal{S}_{v2}\cap\mathbf{B}$	0	0	$-\frac{\omega}{24}+\frac{\varepsilon}{32}+\frac{7}{96}$	$\frac{\omega}{16}-\frac{\varepsilon}{16}-\frac{3}{32}$	$\frac{\omega}{32}-\frac{\varepsilon}{32}-\frac{13}{192}$
$\mathcal{S}_{pcb}\cap\mathbf{C}$	0	0	$-\frac{\omega}{24}+\frac{\varepsilon}{64}+\frac{17}{192}$	$-\frac{\omega}{16}+\frac{7\varepsilon}{192}+\frac{23}{192}$	$-\frac{\omega}{32}+\frac{5\varepsilon}{256}+\frac{29}{768}$
$\mathcal{S}_{v2}\cap\mathbf{C}$	0	0	$-\frac{\omega}{24}-\frac{\varepsilon}{32}+\frac{13}{96}$	$-\frac{\omega}{16}-\frac{\varepsilon}{16}+\frac{7}{32}$	$-\frac{\omega}{32}-\frac{\varepsilon}{32}+\frac{17}{192}$
$\mathcal{S}_{d1}\cap\mathbf{C}$	0	0	$\frac{\omega}{192}+\frac{\varepsilon}{64}-\frac{47}{384}$	$\frac{7\omega}{192}+\frac{7\varepsilon}{192}-\frac{125}{384}$	$\frac{5\omega}{256}+\frac{5\varepsilon}{256}-\frac{293}{1536}$

Table 10: The case of isotropic n.n. hopping only. The set of zero-potential coefficients $\{\alpha_i\}$ in the case of fermions and for $\varepsilon = 0$. In the first column the sets of the α-partition are specified. For more comments see the text in Appendix C.

	α_1	α_2	α_3	α_4	α_5
$\mathcal{S}_- \cap \mathbf{D}$	$-\frac{201\delta}{3200}$	$-\frac{\delta}{8}$	$-\frac{\omega}{96} + \frac{\delta}{6400} + \frac{3}{64}$	0	$-\frac{1}{48}$
$\mathcal{S}_- \cap \mathbf{E}$	$\frac{\omega}{32} - \frac{\delta}{16} + \frac{3}{64}$	$-\frac{\delta}{8}$	$-\frac{\omega}{96} + \frac{3}{64}$	0	$-\frac{1}{48}$
$\mathcal{S}_- \cap \mathbf{F}$	$\frac{\omega}{48} - \frac{\delta}{16} + \frac{5}{96}$	$-\frac{\delta}{8}$	$\frac{1}{24}$	0	$-\frac{1}{48}$
$\mathcal{S}_1 \cap \mathbf{G}$	$\frac{11\omega}{960} - \frac{9\delta}{160} + \frac{121}{1920}$	$-\frac{\delta}{8}$	$-\frac{7\omega}{5760} + \frac{\delta}{320} + \frac{403}{11520}$	$-\frac{\omega}{180} - \frac{\delta}{80} - \frac{11}{360}$	$-\frac{\omega}{144} + \frac{1}{288}$
$\mathcal{S}_1 \cap \mathbf{H}$	$-\frac{3\omega}{160} - \frac{13\delta}{160} + \frac{11}{160}$	$\frac{\omega}{40} - \frac{\delta}{10} + \frac{1}{80}$	$-\frac{13\omega}{960} - \frac{\delta}{320} + \frac{17}{320}$	$-\frac{\omega}{40} - \frac{\delta}{40} - \frac{1}{80}$	$-\frac{1}{48}$
$\mathcal{S}_2 \cap \mathbf{I}$	$-\frac{9\delta}{128} + \frac{21}{256}$	$-\frac{5\delta}{64} + \frac{9}{128}$	$-\frac{\omega}{96} + \frac{\delta}{128} + \frac{19}{256}$	$-\frac{3\delta}{128} - \frac{17}{256}$	$\frac{\omega}{512} - \frac{13}{3072}$
$\mathcal{S}_2 \cap \mathbf{J}$	$\frac{\omega}{128} - \frac{7\delta}{128} + \frac{3}{64}$	$-\frac{\omega}{64} - \frac{9\delta}{64} + \frac{3}{32}$	$-\frac{\omega}{96} + \frac{1}{16}$	$\frac{\omega}{128} + \frac{\delta}{128} - \frac{5}{64}$	$\frac{\omega}{128} + \frac{\delta}{128} - \frac{7}{192}$
$\mathcal{S}_3$	$-\frac{7\omega}{384} - \frac{17\delta}{192} + \frac{49}{256}$	$-\frac{\delta}{8}$	$-\frac{29\omega}{2304} - \frac{7\delta}{1152} + \frac{107}{1536}$	$\frac{\omega}{144} + \frac{\delta}{144} - \frac{7}{96}$	$-\frac{\omega}{144} - \frac{\delta}{144} + \frac{5}{96}$
$\mathcal{S}_{cb}$	$-\frac{359\delta}{5728}$	$-\frac{\delta}{8}$	$-\frac{173\omega}{17184} + \frac{3\delta}{11456} + \frac{495}{11456}$	0	$-\frac{1}{48}$
$\mathcal{S}_{dd} \cap \mathbf{A}$	$-\frac{\delta}{8}$	$-\frac{\delta}{8}$	$-\frac{\omega}{96} + \frac{\delta}{96} + \frac{3}{64}$	$\frac{\delta}{48}$	$-\frac{\delta}{48} - \frac{1}{48}$
$\mathcal{S}_{dd} \cap \mathbf{B}$	$-\frac{\delta}{8}$	$-\frac{\delta}{8}$	$\frac{\delta}{96} + \frac{1}{24}$	$\frac{\delta}{48}$	$-\frac{\delta}{48} - \frac{1}{48}$
$\mathcal{S}_{dd} \cap \mathbf{C}$	$-\frac{\delta}{8}$	$-\frac{\delta}{8}$	$-\frac{\omega}{96} - \frac{\delta}{96} + \frac{3}{64}$	$\frac{\delta}{48}$	$-\frac{\delta}{48} - \frac{1}{48}$

Table 11: The case of isotropic n.n. hopping only. The set of zero-potential coefficients $\{\alpha_i\}$ in the case of hardcore bosons and for $\varepsilon = 0$. In the first column the sets of the α-partition are specified. The cases, where the set $\mathcal{S}_{D|T}$ is a proper subset of $\mathcal{S}_{TD}(p)$ are marked by the asterisk. For more comments see the text in Appendix C.

	α_1	α_2	α_3	α_4	α_5
$\mathcal{S}_{-}\cap\mathbf{I}$	$-\frac{\delta}{16}$	$-\frac{\delta}{8}$	$-\frac{\omega}{96}-\frac{1}{192}$	0	$-\frac{1}{48}$
$\mathcal{S}_{-}\cap\mathbf{J}$	$\frac{\omega}{32}-\frac{\delta}{16}+\frac{9}{64}$	$-\frac{\delta}{8}$	$\frac{7\omega}{192}+\frac{3\delta}{32}+\frac{91}{384}$	$-\frac{3\omega}{64}-\frac{3\delta}{32}-\frac{27}{128}$	$-\frac{1}{48}$
$\mathcal{S}_{-}\cap\mathbf{K}$	$-\frac{3\omega}{128}-\frac{\delta}{16}-\frac{7}{256}$	$\frac{3\omega}{64}-\frac{\delta}{8}+\frac{23}{128}$	$\frac{\omega}{48}+\frac{\delta}{16}+\frac{19}{96}$	$-\frac{\omega}{32}-\frac{3\delta}{64}-\frac{21}{128}$	$-\frac{15\omega}{512}-\frac{7\delta}{256}-\frac{331}{3072}$
$\mathcal{S}_{-}\cap\mathbf{L}$	$\frac{\omega}{16}-\frac{\delta}{16}-\frac{5}{32}$	$-\frac{\omega}{8}-\frac{\delta}{8}+\frac{7}{16}$	$\frac{11\omega}{384}+\frac{3\delta}{32}+\frac{203}{768}$	$\frac{21\omega}{128}+\frac{5\delta}{32}+\frac{13}{256}$	$-\frac{41\omega}{512}-\frac{19\delta}{128}-\frac{1027}{3072}$
$\mathcal{S}_{-}\cap\mathbf{M}$	$-\frac{\delta}{16}+\frac{1}{16}$	$-\frac{\omega}{32}-\frac{5\delta}{32}-\frac{1}{64}$	$-\frac{23\omega}{768}-\frac{5\delta}{256}+\frac{25}{1536}$	$\frac{7\omega}{128}+\frac{7\delta}{128}+\frac{7}{256}$	$-\frac{\omega}{128}-\frac{\delta}{128}-\frac{19}{768}$
$\mathcal{S}_{1}\cap\mathbf{S}$	$-\frac{9\omega}{160}-\frac{11\delta}{40}-\frac{189}{320}$	$\frac{\omega}{20}+\frac{\delta}{20}+\frac{21}{40}$	$-\frac{5\omega}{192}-\frac{\delta}{16}-\frac{65}{384}$	$-\frac{3\omega}{80}-\frac{\delta}{10}-\frac{43}{160}$	$-\frac{\omega}{80}-\frac{3\delta}{40}-\frac{133}{480}$
$\mathcal{S}_{1}\cap\mathbf{T}$	$-\frac{\omega}{40}-\frac{7\delta}{80}+\frac{1}{20}$	$\frac{\omega}{40}-\frac{\delta}{10}+\frac{1}{80}$	$-\frac{\omega}{60}-\frac{\delta}{160}+\frac{11}{480}$	$-\frac{\omega}{40}-\frac{\delta}{40}-\frac{1}{80}$	$-\frac{1}{48}$
$\mathcal{S}_{3}\cap\mathbf{P}$	$-\frac{\omega}{192}-\frac{\delta}{12}-\frac{5}{384}$	$-\frac{\delta}{8}$	$-\frac{\omega}{288}-\frac{5\delta}{144}-\frac{83}{576}$	$\frac{\omega}{192}-\frac{\delta}{24}-\frac{67}{384}$	$-\frac{\omega}{288}-\frac{\delta}{72}-\frac{17}{576}$
$\mathcal{S}_{3}\cap\mathbf{Q}$	$\frac{25\omega}{192}-\frac{\delta}{6}-\frac{475}{384}$	$-\frac{\omega}{8}-\frac{\delta}{16}+\frac{35}{32}$	$\frac{3\omega}{128}-\frac{7\delta}{192}-\frac{269}{768}$	$\frac{\omega}{16}-\frac{\delta}{32}-\frac{37}{64}$	$\frac{5\omega}{96}-\frac{\delta}{24}-\frac{33}{64}$
$\mathcal{S}_{3}\cap\mathbf{R}$	$-\frac{\delta}{16}$	$-\frac{\omega}{72}-\frac{5\delta}{36}+\frac{13}{144}$	$-\frac{\omega}{144}+\frac{\delta}{288}+\frac{1}{288}$	$\frac{\omega}{72}+\frac{\delta}{72}-\frac{13}{144}$	$-\frac{1}{48}$
$\mathcal{S}_{cb}$	$-\frac{\delta}{16}$	$-\frac{\delta}{8}$	$-\frac{\omega}{96}+\frac{5}{192}$	0	$-\frac{1}{48}$
$\mathcal{S}_{v1}$	$-\frac{3\delta}{16}$	$-\frac{\delta}{8}$	$\frac{\omega}{192}+\frac{37}{384}$	$-\frac{\omega}{32}-\frac{\delta}{16}-\frac{9}{64}$	$-\frac{\omega}{64}-\frac{\delta}{8}-\frac{35}{384}$
$\mathcal{S}_{v2}\cap\mathbf{A}$	$-\frac{\delta}{32}$	$-\frac{3\delta}{16}$	$-\frac{\omega}{32}-\frac{\delta}{96}+\frac{5}{64}$	$-\frac{1}{8}$	$-\frac{1}{12}$
$\mathcal{S}_{v2}\cap\mathbf{B}$ *	$\frac{\omega}{32}-\frac{\delta}{16}-\frac{11}{64}$	$-\frac{\omega}{16}-\frac{\delta}{8}+\frac{11}{32}$	$-\frac{\omega}{24}+\frac{13}{96}$	$-\frac{1}{8}$	$-\frac{1}{12}$
$\mathcal{S}_{v3}$	$-\frac{\omega}{192}-\frac{\delta}{24}-\frac{1}{384}$	$-\frac{\omega}{32}-\frac{\delta}{4}-\frac{1}{64}$	$-\frac{7\omega}{192}-\frac{\delta}{48}+\frac{29}{384}$	$-\frac{\omega}{96}-\frac{\delta}{48}-\frac{25}{192}$	$-\frac{1}{12}$
$\mathcal{S}_{d1}\cap\mathbf{C}$	$-\frac{\delta}{16}$	$-\frac{\delta}{8}$	$\frac{\omega}{192}-\frac{47}{384}$	$\frac{3\omega}{64}-\frac{49}{128}$	$\frac{\omega}{32}-\frac{49}{192}$
$\mathcal{S}_{d1}\cap\mathbf{D}$	$-\frac{\delta}{16}$	$-\frac{\delta}{8}$	$\frac{\omega}{192}-\frac{47}{384}$	$\frac{\omega}{64}-\frac{19}{128}$	$-\frac{1}{48}$
$\mathcal{S}_{d2}\cap\mathbf{N}$	$\frac{\omega}{64}-\frac{\delta}{8}-\frac{31}{128}$	$-\frac{5\omega}{64}-\frac{\delta}{16}+\frac{67}{128}$	$-\frac{\omega}{24}+\frac{13}{96}$	$-\frac{\delta}{16}-\frac{1}{4}$	$\frac{\omega}{128}-\frac{\delta}{32}-\frac{133}{768}$
$\mathcal{S}_{d2}\cap\mathbf{O}$	$-\frac{3\omega}{32}-\frac{\delta}{8}+\frac{9}{64}$	$\frac{5\omega}{64}-\frac{\delta}{16}-\frac{3}{128}$	$-\frac{\omega}{24}+\frac{13}{96}$	$-\frac{3\omega}{64}-\frac{\delta}{16}-\frac{11}{128}$	$-\frac{3\omega}{128}-\frac{\delta}{32}-\frac{49}{768}$
$\mathcal{S}_{d3}\cap\mathbf{E}$ *	$\frac{\omega}{32}-\frac{\delta}{16}-\frac{11}{64}$	$-\frac{\omega}{20}-\frac{3\delta}{20}+\frac{1}{4}$	$-\frac{\omega}{60}-\frac{\delta}{20}-\frac{5}{96}$	$\frac{\omega}{32}-\frac{\delta}{16}-\frac{23}{64}$	$\frac{3\omega}{160}-\frac{3\delta}{80}-\frac{43}{192}$
$\mathcal{S}_{d3}\cap\mathbf{F}$ *	$-\frac{\delta}{16}$	$-\frac{3\omega}{160}-\frac{3\delta}{20}+\frac{5}{64}$	$-\frac{31\omega}{960}-\frac{\delta}{20}+\frac{13}{384}$	$-\frac{\delta}{16}-\frac{3}{16}$	$\frac{\omega}{320}-\frac{3\delta}{80}-\frac{53}{384}$
$\mathcal{S}_{d3}\cap\mathbf{G}$ *	$\frac{3\omega}{64}+\frac{\delta}{16}+\frac{3}{128}$	$-\frac{\omega}{16}-\frac{\delta}{4}+\frac{3}{32}$	$-\frac{\omega}{240}+\frac{\delta}{20}+\frac{5}{48}$	$\frac{3\omega}{64}+\frac{\delta}{16}-\frac{21}{128}$	$\frac{9\omega}{320}+\frac{3\delta}{80}-\frac{41}{384}$
$\mathcal{S}_{d3}\cap\mathbf{H}$ *	$\frac{\omega}{64}+\frac{\delta}{16}+\frac{25}{128}$	$-\frac{\omega}{32}-\frac{\delta}{4}-\frac{5}{64}$	$-\frac{19\omega}{960}+\frac{\delta}{20}+\frac{73}{384}$	$\frac{\omega}{64}+\frac{\delta}{16}+\frac{1}{128}$	$\frac{\omega}{80}+\frac{3\delta}{80}-\frac{1}{48}$

Below, in a series of tables, we provide the coefficients $\{\alpha_i\}$, $i = 1, \ldots, 9$, of the zero-potentials for the phase diagrams presented in Section 4. The coefficients that are missing in a table are equal to zero. As in Appendix D, the symbol $\mathcal{S}_1|\mathcal{S}_2$ denotes the boundary between the phases $\mathcal{S}_1$ and $\mathcal{S}_2$, etc.

Table 12: Zero-potentials coefficients for the phase diagram of fermions, shown in Fig. 16, for $\beta_2 = 0$.

$\{\alpha_i\}$	$\mathcal{S}_{seg}\|\mathcal{S}_{cb}$	$\mathcal{S}_{seg}\|\mathcal{S}_{v1}$	$\mathcal{S}_{cb}\|\mathcal{S}_{d1}$	$\mathcal{S}_{v2}\|\mathcal{S}_{v1}$	$\mathcal{S}_{v2}\|\mathcal{S}_{d1}$
α_1	0				
α_2	0				
α_3	0				
α_4	$-\frac{\omega}{96} + \frac{3}{64}$			$-\frac{\omega}{96} + \frac{7}{64}$	$-\frac{\omega}{96} - \frac{1}{64}$
α_5	$-\frac{\omega}{96} + \frac{3}{64}$			$-\frac{\omega}{96} + \frac{7}{64}$	$-\frac{\omega}{96} - \frac{1}{64}$
α_6	0			$-\frac{1}{8}$	
α_7	$-\frac{1}{48}$			$-\frac{1}{12}$	
α_8	$-\frac{1}{48}$			$-\frac{1}{12}$	

Table 13: Zero-potentials coefficients for the phase diagram of fermions, shown in Fig. 16, for $\beta_2 = 7/2$.

$\{\alpha_i\}$	$\mathcal{S}_{seg}\|\mathcal{S}_{cb}$	$\mathcal{S}_{seg}\|\mathcal{S}^v_{v1}$	$\mathcal{S}_{cb}\|\mathcal{S}^v_{d1}$	$\mathcal{S}^v_{v2}\|\mathcal{S}^v_{v1}$	$\mathcal{S}^v_{v2}\|\mathcal{S}^v_{d1}$
α_1	0				
α_2	0				
α_3	0				
α_4	$-\frac{\omega}{96} + \frac{3}{64}$				
α_5	$-\frac{\omega}{96} + \frac{23}{192}$				
α_6	0				
α_7	$-\frac{1}{48}$				
α_8	$-\frac{1}{48}$				

Table 14: Zero-potentials coefficients for the phase diagram of fermions, shown in Fig. 16, for $\beta_2 = 7$.

$\{\alpha_i\}$	$\mathbb{S}_{seg}\|\mathbb{S}_{cb}$	$\mathbb{S}_{seg}\|\mathbb{S}^v_{v1}$	$\mathbb{S}_{cb}\|\mathbb{S}^v_{d1}$	$\mathbb{S}^v_{v2}\|\mathbb{S}^v_{v1}$	$\mathbb{S}^v_{v2}\|\mathbb{S}^v_{d1}$
α_1	0				
α_2	0				
α_3	0				
α_4	$-\frac{\omega}{96} - \frac{1}{64}$			$-\frac{\omega}{96} + \frac{3}{64}$	
α_5	$-\frac{\omega}{96} + \frac{49}{192}$			$-\frac{\omega}{96} + \frac{37}{192}$	
α_6	$\frac{1}{8}$			0	
α_7	$-\frac{1}{12}$			$-\frac{1}{48}$	
α_8	$-\frac{1}{12}$			$-\frac{1}{48}$	

Table 15: Zero-potentials coefficients for the phase diagram of fermions, shown in Fig. 16, for $\beta_2 = 10$.

$\{\alpha_i\}$	$\mathbb{S}_{seg}\|\mathbb{S}_{cb}$	$\mathbb{S}_{seg}\|\mathbb{S}^v_{v1}$	$\mathbb{S}_{cb}\|\mathbb{S}^v_{d1}$	$\mathbb{S}^v_{v2}\|\mathbb{S}^v_{v1}$	$\mathbb{S}^v_{v2}\|\mathbb{S}^v_{d1}$
α_1	0				
α_2	0				
α_3	0				
α_4	$-\frac{1}{6}$			$-\frac{\omega}{96} + \frac{3}{64}$	
α_5	$\frac{1}{6}$			$-\frac{\omega}{96} + \frac{49}{192}$	
α_6	$\frac{1}{8}$			0	
α_7	$-\frac{1}{12}$			$-\frac{1}{48}$	
α_8	$-\frac{1}{12}$			$-\frac{1}{48}$	

Table 16: Zero-potentials coefficients for the phase diagram of hardcore bosons, shown in Fig. 16, for $\beta_2 = 0$.

$\{\alpha_i\}$	$\mathcal{S}_{seg}\|\mathcal{S}_{cb}$	$\mathcal{S}_{seg}\|\mathcal{S}_{v1}$	$\mathcal{S}_{cb}\|\mathcal{S}_{d1}$	$\mathcal{S}_{v2}\|\mathcal{S}_{v1}$	$\mathcal{S}_{v2}\|\mathcal{S}_{d1}$
α_1	0				
α_2	0				
α_3	0				
α_4	$-\frac{\omega}{96}+\frac{5}{192}$			$-\frac{\omega}{96}+\frac{17}{192}$	$-\frac{\omega}{96}-\frac{7}{192}$
α_5	$-\frac{\omega}{96}+\frac{5}{192}$			$-\frac{\omega}{96}+\frac{17}{192}$	$-\frac{\omega}{96}-\frac{7}{192}$
α_6	0			$-\frac{1}{8}$	
α_7	$-\frac{1}{48}$			$-\frac{1}{12}$	
α_8	$-\frac{1}{48}$			$-\frac{1}{12}$	

Table 17: Zero-potentials coefficients for the phase diagram of hardcore bosons, shown in Fig. 16, for $\beta_2 = 1$.

$\{\alpha_i\}$	$\mathcal{S}_{seg}\|\mathcal{S}_{cb}$	$\mathcal{S}_{seg}\|\mathcal{S}^v_{v1}$	$\mathcal{S}_{cb}\|\mathcal{S}^v_{d1}$	$\mathcal{S}^v_{v2}\|\mathcal{S}^v_{v1}$	$\mathcal{S}^v_{v2}\|\mathcal{S}^v_{d1}$
α_1	0				
α_2	0				
α_3	0				
α_4	$-\frac{1}{24}$	$-\frac{\omega}{96}+\frac{5}{192}$			
α_5	$\frac{1}{24}$	$-\frac{\omega}{96}+\frac{3}{64}$			
α_6	0				
α_7	$-\frac{1}{48}$				
α_8	$-\frac{1}{48}$				

Table 18: Zero-potentials coefficients for the phase diagram of hardcore bosons, shown in Fig. 16, for $\beta_2 = 2$.

$\{\alpha_i\}$	$\mathbb{S}_{seg}\|\mathbb{S}_{cb}$	$\mathbb{S}_{seg}\|\mathbb{S}^v_{v1}$	$\mathbb{S}_{cb}\|\mathbb{S}^v_{d1}$	$\mathbb{S}^v_{v2}\|\mathbb{S}^v_{v1}$	$\mathbb{S}^v_{v2}\|\mathbb{S}^v_{d1}$
α_1	0				
α_2	0				
α_3	0				
α_4	$-\frac{1}{12}$	$-\frac{\omega}{96}-\frac{1}{192}$		$-\frac{\omega}{96}+\frac{1}{24}$	
α_5	$\frac{1}{12}$	$-\frac{\omega}{96}+\frac{19}{192}$			
α_6	$\frac{1}{8}$	$\frac{1}{32}$		$-\frac{1}{32}$	
α_7	$-\frac{1}{12}$	$-\frac{1}{48}$		$-\frac{1}{192}$	
α_8	$-\frac{1}{12}$	$-\frac{1}{48}$		$-\frac{5}{96}$	

Table 19: Zero-potentials coefficients for the phase diagram of hardcore bosons, shown in Fig. 16, for $\beta_2 = 5$.

$\{\alpha_i\}$	$\mathbb{S}_{seg}\|\mathbb{S}_{cb}$	$\mathbb{S}_{seg}\|\mathbb{S}^v_{v1}$	$\mathbb{S}_{cb}\|\mathbb{S}^v_{d1}$	$\mathbb{S}^v_{v2}\|\mathbb{S}^v_{v1}$	$\mathbb{S}^v_{v2}\|\mathbb{S}^v_{d1}$
α_1	0				
α_2	0				
α_3	0				
α_4	$-\frac{11}{96}$			$-\frac{\omega}{96}+\frac{1}{24}$	
α_5	$\frac{11}{96}$			$-\frac{\omega}{96}+\frac{19}{192}$	
α_6	$\frac{1}{8}$			$-\frac{1}{32}$	
α_7	$-\frac{1}{12}$			$-\frac{1}{192}$	
α_8	$-\frac{1}{12}$			$-\frac{5}{96}$	

Table 20: Zero-potentials coefficients for the phase diagram shown in Fig. 17, for $\beta_2 = 0$.

$\{\alpha_i\}$	$\mathcal{S}_+\|\mathcal{S}_-$	$\mathcal{S}_-\|\mathcal{S}_1$	$\mathcal{S}_1\|\mathcal{S}_2$	$\mathcal{S}_2\|\mathcal{S}_3$	$\mathcal{S}_3\|\mathcal{S}_{cb}$	$\delta = 0,\ \omega \geqslant \frac{21}{2}$
α_1	0	$\frac{\omega}{16} + \frac{3}{32}$	$\frac{\omega}{16} - \frac{3}{32}$	$\frac{\omega}{16} - \frac{9}{32}$	$\frac{\omega}{16} - \frac{21}{32}$	0
α_2	0	$\frac{\omega}{8} + \frac{1}{16}$	$\frac{\omega}{8} - \frac{3}{16}$	$\frac{\omega}{8} - \frac{3}{4}$	$\frac{\omega}{8} - \frac{21}{16}$	0
α_3	0	$\frac{\omega}{8} + \frac{1}{16}$	$\frac{\omega}{8} - \frac{3}{16}$	$\frac{\omega}{8} - \frac{3}{4}$	$\frac{\omega}{8} - \frac{21}{16}$	0
α_4	$-\frac{\omega}{96} + \frac{3}{64}$			$-\frac{\omega}{96} + \frac{1}{16}$	$-\frac{\omega}{96} + \frac{3}{64}$	
α_5	$-\frac{\omega}{96} + \frac{3}{64}$			$-\frac{\omega}{96} + \frac{1}{16}$	$-\frac{\omega}{96} + \frac{3}{64}$	
α_6	0		$-\frac{1}{16}$	$-\frac{1}{32}$	0	
α_7	$-\frac{1}{48}$			$\frac{1}{96}$	$-\frac{1}{48}$	
α_8	$-\frac{1}{48}$			$\frac{1}{96}$	$-\frac{1}{48}$	

Table 21: Zero-potentials coefficients for the phase diagram shown in Fig. 17, for $\beta_2 = 1$.

$\{\alpha_i\}$	$\mathcal{S}_+\|\mathcal{S}_-$	$\mathcal{S}_-\|\mathcal{S}_1$	$\mathcal{S}_1\|\mathcal{S}_2$	$\mathcal{S}_2\|\mathcal{S}_3$	$\mathcal{S}_3\|\mathcal{S}_{cb}$	$\delta = 0,\ \omega \geqslant \frac{23}{2}$
α_1	0	$\frac{\omega}{16} + \frac{1}{32}$	$\frac{\omega}{16} - \frac{3}{32}$	$\frac{\omega}{16} - \frac{11}{32}$	$\frac{\omega}{16} - \frac{23}{32}$	0
α_2	0	$\frac{\omega}{8} - \frac{1}{16}$	$\frac{\omega}{8} - \frac{11}{32}$	$\frac{\omega}{8} - \frac{41}{48}$	$\frac{\omega}{8} - \frac{23}{16}$	0
α_3	0	$\frac{\omega}{8} - \frac{1}{16}$	$\frac{\omega}{8} - \frac{13}{32}$	$\frac{\omega}{8} - \frac{43}{48}$	$\frac{\omega}{8} - \frac{23}{16}$	0
α_4	$-\frac{\omega}{96} + \frac{3}{64}$		$-\frac{\omega}{96} + \frac{9}{128}$	$-\frac{\omega}{96} + \frac{13}{192}$	$-\frac{\omega}{96} + \frac{3}{64}$	
α_5	$-\frac{\omega}{96} + \frac{13}{192}$		$-\frac{\omega}{96} + \frac{29}{384}$	$-\frac{\omega}{96} + \frac{5}{64}$	$-\frac{\omega}{96} + \frac{13}{192}$	
α_6	0		$-\frac{1}{32}$		0	
α_7	$-\frac{1}{48}$		$\frac{1}{96}$	$-\frac{1}{192}$	$-\frac{1}{48}$	
α_8	$-\frac{1}{48}$		$\frac{1}{96}$	$\frac{5}{192}$	$-\frac{1}{48}$	

Table 22: Zero-potentials coefficients for the phase diagram shown in Fig. 17, for $\beta_2 = 3/2$.

lines & points	α_1	α_2	α_3	α_4	α_5	α_6	α_7	α_8	α_9
$\mathcal{S}_+\|\mathcal{S}_-$	0	0	0	$-\frac{\omega}{96}+\frac{3}{64}$	$-\frac{\omega}{96}+\frac{5}{64}$	$\frac{1}{64}$	$-\frac{7}{192}$	$-\frac{1}{48}$	0
$\mathcal{S}_-\|\mathcal{S}_1$	$\frac{\omega}{16}$	$\frac{\omega}{8}-\frac{1}{8}$	$\frac{\omega}{8}-\frac{3}{32}$	$-\frac{\omega}{96}+\frac{15}{256}$	$-\frac{\omega}{96}+\frac{5}{64}$	$-\frac{1}{256}$	$-\frac{17}{384}$	$-\frac{1}{192}$	0
$\mathcal{S}_1\|\mathcal{S}_2$	$\frac{\omega}{16}-\frac{49}{256}$	$\frac{\omega}{8}-\frac{31}{64}$	$\frac{\omega}{8}-\frac{13}{32}$	$-\frac{\omega}{96}+\frac{7}{128}$	$-\frac{\omega}{96}+\frac{27}{256}$	$-\frac{7}{256}$	$-\frac{23}{384}$	$-\frac{23}{384}$	$\frac{19}{256}$
$\mathcal{S}_2\|\mathcal{S}_3$	$\frac{\omega}{16}-\frac{105}{256}$	$\frac{\omega}{8}-\frac{115}{128}$	$\frac{\omega}{8}-\frac{29}{32}$	$-\frac{\omega}{96}+\frac{7}{128}$	$-\frac{\omega}{96}+\frac{43}{512}$	$-\frac{25}{512}$	$-\frac{157}{3072}$	$\frac{113}{3072}$	0
$\mathcal{S}_3\|\mathcal{S}_{cb}$	$\frac{\omega}{16}-\frac{3}{4}$	$\frac{\omega}{8}-\frac{3}{2}$	$\frac{\omega}{8}-\frac{3}{2}$	$-\frac{\omega}{96}+\frac{3}{64}$	$-\frac{\omega}{96}+\frac{5}{64}$	0	$-\frac{1}{48}$	$-\frac{1}{48}$	0
$\delta = 0,\ \omega \geqslant \frac{25}{2}$	0	0	0	$-\frac{\omega}{96}+\frac{3}{64}$	$-\frac{\omega}{96}+\frac{5}{64}$	$\frac{1}{64}$	$-\frac{1}{48}$	$-\frac{7}{192}$	0
$\left(\frac{1}{2},0\right)$	0	0	0	$\frac{1}{24}$	$\frac{7}{96}$	0	$-\frac{1}{48}$	$-\frac{1}{48}$	0
$\left(\frac{23}{2},0\right)$	0	0	0	$-\frac{7}{96}$	$-\frac{1}{24}$	0	$-\frac{1}{48}$	$-\frac{1}{48}$	0
b	$\frac{1}{32}$	0	$\frac{1}{16}$	$\frac{1}{24}$	$\frac{7}{96}$	0	$-\frac{1}{48}$	$-\frac{1}{48}$	0
c	$\frac{1}{32}$	$\frac{1}{16}$	0	$-\frac{7}{96}$	$-\frac{1}{24}$	0	$-\frac{1}{48}$	$-\frac{1}{48}$	0
e	$\frac{3}{32}$	$\frac{1}{16}$	$\frac{1}{8}$	$\frac{1}{32}$	$\frac{1}{16}$	0	$-\frac{1}{48}$	$-\frac{1}{48}$	0
f	$\frac{7}{64}$	$\frac{1}{8}$	$\frac{3}{16}$	$\frac{1}{96}$	$\frac{11}{192}$	$-\frac{1}{64}$	$-\frac{5}{96}$	$-\frac{5}{96}$	$\frac{3}{64}$

Table 23: Zero-potentials coefficients for the phase diagram shown in Fig. 17, for $\beta_2 = 2$.

lines & points	α_1	α_2	α_3	α_4	α_5	α_6	α_7	α_8	α_9
$\mathcal{S}_+\|\mathcal{S}_-$	0	0	0	$-\frac{\omega}{96}+\frac{3}{64}$	$-\frac{\omega}{96}+\frac{17}{192}$	$\frac{1}{32}$	$-\frac{5}{96}$	$-\frac{1}{48}$	0
$\mathcal{S}_-\|\mathcal{S}_1$	$\frac{\omega}{16}-\frac{1}{32}$	$\frac{\omega}{8}-\frac{3}{16}$	$\frac{\omega}{8}-\frac{3}{16}$	$-\frac{\omega}{96}+\frac{3}{64}$	$-\frac{\omega}{96}+\frac{17}{192}$	0	$-\frac{1}{48}$	$-\frac{1}{48}$	0
$\mathcal{S}_1\|\mathcal{S}_2$	$\frac{\omega}{16}-\frac{1}{4}$	$\frac{\omega}{8}-\frac{9}{16}$	$\frac{\omega}{8}-\frac{7}{16}$	$-\frac{\omega}{96}+\frac{3}{64}$	$-\frac{\omega}{96}+\frac{23}{192}$	$-\frac{1}{32}$	$-\frac{1}{12}$	$-\frac{1}{12}$	$\frac{3}{32}$
$\mathcal{S}_2\|\mathcal{S}_3$	$\frac{\omega}{16}-\frac{15}{32}$	$\frac{\omega}{8}-\frac{15}{16}$	$\frac{\omega}{8}-\frac{15}{16}$	$-\frac{\omega}{96}+\frac{3}{64}$	$-\frac{\omega}{96}+\frac{17}{192}$	$-\frac{1}{16}$	$-\frac{1}{12}$	$\frac{1}{24}$	0
$\mathcal{S}_3\|\mathcal{S}_{cb}$	$\frac{\omega}{16}-\frac{25}{32}$	$\frac{\omega}{8}-\frac{25}{16}$	$\frac{\omega}{8}-\frac{25}{16}$	$-\frac{\omega}{96}+\frac{3}{64}$	$-\frac{\omega}{96}+\frac{17}{192}$	0	$-\frac{1}{48}$	$-\frac{1}{48}$	0
$\delta = 0,\ \omega \geqslant \frac{27}{2}$	0	0	0	$-\frac{\omega}{96}+\frac{3}{64}$	$-\frac{\omega}{96}+\frac{17}{192}$	$\frac{1}{32}$	$-\frac{1}{48}$	$-\frac{5}{96}$	0
$\left(\frac{3}{2},0\right)$	0	0	0	$\frac{1}{32}$	$\frac{7}{96}$	0	$-\frac{1}{48}$	$-\frac{1}{48}$	0
$\left(\frac{23}{2},0\right)$	0	0	0	$-\frac{7}{96}$	$-\frac{1}{32}$	0	$-\frac{1}{48}$	$-\frac{1}{48}$	0
b(**e**)	$\frac{1}{16}$	0	$\frac{1}{8}$	$\frac{1}{32}$	$\frac{7}{96}$	0	$-\frac{1}{48}$	$-\frac{1}{48}$	0
c	$\frac{1}{16}$	$\frac{1}{8}$	0	$-\frac{7}{96}$	$-\frac{1}{32}$	0	$-\frac{1}{48}$	$-\frac{1}{48}$	0

Table 24: Zero-potentials coefficients for the phase diagram shown in Fig. 17, for $\beta_2 = 5/2$.

lines & points	α_1	α_2	α_3	α_4	α_5	α_6	α_7	α_8	α_9
$\mathcal{S}_+\|\mathcal{S}_-$	0	0	0	$-\frac{\omega}{96}+\frac{3}{64}$	$-\frac{\omega}{96}+\frac{19}{192}$	$\frac{1}{32}$	$-\frac{5}{96}$	$-\frac{1}{48}$	0
$\mathcal{S}_-\|\mathcal{S}_1$	$\frac{\omega}{16}-\frac{1}{16}$	$\frac{\omega}{8}-\frac{1}{4}$	$\frac{\omega}{8}-\frac{1}{4}$	$-\frac{\omega}{96}+\frac{3}{64}$	$-\frac{\omega}{96}+\frac{19}{192}$	0	$-\frac{1}{48}$	$-\frac{1}{48}$	0
$\mathcal{S}_1\|\mathcal{S}_2$	$\frac{\omega}{16}-\frac{9}{32}$	$\frac{\omega}{8}-\frac{5}{8}$	$\frac{\omega}{8}-\frac{1}{2}$	$-\frac{\omega}{96}+\frac{3}{64}$	$-\frac{\omega}{96}+\frac{25}{192}$	$-\frac{1}{32}$	$-\frac{1}{12}$	$-\frac{1}{12}$	$\frac{3}{32}$
$\mathcal{S}_2\|\mathcal{S}_3$	$\frac{\omega}{16}-\frac{33}{64}$	$\frac{\omega}{8}-\frac{31}{32}$	$\frac{\omega}{8}-1$	$-\frac{\omega}{96}+\frac{3}{64}$	$-\frac{\omega}{96}+\frac{35}{384}$	$-\frac{9}{128}$	$-\frac{1}{12}$	$\frac{5}{192}$	0
$\mathcal{S}_3\|\mathcal{S}_{cb}$	$\frac{\omega}{16}-\frac{13}{16}$	$\frac{\omega}{8}-\frac{13}{8}$	$\frac{\omega}{8}-\frac{13}{8}$	$-\frac{\omega}{96}+\frac{3}{64}$	$-\frac{\omega}{96}+\frac{19}{192}$	0	$-\frac{1}{48}$	$-\frac{1}{48}$	0
$\delta=0,\ \omega\geqslant\frac{29}{2}$	0	0	0	$-\frac{\omega}{96}+\frac{3}{64}$	$-\frac{\omega}{96}+\frac{19}{192}$	$\frac{1}{32}$	$-\frac{1}{48}$	$-\frac{5}{96}$	0
$\left(\frac{5}{2},0\right)$	0	0	0	$\frac{1}{48}$	$\frac{7}{96}$	0	$-\frac{1}{48}$	$-\frac{1}{48}$	0
$\left(\frac{23}{2},0\right)$	0	0	0	$-\frac{7}{96}$	$-\frac{1}{48}$	0	$-\frac{1}{48}$	$-\frac{1}{48}$	0
b	$\frac{1}{16}$	$\frac{1}{4}$	$\frac{1}{4}$	$-\frac{5}{96}$	0	$-\frac{3}{32}$	$-\frac{1}{12}$	$-\frac{1}{48}$	0
c	$\frac{1}{32}$	$\frac{1}{16}$	0	$-\frac{7}{96}$	$-\frac{1}{48}$	0	$-\frac{1}{48}$	$-\frac{1}{48}$	0
d	$\frac{1}{16}$	0	$\frac{1}{8}$	$\frac{1}{32}$	$\frac{1}{12}$	0	$-\frac{1}{48}$	$-\frac{1}{48}$	0
e	$\frac{1}{32}$	$\frac{1}{8}$	$\frac{3}{16}$	$\frac{1}{96}$	$\frac{1}{16}$	$-\frac{1}{16}$	$-\frac{5}{96}$	$-\frac{5}{96}$	0
f	$\frac{1}{8}$	$\frac{1}{8}$	$\frac{1}{8}$	$\frac{7}{192}$	$\frac{7}{96}$	$-\frac{1}{64}$	$\frac{1}{96}$	$-\frac{1}{48}$	0
g	$\frac{3}{32}$	$\frac{3}{16}$	$\frac{1}{16}$	$-\frac{1}{12}$	$-\frac{3}{64}$	$-\frac{1}{64}$	$-\frac{1}{48}$	$-\frac{1}{48}$	0
h	$\frac{1}{16}$	$\frac{1}{8}$	$\frac{1}{4}$	$-\frac{1}{96}$	$\frac{7}{96}$	$-\frac{1}{16}$	$-\frac{1}{12}$	$-\frac{1}{12}$	$\frac{1}{16}$
i	$\frac{1}{16}$	$\frac{1}{4}$	$\frac{1}{4}$	$-\frac{5}{96}$	0	$-\frac{3}{32}$	$-\frac{1}{12}$	$-\frac{1}{48}$	0

Table 25: Zero-potentials coefficients for the phase diagram shown in Fig. 17, for $\beta_2 = 3$.

lines & points	α_1	α_2	α_3	α_4	α_5	α_6	α_7	α_8
$\mathcal{S}_+\|\mathcal{S}_-$	0	0	0	$-\frac{\omega}{96}+\frac{3}{64}$	$-\frac{\omega}{96}+\frac{7}{64}$	$\frac{1}{32}$	$-\frac{5}{96}$	$-\frac{1}{48}$
$\mathcal{S}_-\|\mathcal{S}_1$	$\frac{\omega}{16}-\frac{3}{32}$	$\frac{\omega}{8}-\frac{5}{16}$	$\frac{\omega}{8}-\frac{5}{16}$	$-\frac{\omega}{96}+\frac{3}{64}$	$-\frac{\omega}{96}+\frac{7}{64}$	0	$-\frac{1}{48}$	$-\frac{1}{48}$
$\mathcal{S}_1\|\mathcal{S}_2$	$\frac{\omega}{16}-\frac{11}{32}$	$\frac{\omega}{8}-\frac{7}{16}$	$\frac{\omega}{8}-\frac{11}{16}$	$-\frac{\omega}{96}+\frac{3}{64}$	$-\frac{\omega}{96}+\frac{3}{64}$	$-\frac{1}{16}$	$-\frac{1}{12}$	$-\frac{1}{12}$
$\mathcal{S}_2\|\mathcal{S}_3$	$\frac{\omega}{16}-\frac{9}{16}$	$\frac{\omega}{8}-1$	$\frac{\omega}{8}-\frac{17}{16}$	$-\frac{\omega}{96}+\frac{3}{64}$	$-\frac{\omega}{96}+\frac{3}{32}$	$-\frac{5}{64}$	$-\frac{1}{12}$	$\frac{1}{96}$
$\mathcal{S}_3\|\mathcal{S}_{cb}$	$\frac{\omega}{16}-\frac{27}{32}$	$\frac{\omega}{8}-\frac{27}{16}$	$\frac{\omega}{8}-\frac{27}{16}$	$-\frac{\omega}{96}+\frac{3}{64}$	$-\frac{\omega}{96}+\frac{7}{64}$	0	$-\frac{1}{48}$	$-\frac{1}{48}$
$\delta=0,\ \omega\geqslant\frac{31}{2}$	0	0	0	$-\frac{\omega}{96}+\frac{3}{64}$	$-\frac{\omega}{96}+\frac{7}{64}$	$\frac{1}{32}$	$-\frac{1}{48}$	$-\frac{5}{96}$
$\left(\frac{7}{2},0\right)$ (**b**)	0	0	0	$\frac{1}{96}$	$\frac{7}{96}$	0	$-\frac{1}{48}$	$-\frac{1}{48}$
$\left(\frac{23}{2},0\right)$ (**c**)	0	0	0	$-\frac{7}{96}$	$-\frac{1}{96}$	0	$-\frac{1}{48}$	$-\frac{1}{48}$
d	$\frac{1}{16}$	0	$\frac{1}{8}$	$\frac{1}{32}$	$\frac{3}{32}$	0	$-\frac{1}{48}$	$-\frac{1}{48}$
e (**h**)	0	$\frac{1}{4}$	$\frac{1}{4}$	$-\frac{1}{96}$	$\frac{5}{96}$	$-\frac{1}{8}$	$-\frac{1}{12}$	$-\frac{1}{12}$
i	0	$\frac{1}{4}$	$\frac{1}{4}$	$-\frac{5}{96}$	$\frac{1}{96}$	$-\frac{1}{8}$	$-\frac{1}{12}$	$-\frac{1}{12}$
f	$\frac{5}{32}$	$\frac{7}{32}$	$\frac{3}{16}$	$\frac{35}{768}$	$\frac{7}{96}$	$-\frac{3}{256}$	$-\frac{5}{384}$	$-\frac{1}{48}$
g	$\frac{1}{8}$	$\frac{1}{4}$	$\frac{1}{8}$	$-\frac{3}{32}$	$-\frac{3}{64}$	$-\frac{1}{64}$	$-\frac{1}{48}$	$-\frac{1}{48}$

Table 26: Zero-potentials coefficients for the phase diagram shown in Fig. 17, for $\beta_2 = 6$.

lines & points	α_1	α_2	α_3	α_4	α_5	α_6	α_7	α_8
$\mathcal{S}_+\|\mathcal{S}_-$	0	0	0	$-\frac{\omega}{96}+\frac{3}{64}$	$-\frac{\omega}{96}+\frac{11}{64}$	$\frac{1}{32}$	$-\frac{5}{96}$	$-\frac{1}{48}$
$\mathcal{S}_-\|\mathcal{S}_1$	$\frac{\omega}{16}-\frac{9}{32}$	$\frac{\omega}{8}-\frac{11}{16}$	$\frac{\omega}{8}-\frac{11}{16}$	$-\frac{\omega}{96}+\frac{3}{64}$	$-\frac{\omega}{96}+\frac{11}{64}$	0	$-\frac{1}{48}$	$-\frac{1}{48}$
$\mathcal{S}_1\|\mathcal{S}_2$	$\frac{\omega}{16}-\frac{19}{32}$	$\frac{\omega}{8}-\frac{11}{16}$	$\frac{\omega}{8}-\frac{15}{16}$	$-\frac{\omega}{96}+\frac{3}{64}$	$-\frac{\omega}{96}+\frac{7}{64}$	$-\frac{1}{8}$	$-\frac{1}{12}$	$-\frac{1}{12}$
$\mathcal{S}_2\|\mathcal{S}_3$	$\frac{\omega}{16}-\frac{25}{32}$	$\frac{\omega}{8}-\frac{21}{16}$	$\frac{\omega}{8}-\frac{23}{16}$	$-\frac{\omega}{96}+\frac{3}{64}$	$-\frac{\omega}{96}+\frac{9}{64}$	$-\frac{3}{32}$	$-\frac{1}{12}$	$-\frac{1}{48}$
$\mathcal{S}_3\|\mathcal{S}_{cb}$	$\frac{\omega}{16}-\frac{33}{32}$	$\frac{\omega}{8}-\frac{33}{16}$	$\frac{\omega}{8}-\frac{33}{16}$	$-\frac{\omega}{96}+\frac{3}{64}$	$-\frac{\omega}{96}+\frac{11}{64}$	0	$-\frac{1}{48}$	$-\frac{1}{48}$
$\delta=0,\ \omega\geqslant\frac{43}{2}$	0	0	0	$-\frac{\omega}{96}+\frac{3}{64}$	$-\frac{\omega}{96}+\frac{11}{64}$	$\frac{1}{32}$	$-\frac{1}{48}$	$-\frac{5}{96}$
b	0	0	0	$\frac{1}{96}$	$\frac{13}{96}$	$-\frac{1}{32}$	$-\frac{5}{96}$	$-\frac{1}{48}$
$\left(\frac{35}{2},0\right)$	0	0	0	$-\frac{13}{96}$	$-\frac{1}{96}$	$-\frac{1}{32}$	$-\frac{1}{48}$	$-\frac{5}{96}$
c	$\frac{1}{16}$	0	$\frac{1}{8}$	$\frac{1}{32}$	$\frac{5}{32}$	0	$-\frac{1}{48}$	$-\frac{1}{48}$
d	$\frac{3}{16}$	$\frac{3}{8}$	$\frac{3}{8}$	$-\frac{13}{96}$	$-\frac{5}{192}$	$-\frac{1}{64}$	$-\frac{1}{48}$	$-\frac{1}{48}$
e	$\frac{7}{32}$	$\frac{5}{8}$	$\frac{9}{16}$	$-\frac{11}{192}$	$\frac{5}{96}$	$-\frac{7}{64}$	$-\frac{1}{12}$	$-\frac{1}{12}$
f	$\frac{3}{16}$	$\frac{5}{8}$	$\frac{5}{8}$	$-\frac{11}{96}$	$-\frac{1}{48}$	$-\frac{3}{32}$	$-\frac{1}{12}$	$-\frac{1}{48}$
g	$\frac{11}{32}$	$\frac{5}{8}$	$\frac{9}{16}$	$-\frac{1}{192}$	$\frac{7}{96}$	$-\frac{1}{64}$	$-\frac{1}{48}$	$-\frac{1}{48}$
h	$\frac{5}{16}$	$\frac{5}{8}$	$\frac{1}{2}$	$-\frac{5}{32}$	$-\frac{3}{64}$	$-\frac{1}{64}$	$-\frac{1}{48}$	$-\frac{1}{48}$

Table 27: Zero-potentials coefficients for the phase diagram shown in Fig. 18, for $\beta_2 = 0$.

lines & points	α_1	α_2	α_3	α_4	α_5	α_6	α_7	α_8
$\mathcal{S}_+\|\mathcal{S}_-$	0	0	0	$-\frac{\omega}{96}+\frac{5}{192}$	$-\frac{\omega}{96}+\frac{5}{192}$	0	$-\frac{1}{48}$	$-\frac{1}{48}$
$\mathcal{S}_-\|\mathcal{S}_1$	$\frac{\omega}{16}+\frac{3}{32}$	$\frac{\omega}{8}+\frac{1}{16}$	$\frac{\omega}{8}+\frac{1}{16}$	$-\frac{\omega}{96}+\frac{5}{192}$	$-\frac{\omega}{96}+\frac{5}{192}$	0	$-\frac{1}{48}$	$-\frac{1}{48}$
$\mathcal{S}_1\|\mathcal{S}_3$	$\frac{\omega}{16}-\frac{9}{32}$	$\frac{\omega}{8}-\frac{1}{16}$	$\frac{\omega}{8}-\frac{1}{16}$	$-\frac{\omega}{96}-\frac{7}{192}$	$-\frac{\omega}{96}-\frac{7}{192}$	$-\frac{1}{8}$	$-\frac{1}{12}$	$-\frac{1}{12}$
$\mathcal{S}_3\|\mathcal{S}_{cb}$	$\frac{\omega}{16}-\frac{13}{32}$	$\frac{\omega}{8}-\frac{13}{16}$	$\frac{\omega}{8}-\frac{13}{16}$	$-\frac{\omega}{96}+\frac{5}{192}$	$-\frac{\omega}{96}+\frac{5}{192}$	0	$-\frac{1}{48}$	$-\frac{1}{48}$
$\delta = 0,\ \omega \geqslant \frac{19}{2}$	0	0	0	$-\frac{\omega}{96}+\frac{5}{192}$	$-\frac{\omega}{96}+\frac{5}{192}$	0	$-\frac{1}{48}$	$-\frac{1}{48}$
b	0	0	0	$\frac{3}{32}$	$\frac{3}{32}$	$-\frac{1}{8}$	$-\frac{1}{12}$	$-\frac{1}{12}$
$\left(\frac{11}{2}, 0\right)$	0	0	0	$-\frac{3}{32}$	$-\frac{3}{32}$	$-\frac{1}{8}$	$-\frac{1}{12}$	$-\frac{1}{12}$
c	$\frac{3}{32}$	$\frac{1}{16}$	$\frac{1}{16}$	$\frac{1}{12}$	$\frac{1}{12}$	$-\frac{1}{32}$	$\frac{1}{96}$	$\frac{1}{96}$
d	$\frac{1}{16}$	$\frac{1}{8}$	$\frac{1}{8}$	$-\frac{3}{32}$	$-\frac{3}{32}$	$-\frac{1}{8}$	$-\frac{1}{12}$	$-\frac{1}{12}$
e	$\frac{1}{16}$	$\frac{3}{8}$	$\frac{3}{8}$	$-\frac{1}{96}$	$-\frac{1}{96}$	$-\frac{1}{8}$	$-\frac{1}{12}$	$-\frac{1}{12}$
f	$\frac{3}{32}$	$\frac{9}{16}$	$\frac{9}{16}$	$\frac{7}{96}$	$\frac{7}{96}$	$-\frac{3}{32}$	$-\frac{1}{12}$	$-\frac{1}{12}$
g	$\frac{5}{32}$	$\frac{5}{16}$	$\frac{5}{16}$	$-\frac{1}{12}$	$-\frac{1}{12}$	$-\frac{1}{32}$	$-\frac{1}{48}$	$-\frac{1}{48}$

Table 28: Zero-potentials coefficients for the phase diagram shown in Fig. 18, for $\beta_2 = 3$.

lines & points	α_1	α_2	α_3	α_4	α_5	α_6	α_7	α_8
$\mathcal{S}_+\|\mathcal{S}_-$	0	0	0	$-\frac{\omega}{96}+\frac{5}{192}$	$-\frac{\omega}{96}+\frac{17}{192}$	$\frac{1}{32}$	$-\frac{5}{96}$	$-\frac{1}{48}$
$\mathcal{S}_-\|\mathcal{S}_1$	$\frac{\omega}{16}-\frac{3}{32}$	$\frac{\omega}{8}-\frac{5}{16}$	$\frac{\omega}{8}-\frac{5}{16}$	$-\frac{\omega}{96}+\frac{5}{192}$	$-\frac{\omega}{96}+\frac{17}{192}$	0	$-\frac{1}{48}$	$-\frac{1}{48}$
$\mathcal{S}_1\|\mathcal{S}_3$	$\frac{\omega}{16}-\frac{15}{32}$	$\frac{\omega}{8}-\frac{7}{16}$	$\frac{\omega}{8}-\frac{7}{16}$	$-\frac{\omega}{96}-\frac{7}{192}$	$-\frac{\omega}{96}+\frac{5}{192}$	$-\frac{1}{8}$	$-\frac{1}{12}$	$-\frac{1}{12}$
$\mathcal{S}_3\|\mathcal{S}_{cb}$	$\frac{\omega}{16}-\frac{19}{32}$	$\frac{\omega}{8}-\frac{19}{16}$	$\frac{\omega}{8}-\frac{19}{16}$	$-\frac{\omega}{96}+\frac{5}{192}$	$-\frac{\omega}{96}+\frac{17}{192}$	0	$-\frac{1}{48}$	$-\frac{1}{48}$
$\delta = 0,\ \omega \geqslant \frac{31}{2}$	0	0	0	$-\frac{\omega}{96}+\frac{5}{192}$	$-\frac{\omega}{96}+\frac{17}{192}$	$\frac{1}{32}$	$-\frac{1}{48}$	$-\frac{5}{96}$
b	0	0	0	$\frac{1}{32}$	$\frac{3}{32}$	$-\frac{1}{32}$	$-\frac{5}{96}$	$-\frac{1}{48}$
$\left(\frac{23}{2}, 0\right)$	0	0	0	$-\frac{3}{32}$	$-\frac{1}{32}$	$-\frac{1}{32}$	$-\frac{1}{48}$	$-\frac{5}{96}$
c	$\frac{3}{32}$	$\frac{1}{16}$	$\frac{1}{16}$	$\frac{13}{192}$	$\frac{25}{192}$	$-\frac{1}{64}$	$\frac{1}{96}$	$-\frac{1}{48}$
d	$\frac{1}{4}$	$\frac{1}{2}$	$\frac{1}{2}$	$-\frac{3}{32}$	$-\frac{3}{64}$	$-\frac{1}{64}$	$-\frac{1}{48}$	$-\frac{1}{48}$
e	$\frac{1}{4}$	$\frac{3}{4}$	$\frac{3}{4}$	$-\frac{7}{96}$	$-\frac{1}{96}$	$-\frac{1}{8}$	$-\frac{1}{12}$	$-\frac{1}{12}$
f	$\frac{13}{32}$	$\frac{23}{32}$	$\frac{11}{16}$	$-\frac{5}{384}$	$\frac{1}{96}$	$-\frac{1}{128}$	$-\frac{1}{48}$	$-\frac{1}{48}$
g	$\frac{11}{32}$	$\frac{11}{16}$	$\frac{11}{16}$	$-\frac{7}{48}$	$-\frac{13}{192}$	$-\frac{1}{64}$	$-\frac{1}{48}$	$-\frac{1}{48}$

Table 29: Zero-potentials coefficients for the phase diagram shown in Fig. 24.

lines	α_1
$\mathbb{S}_+\|\mathbb{S}_-$	0
$\mathbb{S}_-\|\mathbb{S}^v_{v3}$	$\frac{\omega}{16}+\frac{1}{32}$
$\mathbb{S}^v_{v3}\|\mathbb{S}^v_{v2}$	$\frac{\omega}{16}-\frac{7}{32}$
$\delta=0,\ \omega\geqslant\frac{7}{2}$	0

Table 30: Zero-potentials coefficients for the phase diagram shown in Fig. 25.

lines	α_1
$\mathbb{S}_+\|\mathbb{S}_-$	0
$\mathbb{S}_-\|\mathbb{S}^v_{v3}$	$\frac{\omega}{16}+\frac{9}{32}$
$\mathbb{S}^v_{v3}\|\mathbb{S}^v_{v2}$	$\frac{\omega}{16}+\frac{1}{32}$
$\delta=0,\ \omega\geqslant-\frac{1}{2}$	0

Table 31: Zero-potentials coefficients for the phase diagram shown in Fig. 26.

lines & points	α_1	α_2	α_3	α_4	α_5	α_6	α_7	α_8
$\mathbb{S}_-\|\mathbb{S}^v_{v3}$	0	0	$\frac{\omega}{8}+\frac{1}{16}$	$-\frac{\omega}{24}+\frac{1}{16}$	$-\frac{\omega}{96}+\frac{3}{64}$	$-\frac{1}{32}$	$-\frac{1}{48}$	$-\frac{1}{48}$
$\mathbb{S}_-\|\mathbb{S}_1$	0	$-\frac{1}{8}$	$\frac{\omega}{4}+\frac{1}{4}$	$-\frac{7\omega}{96}-\frac{3}{64}$	$-\frac{\omega}{96}+\frac{3}{64}$	0	$-\frac{1}{48}$	$-\frac{1}{48}$
$\mathbb{S}_1\|\mathbb{S}_2$	$\frac{7\omega}{96}-\frac{17}{64}$	$\frac{7\omega}{48}-\frac{1}{32}$	$\frac{5\omega}{48}-\frac{3}{32}$	0	$-\frac{\omega}{96}-\frac{1}{64}$	$-\frac{1}{8}$	$-\frac{1}{12}$	$-\frac{1}{12}$
$\mathbb{S}_2\|\mathbb{S}_3$	$\frac{7\omega}{96}-\frac{29}{64}$	$\frac{7\omega}{48}-\frac{21}{32}$	$\frac{5\omega}{48}-\frac{19}{32}$	0	$-\frac{\omega}{96}+\frac{1}{64}$	$-\frac{3}{32}$	$-\frac{1}{12}$	$-\frac{1}{48}$
$\mathbb{S}_3\|\mathbb{S}_{cb}$	0	0	$\frac{\omega}{4}-\frac{21}{8}$	$-\frac{7\omega}{96}+\frac{45}{64}$	$-\frac{\omega}{96}+\frac{3}{64}$	0	$-\frac{1}{48}$	$-\frac{1}{48}$
$\mathbb{S}^v_{d1}\|\mathbb{S}_{cb}$	0	0	$-\frac{\delta}{4}$	$\frac{\delta}{16}-\frac{5}{96}$	$-\frac{5}{96}$	0	$-\frac{1}{48}$	$-\frac{1}{48}$
$\mathbb{S}^v_{v2}\|\mathbb{S}^v_{d1}$	0	0	$-\frac{\delta}{4}$	$\frac{\delta}{16}-\frac{1}{96}$	$-\frac{5}{192}$	$-\frac{1}{64}$	$-\frac{1}{48}$	$-\frac{1}{48}$
$\mathbb{S}^v_{v3}\|\mathbb{S}^v_{v2}$	$-\frac{1}{8}$	0	$\frac{\omega}{8}-\frac{3}{16}$	$-\frac{\omega}{24}+\frac{3}{32}$	$-\frac{\omega}{96}+\frac{3}{64}$	$-\frac{1}{8}$	$-\frac{1}{12}$	$-\frac{1}{12}$
c	$-\frac{1}{8}$	0	$-\frac{1}{4}$	$\frac{7}{96}$	$-\frac{1}{48}$	$-\frac{3}{32}$	$-\frac{1}{12}$	$-\frac{1}{48}$
e	0	0	$-\frac{3}{8}$	$\frac{1}{32}$	$-\frac{3}{64}$	$-\frac{1}{64}$	$-\frac{1}{48}$	$-\frac{1}{48}$

Table 32: Zero-potentials coefficients for the phase diagram shown in Fig. 27.

lines & points	α_1	α_2	α_3	α_4	α_5	α_6	α_7	α_8
$\mathbb{S}_-\|\mathbb{S}^v_{v3}$	0	$-\frac{1}{4}$	$\frac{\omega}{8}+\frac{9}{16}$	$-\frac{\omega}{24}-\frac{7}{48}$	$-\frac{\omega}{96}+\frac{5}{192}$	$\frac{1}{32}$	$-\frac{1}{48}$	$-\frac{1}{48}$
$\mathbb{S}_-\|\mathbb{S}_1$	0	$-\frac{1}{8}$	$\frac{\omega}{4}+\frac{1}{4}$	$-\frac{7\omega}{96}-\frac{13}{192}$	$-\frac{\omega}{96}+\frac{5}{192}$	0	$-\frac{1}{48}$	$-\frac{1}{48}$
$\mathbb{S}_1\|\mathbb{S}_3$	$-\frac{1}{4}$	0	$\frac{\omega}{4}-\frac{1}{8}$	$-\frac{7\omega}{96}-\frac{1}{192}$	$-\frac{\omega}{96}-\frac{7}{192}$	$-\frac{1}{8}$	$-\frac{1}{12}$	$-\frac{1}{12}$
$\mathbb{S}_3\|\mathbb{S}_{cb}$	0	0	$\frac{\omega}{4}-\frac{13}{8}$	$-\frac{7\omega}{96}+\frac{83}{192}$	$-\frac{\omega}{96}+\frac{5}{192}$	0	$-\frac{1}{48}$	$-\frac{1}{48}$
$\mathbb{S}^v_{d1}\|\mathbb{S}_{cb}$	0	0	$-\frac{\delta}{4}$	$\frac{\delta}{16}-\frac{7}{96}$	$-\frac{7}{96}$	0	$-\frac{1}{48}$	$-\frac{1}{48}$
$\mathbb{S}^v_{v2}\|\mathbb{S}^v_{d1}$	0	0	$-\frac{\delta}{4}$	$\frac{\delta}{16}-\frac{1}{32}$	$-\frac{3}{64}$	$-\frac{1}{64}$	$-\frac{1}{48}$	$-\frac{1}{48}$
$\mathbb{S}^v_{v3}\|\mathbb{S}^v_{v2}$	$-\frac{1}{8}$	0	$\frac{\omega}{8}+\frac{5}{16}$	$-\frac{\omega}{24}-\frac{5}{96}$	$-\frac{\omega}{96}+\frac{5}{192}$	$-\frac{1}{8}$	$-\frac{1}{12}$	$-\frac{1}{12}$
d	0	0	$\frac{5}{8}$	$-\frac{23}{96}$	$-\frac{13}{192}$	$-\frac{1}{64}$	$-\frac{1}{48}$	$-\frac{1}{48}$

Here we present the zero-potential coefficients α_i in the generating points of phase diagram shown in Fig. 28.

Table 33: Zero-potentials coefficients for the phase diagram shown in Fig. 28.

Points (d_1, d_2)	$(0,0)$	$(2,0)$	$(0,1)$	$(2,1)$	$(0,4)$	$(2,4)$
α_1	$-\frac{83}{1536}$	$-\frac{259}{3072}$	$-\frac{79}{1536}$	$-\frac{253}{3072}$	$-\frac{67}{1536}$	$-\frac{217}{3072}$
α_2	$-\frac{25}{1536}$	$-\frac{245}{3072}$	$-\frac{29}{1536}$	$-\frac{251}{3072}$	$-\frac{41}{1536}$	$-\frac{287}{3072}$
α_3	$-\frac{47}{1536}$	$-\frac{331}{3072}$	$-\frac{43}{1536}$	$-\frac{325}{3072}$	$-\frac{31}{1536}$	$-\frac{289}{3072}$
α_4	$-\frac{25}{1536}$	$-\frac{245}{3072}$	$-\frac{29}{1536}$	$-\frac{251}{3072}$	$-\frac{41}{1536}$	$-\frac{287}{3072}$
α_5	$\frac{53}{3072}$	$\frac{137}{8192}$	$\frac{19}{1024}$	$\frac{139}{8192}$	$\frac{3}{128}$	$\frac{91}{8192}$
α_6	$-\frac{53}{3072}$	$-\frac{335}{24576}$	$-\frac{19}{1024}$	$-\frac{365}{24576}$	$-\frac{3}{128}$	$-\frac{91}{8192}$
α_7	$\frac{53}{3072}$	$\frac{401}{8192}$	$\frac{19}{1024}$	$\frac{403}{8192}$	$\frac{3}{128}$	$\frac{1117}{24576}$
α_8	$-\frac{53}{3072}$	$-\frac{571}{24576}$	$-\frac{19}{1024}$	$-\frac{589}{24576}$	$-\frac{3}{128}$	$-\frac{139}{6144}$
α_9	$-\frac{19}{3072}$	$\frac{101}{2048}$	$-\frac{19}{3072}$	$\frac{13}{256}$	$-\frac{19}{3072}$	$\frac{1451}{24576}$